TÜBİTAK

Turkish Journal of Earth Sciences

http://journals.tubitak.gov.tr/earth/

Research Article

Turkish J Earth Sci
(2013) 22: 931-995

doi:10.3906/yer-1204-6

First 15 probability-based multidimensional tectonic discrimination diagrams for intermediate magmas and their robustness against postemplacement compositional changes and petrogenetic processes

Surendra P. VERMA[1,*], Sanjeet K. VERMA[2,3]

[1]Department of Energy Systems, Energy Research Center, Universidad Nacional Autónoma de México, Temixco, Morelos 62580, Mexico
[2]Energy Research Center, Universidad Nacional Autónoma de México, Temixco, Morelos 62580, Mexico
[3]Department of Geology and Natural Resources, Institute of Geosciences, University of Campinas—UNICAMP, 13083-970 Campinas, Sao Paulo, Brazil (present address)

Received: 13.04.2012 • **Accepted:** 05.01.2013 • **Published Online:** 11.10.2013 • **Printed:** 08.11.2013

Abstract: Although for ultrabasic and basic magmas a plethora of tectonomagmatic diagrams have been used, with the exception of one bivariate diagram for refined tectonic setting of orogenic andesites, none is available for highly abundant intermediate magma. We present 3 sets of discrimination diagrams obtained from the correct statistical methodology of $\log_e$-ratio transformation and linear discriminant analysis. All major element $\log_e$-ratio variables in 3664 samples, only immobile major and trace element $\log_e$-ratio variables in 1858 samples, and immobile trace element $\log_e$-ratio variables in 1512 samples were used. These diagrams with probability-based tectonic field boundaries and high success rates (about 69%–96%, 63%–100%, and 64%–100%, respectively, for diagrams based on all major elements, immobile major and trace elements, and immobile trace elements) were first tested for fresh and highly altered rocks. The expected tectonic setting was indicated from our diagrams. The probability-based decisions and total percent probability estimates can fully replace the actual plotting of samples in the diagrams. The probability calculations were then used for tectonic discrimination of 7 case studies of Archean to Proterozoic rocks. An island arc setting was indicated for the Wawa greenstone belt (Canada), implying the existence of plate tectonic processes during the Late Archean, for western Tasmania (Australia) during the Cambrian, and for Chichijima Island (Bonin Islands, Japan) during the Eocene. Similarly, an arc setting (indecisive island or continental type) was obtained for south-central Sweden during the Paleoproterozoic and for Adola (southern Ethiopia) during the Neoproterozoic. A within-plate setting was inferred for the Neoproterozoic Malani igneous complex, Rajasthan, India. A collision setting was indicated for the Alps (France-Italy-Switzerland) during the Late Carboniferous. Modeling of likely as well as extreme processes indicates that these diagrams are robust against postemplacement compositional changes caused by analytical errors, element mobility, Fe-oxidation, alteration, and petrogenetic processes.

Key words: Arc, collision, natural logarithm transformation of element ratios, tectonomagmatic discrimination, within-plate tectonic setting

1. Introduction

Magmas, subdivided into 4 main categories on the basis of anhydrous 100% adjusted SiO_2 contents (Le Bas *et al.* 1986; ultrabasic with $(SiO_2)_{adj}$ = 35%–45%, basic with 45%–52%, intermediate with 52%–63%, and acid with >63%), may originate in different tectonic settings (island arc [IA], continental arc [CA], continental rift [CR], ocean-island [OI], collision [Col], and mid-ocean ridge [MOR]). To reconstruct the geologic-tectonic history, especially in older or tectonically complex areas, it is mandatory to know the most likely tectonic setting that gave rise to magmas in a given region. One commonly used method is the application of tectonomagmatic discrimination diagrams (e.g., Rollinson 1993). Numerous such diagrams (bivariate [x-y], ternary [x-y-z], and multidimensional [DF1-DF2]) are available for ultrabasic, basic, or acid magmas (e.g., Pearce & Cann 1971, 1973; Wood 1980; Shervais 1982; Pearce *et al.* 1984; Meschede 1986; Verma 2010; Verma & Agrawal 2011; Verma *et al.* 2012). Only 1 bivariate-type diagram (Bailey 1981) has been proposed for fine-scale discrimination of only 1 type of intermediate magma (orogenic or arc andesite). For its application to old terrains, the user will have to ensure that the samples actually come from an arc setting.

* Correspondence: spv@ier.unam.mx

Therefore, tectonic origin of intermediate magma (basaltic andesite, andesite, basaltic trachyandesite, trachyandesite, tephriphonolite, phonolite, and boninite) cannot be inferred from discrimination diagrams, and new ones are very much required to fill this important deficiency of the widely used geochemical technique. For intermediate magma, we propose a total of 15 multidimensional diagrams (in 3 sets of 5 diagrams each), evaluate their success rates, argue in favor of the refined procedure of probability calculations for individual samples, test their functioning for fresh and altered samples from known tectonic settings, and efficiently use the probability estimates for 7 case studies demonstrating the versatility of these diagrams. More importantly, we also demonstrate their robustness against extreme compositional changes related to analytical errors and postemplacement changes, bulk assimilation, and petrogenetic processes.

2. Database and the statistically correct procedure

For constructing the new diagrams, a representative 5-part database (IA, CA, CR, OI, and Col, in which MOR was not included due to the scarcity of intermediate magma from mid-ocean ridges) was established from Miocene to Recent rocks from different parts of the world (see Table S1 in the electronic supplement to this paper; the relevant references are, however, included in the main paper in order to give due credit to the authors whose data were used for constructing our database and proposing new diagrams), where the tectonic setting is clearly and unambiguously known. Although we have assigned IA to samples from Japan and New Zealand, it could have been CA. It could be checked in the future if this change in assignment would improve the success rates of IA and CA discrimination. Importantly, the character of intermediate magma for each sample included in the database was confirmed by SINCLAS software (Verma *et al.* 2002).

Natural logarithm (ln or $\log_e$) transformation of element ratios (Aitchison 1986; Agrawal & Verma 2007) was used to provide the normal or Gaussian variable space, because compositional data represent a closed space with unit sum constraint and linear discriminant analysis (LDA) requires that the LDA variables be normally distributed. Before applying the LDA, the compiled data from each tectonic setting were processed using DODESSYS software (Verma & Díaz-González 2012) for identifying and separating discordant outliers (Barnett & Lewis 1994) in the 10 variables of logarithms of element ratios (natural logarithms of the ratio of all major elements, TiO_2 to P_2O_5, with SiO_2 as the common denominator). The choice of the element used as the common denominator is immaterial (Aitchison 1986) and does not actually affect the proposal and functioning of the multidimensional diagrams.

The samples with complete analyses and discordant outlier-free $\log_e$-ratio data were used to propose the diagrams. The total number of samples from each tectonic setting available for the different combination of elements is listed in Table S2. Commercial software Statistica was used to perform LDA. No attempt was made to randomly separate the database in training and testing sets, because in all previous studies when the diagrams were proposed from training-set data, the evaluation by testing-set data provided similarly high success rates (high values of correct classification expressed as percentages) as the original proposal (Verma *et al.* 2006; Agrawal *et al.* 2008; Verma & Agrawal 2011; Verma *et al.* 2012). Thus, the generally similar success rates for the training and testing sets made it unnecessary to split the data into training and testing sets.

Success rates were calculated from counting the correctly discriminated samples. The probability-based boundaries following the initial suggestion of Agrawal (1999) and the probabilities for individual samples were computed from the method recently outlined by Verma and Agrawal (2011). For applications, probabilities for individual samples of intermediate magma were used to infer the dominant tectonic setting. The concept recently proposed by Verma (2012) of total percent probability of samples from a given area corresponding to each tectonic setting was used to better illustrate the functioning and inferences from our diagrams.

Similar procedures were adopted for the other 2 sets of diagrams based on relatively immobile elements.

3. New multidimensional diagrams

We have proposed 3 sets of diagrams. Each set consists of 5 diagrams to discriminate 4 tectonic settings of island arc, continental arc, continental rift and ocean island together as within-plate, and collision. The very similar tectonic settings of island and continental arcs are separated for the first time from such complex diagrams for intermediate magma. We recall that it was not possible to do so from major elements in basic and ultrabasic rocks (Agrawal *et al.* 2004; Verma *et al.* 2006), nor was it attempted from immobile element-based diagrams (Agrawal *et al.* 2008; Verma & Agrawal 2011), although such a discrimination was successfully achieved from diagrams for acid magma (Verma *et al.* 2012). All diagrams were obtained from LDA of natural logarithms of element ratios. These 3 sets of diagrams are based, respectively, on the complete set of all major elements including the 2 Fe-oxidation varieties obtained from the Middlemost (1989) Fe subdivision with the SINCLAS computer program (Verma *et al.* 2002), relatively immobile selected major and trace elements easily determinable by conventional X-ray fluorescence spectrometry, and immobile elements involving a combination of trace and rare earth elements. Finally, no attempt was made to discriminate the within-plate setting in its 2 tectonic types (continental rift and ocean island). This is best achieved from basic and ultrabasic

magmas (Verma *et al.* 2006; Agrawal *et al.* 2008; Verma & Agrawal 2011), which are highly abundant in these 2 environments. Intermediate rock samples are much less abundant, especially in the ocean island setting (Table S2), and, therefore, it is not advisable at present to attempt their discrimination from the continental rift setting. Furthermore, 4 additional diagrams for each set of 5 diagrams would be required if we were to attempt it.

3.1. Major element-based diagrams

A total of 4023 intermediate rock samples with complete major-element analyses were available in our complete database. The results of LDA performed on these samples (success rates) can be summarized as follows: 84.56% for IA+CA together, 76.84% for CR+OI together, and 84.44% for Col. When the LDA was applied to the 3664 discordant outlier-free samples (remaining after the application of the DODESSYS software to 4023 analyses; Table S2), the success rates increased by about 2.05%, 3.39%, and 2.38%, respectively. Similar improvements were observed for all other combinations of 3 tectonic settings (average increase of about 0.98% to 5.90% in success rates). This increment of success rates clearly showed the advantage of fulfilling the basic requirement of LDA that this multivariate technique should be applied to data drawn from a normal distribution (Morrison 1990).

The geochemical characteristics of adjusted major-element and $\log_e$-ratios of discordant outlier-free 3664 complete major element analyses of intermediate rocks from the 5 tectonic settings are presented in Table S3. The statistical data for $\log_e$-ratio variables (Table S3; note the data in this and other tables are reported as rounded values following the flexible rules put forth by Verma [2005]) showed that although IA and CA as well as CR and OI are somewhat similar, there are differences among them, which can be tested by Wilks' lambda and F-ratio statistics. Thus, the $\log_e$-transformed ratios for these 5 tectonic groups or classes showed statistically significant differences inferred from both statistical tests (Wilks' lambda = 0.2002–0.2522, i.e. Wilks' lambda << 1, and F-ratio = 8.4–247.5, i.e. F-ratio >> 1) at an extremely low significance level approaching 0 (equivalently at a very high confidence level approaching 100%) for all variables (Table S4). These differences were enhanced by the multivariate technique of LDA practiced here.

The LDA was performed 5 times on 3664 samples of the training set, the first time being for all groups with IA+CA (arc samples were kept together), CR+OI (within-plate samples were maintained together), and Col settings (Figure 1a), and 4 times for all possible combinations of 3 groups at a time out of 4 groups, IA, CA, CR+OI, and Col (Figures 1b–1e). The equations for the DF1 and DF2 functions (x- and y-axes; Figures 1a–1e) obtained from the LDA (canonical analysis) are as follows.

For Figure 1a, Eqs. (1) and (2) are used to calculate the x- and y-axis variables, $DF1_{(IA+CA-CR+OI-Col)mint}$ and $DF2_{(IA+CA-CR+OI-Col)mint}$, respectively, where the subscript $_{mint}$ stands for the major element ($_m$)-based diagram for intermediate ($_{int}$) magmas. The multiplication factors and the constant are the raw coefficients from the canonical analysis (LDA; Root 1 and Root 2 values from Statistica).

$$\begin{aligned} DF1_{(IA+CA-CR+OI-Col)_{mint}} = {} & (-2.45605 \times \ln(TiO_2/SiO_2)_{adj}) + (1.11985 \times \ln(Al_2O_3/SiO_2)_{adj}) + \\ & (-2.22475 \times \ln(Fe_2O_3/SiO_2)_{adj}) + (2.48861 \times \ln(FeO/SiO_2)_{adj}) + \\ & (-0.212024 \times \ln(MnO/SiO_2)_{adj}) + (-0.06661 \times \ln(MgO/SiO_2)_{adj}) + \\ & (1.29066 \times \ln(CaO/SiO_2)_{adj}) + (-0.28377 \times \ln(Na_2O/SiO_2)_{adj}) + \\ & (-0.40211 \times \ln(K_2O/SiO_2)_{adj}) + (0.030635 \times \ln(P_2O_5/SiO_2)_{adj}) - 11.43097347 \end{aligned} \quad (1)$$

$$\begin{aligned} DF2_{(IA+CA-CR+OI-Col)_{mint}} = {} & (-0.57759 \times \ln(TiO_2/SiO_2)_{adj}) + (-0.01121 \times \ln(Al_2O_3/SiO_2)_{adj}) + \\ & (0.69125 \times \ln(Fe_2O_3/SiO_2)_{adj}) + (-1.99798 \times \ln(FeO/SiO_2)_{adj}) + \\ & (-1.72014 \times \ln(MnO/SiO_2)_{adj}) + (0.305275 \times \ln(MgO/SiO_2)_{adj}) + \\ & (0.816018 \times \ln(CaO/SiO_2)_{adj}) + (-1.791727 \times \ln(Na_2O/SiO_2)_{adj}) + \\ & (0.871298 \times \ln(K_2O/SiO_2)_{adj}) + (0.335479 \times \ln(P_2O_5/SiO_2)_{adj}) - 12.20158596 \end{aligned} \quad (2)$$

For Figure 1b, Eqs. (3) and (4) give the x- and y-axis variables, respectively.

$$\begin{aligned} DF1_{(IA-CA-CR+OI)_{mint}} = {} & (-2.51880 \times \ln(TiO_2/SiO_2)_{adj}) + (0.54210 \times \ln(Al_2O_3/SiO_2)_{adj}) + \\ & (-3.790190 \times \ln(Fe_2O_3/SiO_2)_{adj}) + (3.846277 \times \ln(FeO/SiO_2)_{adj}) + \\ & (-0.362718 \times \ln(MnO/SiO_2)_{adj}) + (-0.176632 \times \ln(MgO/SiO_2)_{adj}) + \\ & (1.426496 \times \ln(CaO/SiO_2)_{adj}) + (0.111801 \times \ln(Na_2O/SiO_2)_{adj}) + \\ & (-0.219223 \times \ln(K_2O/SiO_2)_{adj}) + (-0.07248 \times \ln(P_2O_5/SiO_2)_{adj}) - 14.3151255 \end{aligned} \quad (3)$$

$$DF2_{(IA-CA-CR+OI)_{mint}} = (-1.04907 \times \ln(TiO_2/SiO_2)_{adj}) + (3.440438 \times \ln(Al_2O_3/SiO_2)_{adj}) + (-3.43323 \times \ln(Fe_2O_3/SiO_2)_{adj}) + (4.807165 \times \ln(FeO/SiO_2)_{adj}) + (-3.499257 \times \ln(MnO/SiO_2)_{adj}) + (0.373928 \times \ln(MgO/SiO_2)_{adj}) + (-2.147775 \times \ln(CaO/SiO_2)_{adj}) + (3.00229 \times \ln(Na_2O/SiO_2)_{adj}) + (-0.773719 \times \ln(K_2O/SiO_2)_{adj}) + (1.061808 \times \ln(P_2O_5/SiO_2)_{adj}) - 13.4885545 \quad (4)$$

For Figure 1c, Eqs. (5) and (6) are as follows.

$$DF1_{(IA-CA-Col)_{mint}} = (-0.88680 \times \ln(TiO_2/SiO_2)_{adj}) + (-0.781835 \times \ln(Al_2O_3/SiO_2)_{adj}) + (-2.43157 \times \ln(Fe_2O_3/SiO_2)_{adj}) + (4.10644 \times \ln(FeO/SiO_2)_{adj}) + (2.050295 \times \ln(MnO/SiO_2)_{adj}) + (-0.386860 \times \ln(MgO/SiO_2)_{adj}) + (-0.74023 \times \ln(CaO/SiO_2)_{adj}) + (1.35997 \times \ln(Na_2O/SiO_2)_{adj}) + (-0.816315 \times \ln(K_2O/SiO_2)_{adj}) + (-0.468418 \times \ln(P_2O_5/SiO_2)_{adj}) + 4.31214432 \quad (5)$$

$$DF2_{(IA-CA-Col)_{mint}} = (1.760336 \times \ln(TiO_2/SiO_2)_{adj}) + (-4.328944 \times \ln(Al_2O_3/SiO_2)_{adj}) + (2.601111 \times \ln(Fe_2O_3/SiO_2)_{adj}) + (-4.960886 \times \ln(FeO/SiO_2)_{adj}) + (2.896834 \times \ln(MnO/SiO_2)_{adj}) + (-0.362075 \times \ln(MgO/SiO_2)_{adj}) + (2.230186 \times \ln(CaO/SiO_2)_{adj}) + (-2.966776 \times \ln(Na_2O/SiO_2)_{adj}) + (0.790236 \times \ln(K_2O/SiO_2)_{adj}) + (-1.326438 \times \ln(P_2O_5/SiO_2)_{adj}) + 7.586117348 \quad (6)$$

For Figure 1d, Eqs. (7) and (8) provide the respective x- and y-axis variables.

$$DF1_{(IA-CR+OI-Col)_{mint}} = (-2.435655 \times \ln(TiO_2/SiO_2)_{adj}) + (1.539133 \times \ln(Al_2O_3/SiO_2)_{adj}) + (-1.516655 \times \ln(Fe_2O_3/SiO_2)_{adj}) + (1.455822 \times \ln(FeO/SiO_2)_{adj}) + (0.4961937 \times \ln(MnO/SiO_2)_{adj}) + (-0.050128 \times \ln(MgO/SiO_2)_{adj}) + (1.258138 \times \ln(CaO/SiO_2)_{adj}) + (-0.827499 \times \ln(Na_2O/SiO_2)_{adj}) + (-0.488469 \times \ln(K_2O/SiO_2)_{adj}) + (0.1123605 \times \ln(P_2O_5/SiO_2)_{adj}) - 7.894955173 \quad (7)$$

$$DF2_{(IA-CR+OI-Col)_{mint}} = (-0.736658 \times \ln(TiO_2/SiO_2)_{adj}) + (-0.078809 \times \ln(Al_2O_3/SiO_2)_{adj}) + (0.065533 \times \ln(Fe_2O_3/SiO_2)_{adj}) + (-1.130176 \times \ln(FeO/SiO_2)_{adj}) + (-2.130889 \times \ln(MnO/SiO_2)_{adj}) + (0.245709 \times \ln(MgO/SiO_2)_{adj}) + (0.681694 \times \ln(CaO/SiO_2)_{adj}) + (-1.328430 \times \ln(Na_2O/SiO_2)_{adj}) + (0.770940 \times \ln(K_2O/SiO_2)_{adj}) + (0.295664 \times \ln(P_2O_5/SiO_2)_{adj}) - 15.24062267 \quad (8)$$

Finally, for Figure 1e, Eqs. (9) and (10) are used for calculating the respective x- and y-axis variables.

$$DF1_{(CA-CR+OI-Col)_{mint}} = (-2.32173 \times \ln(TiO_2/SiO_2)_{adj}) + (1.97128 \times \ln(Al_2O_3/SiO_2)_{adj}) + (-0.537435 \times \ln(Fe_2O_3/SiO_2)_{adj}) + (0.431388 \times \ln(FeO/SiO_2)_{adj}) + (-1.139286 \times \ln(MnO/SiO_2)_{adj}) + (0.527984 \times \ln(MgO/SiO_2)_{adj}) + (0.9884038 \times \ln(CaO/SiO_2)_{adj}) + (-0.894467 \times \ln(Na_2O/SiO_2)_{adj}) + (0.16138688 \times \ln(K_2O/SiO_2)_{adj}) + (0.0778358 \times \ln(P_2O_5/SiO_2)_{adj}) - 12.34961873 \quad (9)$$

$$DF2_{(CA\text{-}CR+OI\text{-}Col)_{mint}} = (-0.40691\times\ln(TiO_2/SiO_2)_{adj}) + (2.60576\times\ln(Al_2O_3/SiO_2)_{adj}) + (0.1610669\times\ln(Fe_2O_3/SiO_2)_{adj}) + (1.345967\times\ln(FeO/SiO_2)_{adj}) + (0.4457959\times\ln(MnO/SiO_2)_{adj}) + (-0.260127\times\ln(MgO/SiO_2)_{adj}) + (-0.464534\times\ln(CaO/SiO_2)_{adj}) + (0.9211739\times\ln(Na_2O/SiO_2)_{adj}) + (-1.2769499\times\ln(K_2O/SiO_2)_{adj}) + (-0.142884\times\ln(P_2O_5/SiO_2)_{adj}) + 3.501318155 \quad (10)$$

The 3 boundaries dividing the fields in each diagram (Figures 1a–1e) were based on probability calculations expressed in percentages, as explained by Verma and Agrawal (2011) and Verma *et al.* (2012). Training set group centroid DF1-DF2 values required for these calculations are included in Figures 1a–1e. Each boundary represents 50% probability for the 2 fields that it separates, and this probability decreases to 33.33% at the triple point (the intersection of 3 tectonic boundaries). For all fields (Figure 1a), we also calculated the probability-based curves for 70% (dotted curves) and 90% (dashed curves). The probability to belong to a certain group increases very rapidly for transects from the discrimination boundaries (thick solid lines) into a given field (dotted and dashed curves). To better show the data and the equal probability discrimination boundaries, we did not add these additional 70% and 90% probability curves to other diagrams (Figures 1b–1e). These curves are very similar to those in Figure 1a.

The correct and incorrect discriminations (Table S5) are reported separately for the 5 tectonic settings (Figures 1a–1e). For each tectonic setting, only 4 of the 5 diagrams (Figures 1a–1e) are applicable (the inapplicable diagram is indicated by an asterisk in Table S5). The success rates for IA and CA, discriminated as the combined IA+CA setting, were fairly high (90.1% and 79.3%, respectively). When these IA or CA samples were discriminated as either IA (see IA in Figure 1d) or CA (see CA in Figure 1e) in diagrams from which the CA or IA setting was missing, the success rates were about 89.1% and 80.0%, respectively. The similarity of these 2 arc settings is evident from those diagrams in which the same IA or CA samples were wrongly discriminated as CA and IA, respectively, because 84.5% of IA samples plotted in the CA field in Figure 1e, from which the IA field is absent, and 73.0% of CA samples did so for the IA field in Figure 1d where the CA field is missing. The similarity of these 2 tectonic settings is again clear from the other 2 diagrams (see Figures 1b and 1c), in which the IA and CA samples showed somewhat lower success rates of 69.1% to 72.5%, respectively, because most of the misdiscriminated arc samples are plotted in the other arc field. Nevertheless, these major element-based diagrams do show the feasibility of discriminating these 2 very similar subduction-related tectonic settings. The success rates for CR and OI were, respectively, 71.2%–76.6% and 93.9%–96.4%. Finally, the success rates for the Col magmas were consistently high (85.3%–86.8%, Figures 1a and 1c–1e; Table S5). Thus, the first set of 5 multidimensional diagrams showed success rates of about 69.1% to 96.4% for the discrimination of IA, CA, CR+OI, and Col settings.

3.2. Immobile major and trace element-based diagrams

In our database a total of 1868 samples (Table S2) were available with complete data for the selected immobile elements: 3 major elements $(TiO_2)_{adj}$, $(MgO)_{adj}$, and $(P_2O_5)_{adj}$, and 5 trace elements Nb, Ni, V, Y, and Zr. The selection was based on the feasibility of determining all major and these trace elements by the commonly used analytical technique of X-ray fluorescence spectrometry, which will facilitate the use of these diagrams, as well as those based on only major elements in most applications. We note that for proposing these diagrams, all major element data were first processed by SINCLAS under the Middlemost (1989) option for Fe-oxidation adjustment. The output TiO_2 value from the SINCLAS program, $(TiO_2)_{adj}$, was declared as the common denominator, and the resulting $\log_e$-transformed ratios were used for the LDA of 1868 discordant outlier-free samples. We also note that for all trace to major element $\log_e$-ratios, trace element data were expressed in the same unit (wt.%) as the major element $(TiO_2)_{adj}$. The geochemical characteristics of these elements and $\log_e$-ratios for intermediate rocks from the 5 tectonic settings (Table S2) are presented in Table S6. This statistical synthesis indicated that differences among the tectonic settings do exist. Wilks' lambda and F-ratio tests (Table S7) clearly showed that statistically significant differences (Wilks' lambda = 0.2119–0.2391, i.e. Wilks' lambda << 1, and F-ratio = 25.1–88.0, i.e. F-ratio >> 1) are present at an extremely low significance level approaching 0 for all variables. Therefore, all $\log_e$-ratio variables (Table S7) can be used in the LDA, which was performed 5 times on 1868 samples as done for the earlier set of diagrams. The equations of the $DF1_{(IA+CA\text{-}CR+OI\text{-}Col)_{mtint}}$ and $DF2_{(IA+CACR+)}$ functions (x- and y-axes; Figure 2a; similar nomenclature for other diagrams in Figures 2b–2e) were obtained from the LDA, where the subscript $_{mtint}$ stands for the major ($_m$) and trace ($_t$) element-based diagrams for intermediate ($_{int}$) magmas.

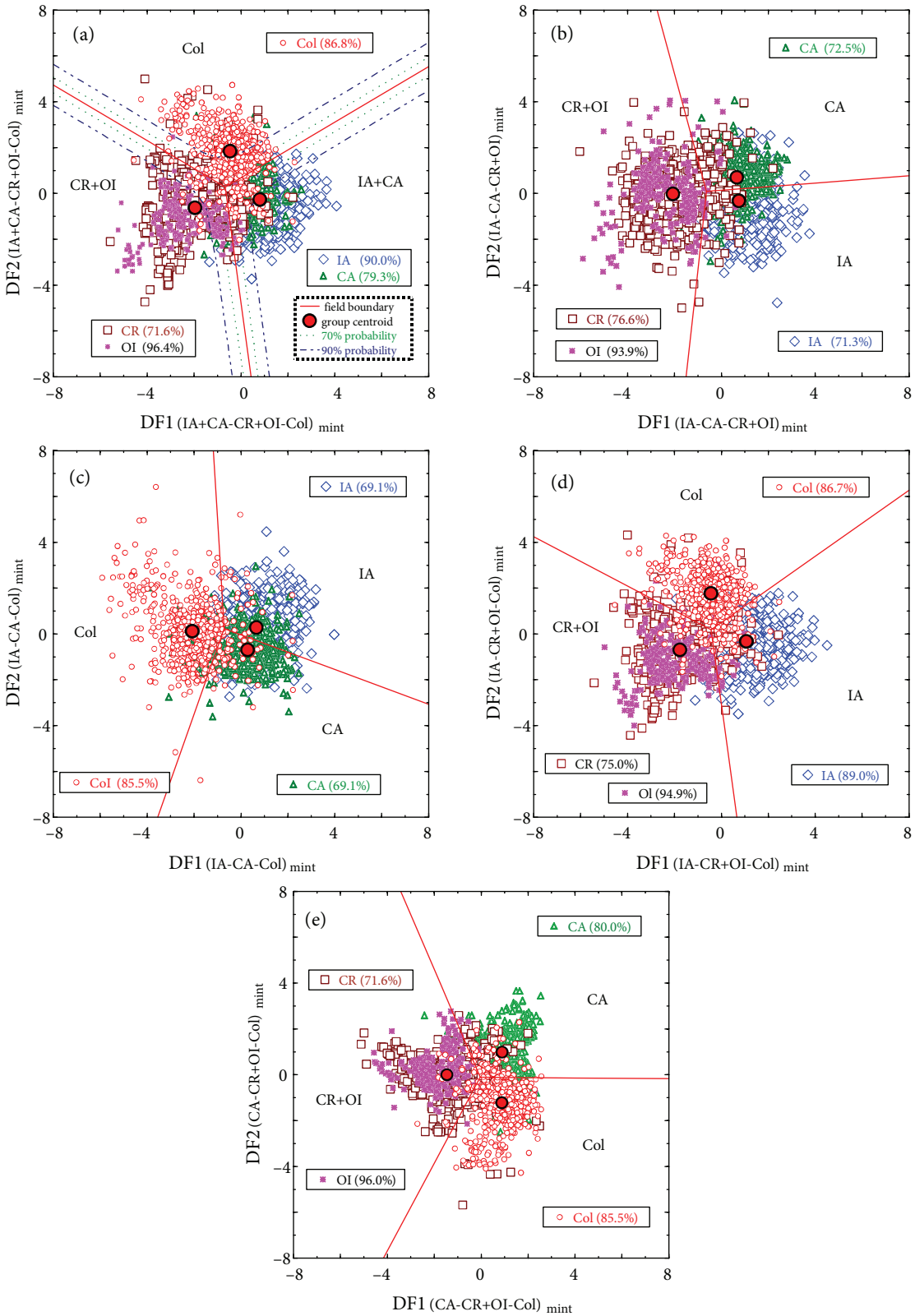

Figure 1. The first set of 5 new discriminant-function multidimensional diagrams based on $\log_e$-transformed ratios of major elements for the discrimination of intermediate rocks from island arc (IA), continental arc (CA), continental rift (CR) and ocean-island (OI) combined together, and collision (Col) tectonic settings, showing samples from the training set. The symbols are explained in the inset

in Figure 1a. In (a), 5 groups are represented as 3 groups by combining IA and CA as IA+CA and CR and OI as CR+OI. The other 4 diagrams (b–e) are for 3 groups at a time. The subscript $_{mint}$ refers to the set of multidimensional diagrams based on natural logarithm-transformed major element ($_{m}$) ratios for intermediate ($_{int}$) magmas. Group centroids (filled circles) refer to the training set samples and are reported in each diagram. The percentages are correct discrimination for training set samples (see Table S5). The thick lines represent equal probability discrimination boundaries in all diagrams. (a) IA+CA–CR+OI–Col (1+2–3+4-5) diagram; the coordinates of the field boundaries are (0.42744, –8.0) and (–0.67554, 0.27663) for IA+CA-CR+OI, (8.0, 5.53331) and (–0.67554, 0.27663) for IA+CA-Col, and (–8.0, 4.73569) and (–0.67554, 0.27663) for CR+OI–Col; the group centroids are (0.8054338548, –0.2585540725) for IA+CA, (–1.964671917, –0.6277101314) for CR+OI, and (–0.4642378707, 1.836804090) for Col; the green dotted curves are for 70% probability and blue dashed curves represent 90% probability. **(b)** IA-CA-CR+OI (1-2-3+4) diagram; the coordinates of the field boundaries are (8.0, 0.76690) and (–0.63205, 0.08764) for IA-CA, (–1.50230, –8.0) and (–0.63205, 0.08764) for IA-CR+OI, and (–2.73408, 8.0) and (–0.63205, 0.08764) for CA-CR+OI; the group centroids are (0.7455503041, –0.3210198532) for IA, (0.6646759663, 0.7065892584) for CA, and (–2.065048896, –0.01859066688) for CR+OI. **(c)** IA-CA-Col (1-2-5) diagram; the coordinates of the field boundaries are (8.0, –3.06676) and (–0.71170, 0.24138) for IA-CA, (–1.18110, 8.0) and (–0.71170, 0.24138) for IA-Col, and (–3.55140, –8.0) and (–0.71170, 0.24138) for CA–Col; the group centroids are (0.6581080574, 0.2819229794) for IA, (0.2861131966, –0.6975830163) for CA, and (–2.0761856179, 0.1163864964) for Col. **(d)** IA-CR+OI-Col (1-3+4-5) diagram; the coordinates of the field boundaries are (0.66776, –8.0) and (–0.44102, 0.17933) for IA-CR+OI, (8.0, 6.27226) and (–0.44102, 0.17933) for IA-Col, and (–8.0, 4.24657) and (–0.44102, 0.17933) for CR+OI-Col; the group centroids are (1.069154781, –0.3163633417) for IA, (–1.764731542, –0.7005214343) for CR+OI, and (–0.4360327298, 1.7689356843) for Col. **(e)** CA-CR+OI-Col (2-3+4-5) diagram; the coordinates of the field boundaries are (–3.42497, 8.0) and (–0.033967, –0.10997) for CA-CR+OI, (8.0, –0.16286) and (–0.033967, –0.10997) for CA-Col, and (–4.17272, –8.0) and (–0.033967, –0.10997) for CR+OI-Col; the group centroids are (0.8905493277, 0.99156690835) for CA, (–1.4673931178, 0.005642657408) for CR+OI, and (0.8759650737, –1.223577442) for Col.

For Figure 2a, Eqs. (11) and (12) are as follows:

$$DF1_{(IA+CA-CR+OI-Col)_{mtint}} = (1.022933\times\ln(MgO/TiO_2)_{adj}) + (0.63053\times\ln(P_2O_5/TiO_2)_{adj}) + (-0.93889\times\ln(Nb/TiO_2)_{adj}) + (-0.41538\times\ln(Ni/TiO_2)_{adj}) + (1.676898\times\ln(V/TiO_2)_{adj}) + (0.453813\times\ln(Y/TiO_2)_{adj}) + (0.583182\,3\times\ln(Zr/TiO_2)_{adj}) + 1.900726416 \quad (11)$$

$$DF2_{(IA+CA-CR+OI-Col)_{mtint}} = (0.248529\times\ln(MgO/TiO_2)_{adj}) + (-0.477177\times\ln(P_2O_5/TiO_2)_{adj}) + (-0.336281\times\ln(Nb/TiO_2)_{adj}) + (-0.131072\times\ln(Ni/TiO_2)_{adj}) + (-1.712035\times\ln(V/TiO_2)_{adj}) + (0.213840\times\ln(Y/TiO_2)_{adj}) + (-2.008435\times\ln(Zr/TiO_2)_{adj}) - 18.63750138 \quad (12)$$

For Figure 2b, the functions are calculated from Eqs. (13) and (14).

$$DF1_{(IA-CA-CR+OI)_{mtint}} = (0.875059\,7\times\ln(MgO/TiO_2)_{adj}) + (0.4279822\times\ln(P_2O_5/TiO_2)_{adj}) + (-0.686496\,7\times\ln(Nb/TiO_2)_{adj}) + (-0.372419\times\ln(Ni/TiO_2)_{adj}) + (1.924254\times\ln(V/TiO_2)_{adj}) + (0.835240\times\ln(Y/TiO_2)_{adj}) + (0.8428416\times\ln(Zr/TiO_2)_{adj}) + 8.228368089 \quad (13)$$

$$DF2_{(IA-CA-CR+OI)_{mtint}} = (-1.171625\times\ln(MgO/TiO_2)_{adj}) + (-2.650912\times\ln(P_2O_5/TiO_2)_{adj}) + (0.176065\times\ln(Nb/TiO_2)_{adj}) + (0.1183849\times\ln(Ni/TiO_2)_{adj}) + (-0.18532\,798\times\ln(V/TiO_2)_{adj}) + (1.9213464\times\ln(Y/TiO_2)_{adj}) + (0.3868149\times\ln(Zr/TiO_2)_{adj}) + 12.45160186 \quad (14)$$

For Figure 2c, Eqs. (15) and (16) are as follows:

$$DF1_{(IA\text{-}CA\text{-}Col)_{mtint}} = (-0.801371\times\ln(MgO/TiO_2)_{adj}) + (0.125028\times\ln(P_2O_5/TiO_2)_{adj}) + (0.908386\times\ln(Nb/TiO_2)_{adj}) + (0.320442\times\ln(Ni/TiO_2)_{adj}) + (-0.3683636\times\ln(V/TiO_2)_{adj}) + (-0.640580 5\times\ln(Y/TiO_2)_{adj}) + (0.72337227\times\ln(Zr/TiO_2)_{adj}) + 8.1087217398 \quad (15)$$

$$DF2_{(IA\text{-}CA\text{-}Col)_{mtint}} = (1.317201\times\ln(MgO/TiO_2)_{adj}) + (2.199955\times\ln(P_2O_5/TiO_2)_{adj}) + (-0.1235449\times\ln(Nb/TiO_2)_{adj}) + (-0.133901 8\times\ln(Ni/TiO_2)_{adj}) + (-0.8720114\times\ln(V/TiO_2)_{adj}) + (-1.7825807\times\ln(Y/TiO_2)_{adj}) + (-1.36498299\times\ln(Zr/TiO_2)_{adj}) - 20.6303644 7 \quad (16)$$

For Figure 2d, Eqs. (17) and (18) are given as follows:

$$DF1_{(IA\text{-}CR+OI\text{-}Col)_{mtint}} = (-0.85601\times\ln(MgO/TiO_2)_{adj}) + (-0.300589\times\ln(P_2O_5/TiO_2)_{adj}) + (0.861909\times\ln(Nb/TiO_2)_{adj}) + (0.384727\times\ln(Ni/TiO_2)_{adj}) + (-1.5827037\times\ln(V/TiO_2)_{adj}) + (-0.757282\times\ln(Y/TiO_2)_{adj}) + (-0.692422\times\ln(Zr/TiO_2)_{adj}) - 4.4685506 46 \quad (17)$$

$$DF2_{(IA\text{-}CR+OI\text{-}Col)_{mtint}} = (0.21504\times\ln(MgO/TiO_2)_{adj}) + (-0.503675\times\ln(P_2O_5/TiO_2)_{adj}) + (-0.32252\times\ln(Nb/TiO_2)_{adj}) + (-0.122383\times\ln(Ni/TiO_2)_{adj}) + (-1.7097486\times\ln(V/TiO_2)_{adj}) + (0.426039\times\ln(Y/TiO_2)_{adj}) + (-1.980676\times\ln(Zr/TiO_2)_{adj}) - 17.0408209 5 \quad (18)$$

Finally, for Figure 2e, the respective equations are as follows:

$$DF1_{(CA\text{-}CR+OI\text{-}Col)_{mtint}} = (-1.25554\times\ln(MgO/TiO_2)_{adj}) + (-1.082014\times\ln(P_2O_5/TiO_2)_{adj}) + (1.437934\times\ln(Nb/TiO_2)_{adj}) + (0.545446 9\times\ln(Ni/TiO_2)_{adj}) + (-1.6196297\times\ln(V/TiO_2)_{adj}) + (0.336872 5\times\ln(Y/TiO_2)_{adj}) + (-0.71359906\times\ln(Zr/TiO_2)_{adj}) + 5.752160917 \quad (19)$$

$$DF2_{(CA\text{-}CR+OI\text{-}Col)_{mtint}} = (-0.02400\times\ln(MgO/TiO_2)_{adj}) + (-0.054413\times\ln(P_2O_5/TiO_2)_{adj}) + (-0.8608025\times\ln(Nb/TiO_2)_{adj}) + (-0.174160\times\ln(Ni/TiO_2)_{adj}) + (-1.6407186\times\ln(V/TiO_2)_{adj}) + (0.068523\times\ln(Y/TiO_2)_{adj}) + (-1.772088\times\ln(Zr/TiO_2)_{adj}) - 21.02758313 \quad (20)$$

The success rates (Table S8) are reported separately for the 5 tectonic settings (Figures 2a–2e). For each tectonic setting, only 4 of the 5 diagrams (Figures 2a–2e) are applicable (the inapplicable diagram is indicated by an asterisk in Table S8). The success rates for IA and CA, discriminated as the combined IA+CA setting, were high (86.3% and 88.5%, respectively), whereas IA and CA were discriminated as IA (Figures 2b–2d) and CA (Figures 2b, 2c, and 2e), respectively, with success rates of 62.8%–85.5% and 76.2%–94.7%. The success rates for CR and OI were, respectively, 72.9%–79.2% and 98.7%–100%. The success rates for the Col magmas were very high (90.2%–92.7%; Table S8), even higher than for the major element-based diagrams (Table S5). Thus, the second set of 5 multidimensional diagrams showed success rates of about 62.8% to 100% for the discrimination of IA, CA, CR+OI, and Col settings.

3.3. Immobile trace element-based diagrams

In our database, a total of 1512 samples (Table S2) were available with discordant outlier-free complete data for the selected immobile trace elements (Yb used as the common denominator, La, Ce, Sm, Nb, Th, Y, and Zr; Table S9). Although, unlike the earlier 2 sets of diagrams, it is not mandatory to use SINCLAS (Verma *et al.* 2002) for these elements, this computer program is still considered useful even for this set of diagrams for ascertaining the intermediate nature of the igneous rock samples. The geochemical characteristics of these elements and $\log_e$-ratios for intermediate rocks from the 5 tectonic settings (Table S2) are presented in Table S9. Statistically significant differences (Wilks' lambda = 0.1466–0.1986, i.e. Wilks' lambda << 1, and F-ratio = 5.0–140.0, i.e. F-ratio >> 1) exist also for these $\log_e$-transformed ratios (Table S10) at an extremely low significance level approaching 0 for all variables, except for ln(La/Yb); for the latter, the differences are significant at the 95% confidence level. All variables were used in the LDA performed 5 times on 1512 samples. The equations of the $DF1_{(IA+CA-CR+OI-Col)_{tint}}$ and $DF2_{(IA+CA-CR+OI-Col)_{tint}}$ functions (x- and y-axes; Figure 3a; similar nomenclature for other diagrams in Figures 3b–3e) obtained from the LDA are now presented where the subscript $_{tint}$ stands for the trace ($_t$) element-based diagrams for intermediate ($_{int}$) magmas.

For Figure 3a, Eqs. (21) and (22) are as follows:

$$DF1_{(IA+CA-CR+OI-Col)_{tint}} = (-0.1672589 \times \ln(La/Yb) + (-1.2542899 \times \ln(Ce/Yb) + (1.295171 \times \ln(Sm/Yb) + (1.3318361 \times \ln(Nb/Yb) + (0.2698636 \times \ln(Th/Yb) + (1.9286976 \times \ln(Y/Yb) + (0.18097357 \times \ln(Zr/Yb) - 3.815745639 \quad (21)$$

$$DF2_{(IA+CA-CR+OI-Col)_{tint}} = (-0.2426713 \times \ln(La/Yb) + (1.7265475 \times \ln(Ce/Yb) + (0.4902224 \times \ln(Sm/Yb) + (-1.2755648 \times \ln(Nb/Yb) + (0.9602491 \times \ln(Th/Yb) + (0.8511852 \times \ln(Y/Yb) + (-0.4894082 \times \ln(Zr/Yb) - 3.305510646 \quad (22)$$

For Figure 3b, the functions are calculated from Eqs. (23) and (24).

$$DF1_{(IA-CA-CR+OI)_{tint}} = (0.0178001 \times \ln(La/Yb) + (-1.26897\,12 \times \ln(Ce/Yb) + (1.7407108 \times \ln(Sm/Yb) + (1.32442143\,8 \times \ln(Nb/Yb) + (0.0288819 \times \ln(Th/Yb) + (1.580888\,497 \times \ln(Y/Yb) + (0.17161461 \times \ln(Zr/Yb) - 3.3845534\,709 \quad (23)$$

$$DF2_{(IA-CA-CR+OI)_{tint}} = (-2.099551 \times \ln(La/Yb) + (-2.044178 \times \ln(Ce/Yb) + (-0.41179008 \times \ln(Sm/Yb) + (1.022466699 \times \ln(Nb/Yb) + (1.24448424 \times \ln(Th/Yb) + (1.87700276 \times \ln(Y/Yb) + (1.07017399797 \times \ln(Zr/Yb) - 0.2920468400 \quad (24)$$

For Figure 3c, Eqs. (25) and (26) are used:

$$DF1_{(IA-CA-Col)_{tint}} = (0.092724 \times \ln(La/Yb) + (0.752143 \times \ln(Ce/Yb) + (0.9296053 \times \ln(Sm/Yb) + (0.12351021 \times \ln(Nb/Yb) + (0.3479451 \times \ln(Th/Yb) + (1.472513 \times \ln(Y/Yb) + (-0.0339674 \times \ln(Zr/Yb) - 5.801482381 \quad (25)$$

$$DF2_{(IA-CA-CR+OI)_{tint}} = (-2.038286 \times \ln(La/Yb) + (-0.073322 \times \ln(Ce/Yb) + (-1.360432 \times \ln(Sm/Yb) + (-0.0782899 \times \ln(Nb/Yb) + (1.8248761 \times \ln(Th/Yb) + (2.7738488 \times \ln(Y/Yb) + (0.44440139 \times \ln(Zr/Yb) - 3.684349292 \quad (26)$$

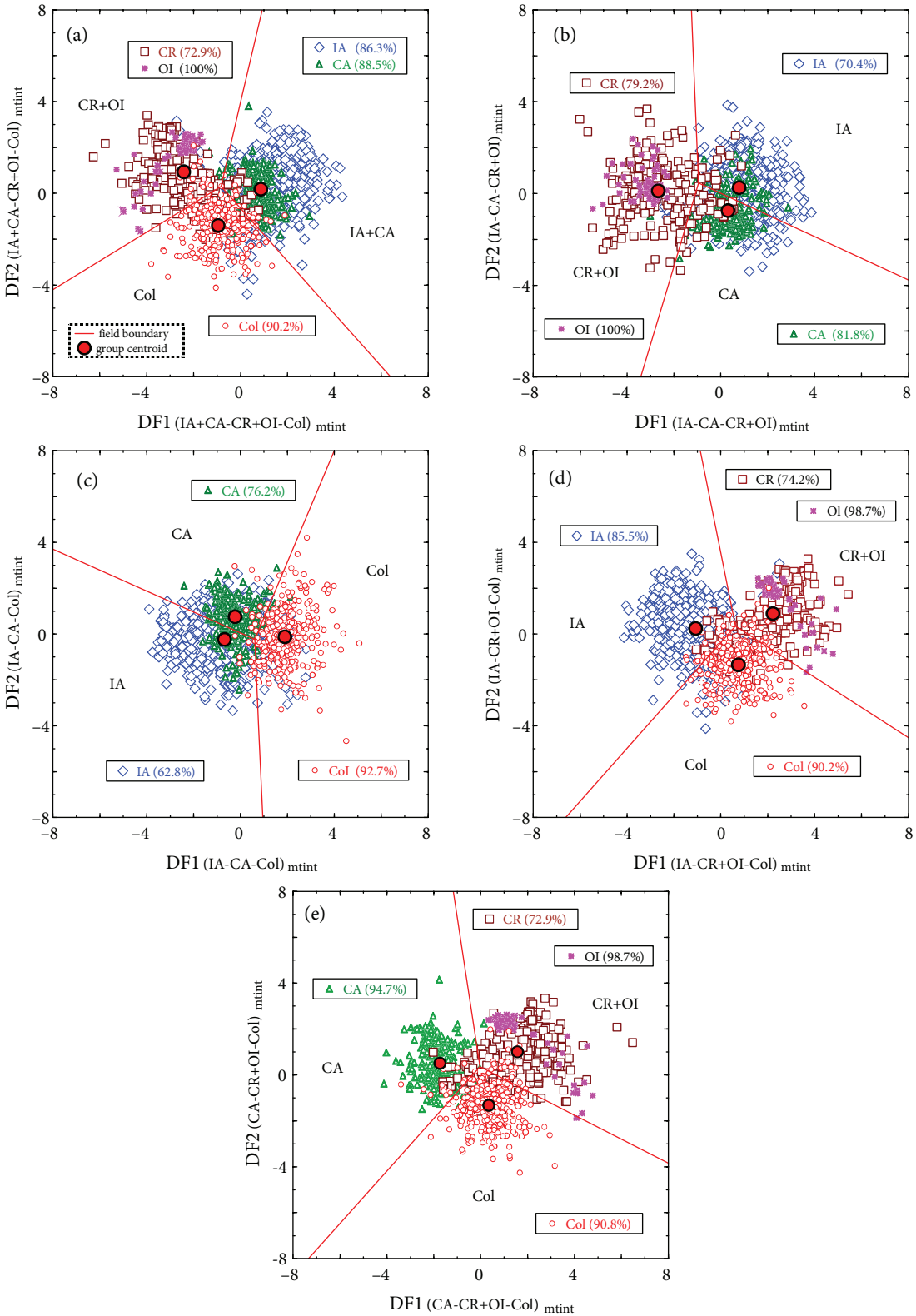

Figure 2. The second set of 5 new discriminant-function multidimensional discrimination diagrams based on $\log_e$-transformed ratios of immobile major and trace elements, showing samples from the training set. The symbols are explained in the inset in Figure 2a. More details are given in Figure 1. The subscript $_{mtint}$ in axis names refers to major and trace element ratios. The percentages in each figure are

correct discriminations for training set samples (see Table S8). **(a)** IA+CA-CR+OI-Col (1+2–3+4-5) diagram; the coordinates of the field boundaries are (0.92190, 8.0) and (–0.82858, 0.29965) for IA+CA-CR+OI, (6.39297, –8.0) and (–0.82858, 0.29965) for IA+CA-Col, and (–8.0, –4.20284) and (–0.82858, 0.29965) for CR+OI-Col; the group centroids are (0.8717919136, 0.1836538565) for IA+CA, (–2.4119835116, 0.9301323744) for CR+OI, and (–0.9487745230, –1.4004245813) for Col. **(b)** IA-CA-CR+OI (1-2-3+4) diagram; the coordinates of the field boundaries are (8.0, –3.76290) and (–0.95018, 0.45941) for IA-CA, (–1.24490, 8.0) and (–0.95018, 0.45941) for IA-CR+OI, and (–3.41007, –8.0) and (–0.95018, 0.45941) for CA-CR+OI; the group centroids are (0.7875504506, 0.2520734663) for IA, (0.3148863535, –0.7498501616) for CA, and (–2.666419140, 0.1170769090) for CR+OI. **(c)** IA-CA-Col (1-2-5) diagram; the coordinates of the field boundaries are (–8.0, 3.71126) and (0.60491, –0.23211) for IA-CA, (0.95093, –8.0) and (0.60491, –0.23211) for IA-Col, and (4.00195, 8.0) and (0.60491, –0.23211) for CA-Col; the group centroids are (–0.6826446433, –0.2400902940) for IA, (–0.2296800482, 0.7483231874) for CA, and (1.8880671989, –0.1255771906) for Col. **(d)** IA-CR+OI-Col (1-3+4-5) diagram; the coordinates of the field boundaries are (–0.87616, 8.0) and (0.62149, 0.34939) for IA-CR+OI, (–6.61289, –8.0) and (0.62149, 0.34939) for IA-Col, and (8.0, –4.51524) and (0.62149, 0.34939) for CR+OI-Col; the group centroids are (–1.0703369201, 0.2441771424) for IA, (2.2277092202, 0.8896913710) for CR+OI, and 0.7578341279, –1.3397609987) for Col. **(e)** CA-CR+OI-Col (2–3+4-5) diagram; the coordinates of the field boundaries are (–1.16430, 8.0) and (–0.028516, 0.35743) for CA-CR+OI, (–7.33632, –8.0) and (–0.028516, 0.35743) for CA-Col, and (8.0, –3.84452) and (–0.028516, 0.35743) for CR+OI-Col; the group centroids are (–1.7443803369, 0.5101687902) for CA, (1.5687968044, 1.0025551371) for CR+OI, and (0.3517867418, –1.3227417914) for Col.

For Figure 3d, Eqs. (27) and (28) are given as follows:

$$DF1_{(IA\text{-}CR+OI\text{-}Col)_{tint}} = (0.720851 \times \ln(La/Yb) + (-1.352147 \times \ln(Ce/Yb) + (1.378563 \times \ln(Sm/Yb) + (1.1641465 \times \ln(Nb/Yb) + (-0.0423769 \times \ln(Th/Yb) + (1.5584709 \times \ln(Y/Yb) + (-0.1644980 \times \ln(Zr/Yb) - 2.9336489118 \quad (27)$$

$$DF2_{(IA\text{-}CR+OI\text{-}Col)_{tint}} = (0.2378909 \times \ln(La/Yb) + (-2.03548886 \times \ln(Ce/Yb) + (-0.2501036699 \times \ln(Sm/Yb) + (1.34733326 \times \ln(Nb/Yb) + (-0.760673982 \times \ln(Th/Yb) + (-0.786605747 \times \ln(Y/Yb) + (0.37736968328 \times \ln(Zr/Yb) + 4.1547322826 \quad (28)$$

Finally, for Figure 3e, the respective equations are as follows:

$$DF1_{(CA\text{-}CR+OI\text{-}Col)_{tint}} = (-0.977026 \times \ln(La/Yb) + (-1.3886489 \times \ln(Ce/Yb) + (1.36560 \times \ln(Sm/Yb) + (1.8999127 \times \ln(Nb/Yb) + (0.5690460 \times \ln(Th/Yb) + (1.65772638 \times \ln(Y/Yb) + (-0.30523813 \times \ln(Zr/Yb) - 0.87680549008 \quad (29)$$

$$DF2_{(CA\text{-}CR+OI\text{-}Col)_{tint}} = (-0.0869677 \times \ln(La/Yb) + (1.1636159 \times \ln(Ce/Yb) + (0.3635930 \times \ln(Sm/Yb) + (-0.90127239 \times \ln(Nb/Yb) + (1.1257989 \times \ln(Th/Yb) + (1.19149068 \times \ln(Y/Yb) + (-0.39964298 \times \ln(Zr/Yb) - 3.915383182 \quad (30)$$

As for the earlier 2 sets of diagrams, only 4 of the 5 diagrams (Figures 3a–3e) are applicable for each tectonic setting (the inapplicable diagram is indicated by an asterisk in Table S11). The success rates for IA and CA (Table S11), discriminated as the combined IA+CA setting, were very high (91.4% and 90.4%, respectively), whereas IA and CA were discriminated as IA (Figures 3b–3d) and CA (Figures 3b, 3c, and 3e), respectively, with success rates of 72.7%–90.3% and 64.5%–95.7%. The success rates for CR and OI were, respectively, 74.3%–80.5% and 94.1%–100%. The success rates for the Col magmas were also high (81.0%–84.7%; Table S11). Thus, the third set of 5 multidimensional diagrams showed success rates of about 64.5% to 100% for the discrimination of IA, CA, CR+OI, and Col settings.

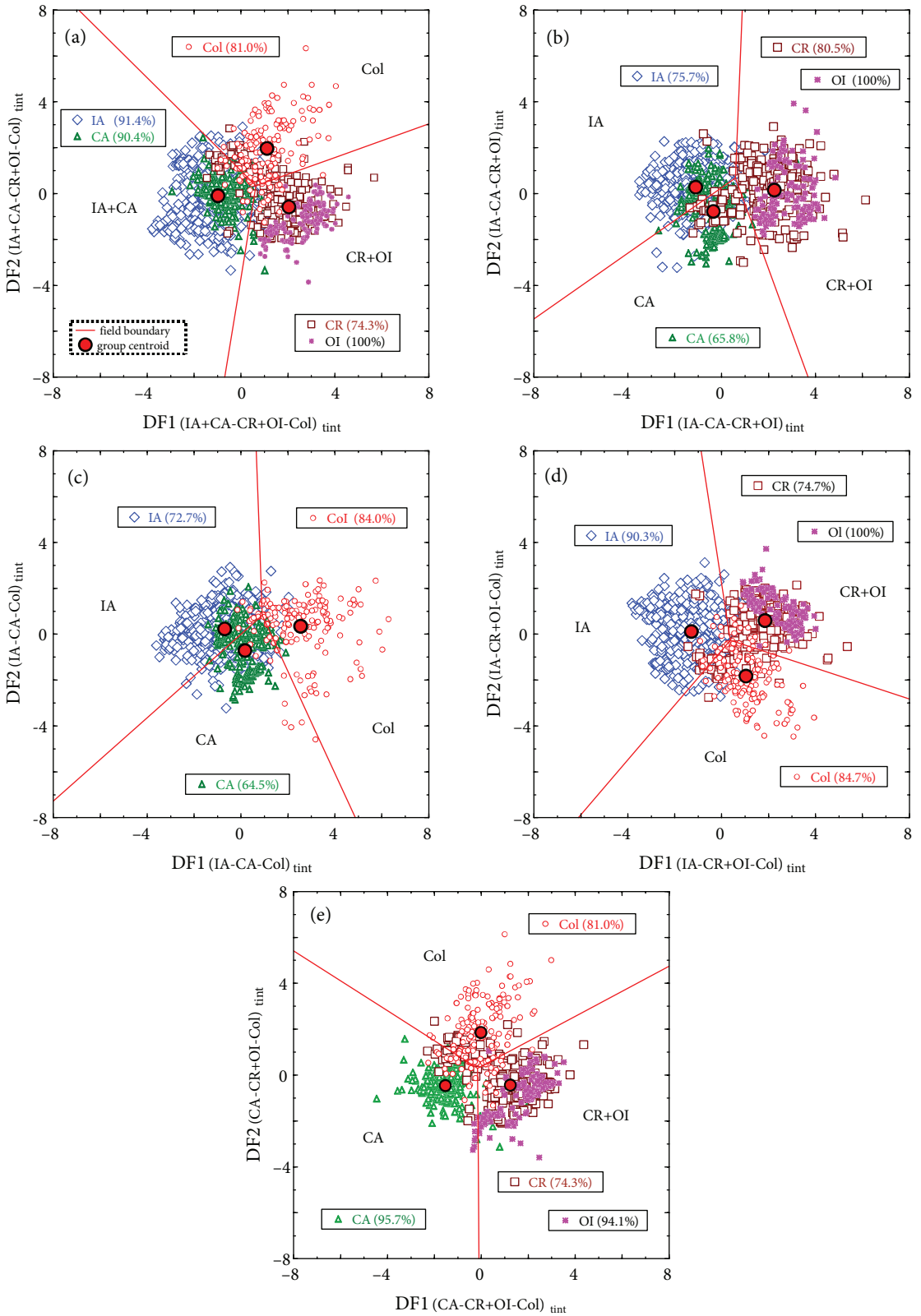

Figure 3. The third set of 5 new discriminant-function multidimensional diagrams based on $\log_e$-transformed ratios of immobile trace elements for the discrimination of intermediate rocks, showing samples from the training set. The symbols are explained in the inset in Figure 3a. More details are given in Figure 1. The subscript $_{tint}$ in axis names refers to the set of multidimensional diagrams based on

$\log_e$-transformed trace element ratios. The percentages in each figure refer to correct discrimination for training set samples (see Table S11). **(a)** IA+CA-CR+OI-Col (1+2–3+4-5) diagram; the coordinates of the field boundaries are (–0.69292, –8.0) and (0.64148, 0.34301) for IA+CA-CR+OI, (–6.91145, 8.0) and (0.64148, 0.34301) for IA+CA-Col, and (8.0, 3.04640) and (0.64148, 0.34301) for CR+OI-Col; the group centroids are (–0.9774289603, –0.1013788344) for IA+CA, (2.0410269070, –0.5841593120) for CR+OI, and (1.1079374566, 1.9556336665) for Col. **(b)** IA-CA-CR+OI (1-2-3+4) diagram; the coordinates of the field boundaries are (–8.0, –5.45793) and (0.58959, 0.68699) for IA-CA, (0.87619, 8.0) and (0.58959, 0.68699) for IA-CR+OI, and (3.67939, –8.0) and (0.58959, 0.68699) for CA-CR+OI; the group centroids are (–1.1051018735, 0.2721190917) for IA, (–0.3503347313, –0.7829225361) for CA, and (2.2466156797, 0.1407633232) for CR+OI. **(c)** IA-CA-Col (1-2-5) diagram; the coordinates of the field boundaries are (–8.0, –7.28196) and (0.90473, 0.82230) for IA-CA, (0.64537, 8.0) and (0.90473, 0.82230) for IA-Col, and (4.86730, –8.0) and (0.90473, 0.82230) for CA-Col; the group centroids are (–0.6933875947, 0.2346902936) for IA, (0.1696340466, –0.7135732664) for CA, and 2.5411240984, 0.3515850688) for Col. **(d)** IA-CR+OI-Col (1-3+4-5) diagram; the coordinates of the field boundaries are (–0.87235, 8.0) and (0.37157, –0.26385) for IA-CR+OI, (–6.10890, –8.0) and (0.37157, –0.26385) for IA-Col, and (8.0, –2.82217) and (0.37157, –0.26385) for CR+OI-Col; the group centroids are (–1.2898249628, 0.1152106837) for IA, (1.8477651525, 0.5874997038) for CR+OI, and (1.0359821323, –1.8330905346) for Col. **(e)** CA-CR+OI-Col (2-3+4-5) diagram; the coordinates of the field boundaries are (–0.10284, –8.0) and (–0.15459, 0.29462) for CA-CR+OI, (–8.0, 5.41425) and (–0.15459, 0.29462) for CA-Col, and (8.0, 4.74335) and (–0.15459, 0.29462) for CR+OI-Col; the group centroids are (–1.5332986559, –0.4569150582) for CA, (1.2333855428, –0.4396529035) for CR+OI, and (–0.02124818532, 1.8606170376) for Col.

4. Applications

4.1. Probability estimates for individual samples

As recently suggested by Verma (2012), we can use the probability calculations (modified from Verma & Agrawal 2011; a few nomenclatural errors are corrected in this work) to fully replace the discrimination diagrams (Figure 1). Therefore, we outline the procedure to calculate the probabilities of individual samples to belong to the 3 tectonic settings discriminated in a given diagram. The subscripts, such as $(IA+CA-CR+OI-Col)_{mint}$, $DF1_{(IA+CA-CR+OI-Col)_{mtint}}$, and $DF1_{(IA+CA-CR+OI-Col)_{tint}}$, are purposely eliminated from Eqs. (31) through (39) to keep them relatively simple. Otherwise, we would have had to list 126 more equations (9 for each diagram).

The distances (d_{g1}, d_{g2}, and d_{g3}) of a sample under evaluation from the 3 group centroids ($mdf1_{g1}$, $mdf2_{g1}$), ($mdf1_{g2}$, $mdf2_{g2}$), and ($mdf1_{g3}$, $mdf2_{g3}$) of the tectonic groups g1, g2, and g3, respectively, in a given diagram are as follows:

$$d_{g1} = \sqrt{(df1_s - mdf1_{g1})^2 + (df2_s - mdf2_{g1})^2} \quad (31)$$

$$d_{g2} = \sqrt{(df1_s - mdf1_{g2})^2 + (df2_s - mdf2_{g2})^2} \quad (32)$$

$$d_{g3} = \sqrt{(df1_s - mdf1_{g3})^2 + (df2_s - mdf2_{g3})^2} \quad (33)$$

where $df1_s$ and $df2_s$ are the coordinates or scores of the sample under evaluation in a given diagram.

New functions sg1, sg2, and sg3 based on distances d_{g1}, d_{g2}, and d_{g3} of Eqs. (31) through (33) for that particular sample are then computed from Eqs. (34) through (36) as follows:

$$sg1 = e^{\{(d_{g1})^2/2\}} \quad (34)$$

$$sg2 = e^{\{(d_{g2})^2/2\}} \quad (35)$$

$$sg3 = e^{\{(d_{g3})^2/2\}} \quad (36)$$

Finally, the probabilities for belonging to each of 3 groups ($P1_s$, $P2_s$, and $P3_s$; if desired, they could be expressed in percentages) are then calculated from the above parameters (sg1, sg2, and sg3) as follows:

$$P1_s = \frac{sg1}{sg1 + sg2 + sg3} \quad (37)$$

$$P2_s = \frac{sg2}{sg1 + sg2 + sg3} \quad (38)$$

$$P3_s = \frac{sg3}{sg1 + sg2 + sg3} \quad (39)$$

These probability estimates ($P1_s$, $P2_s$, and $P3_s$) directly provide the inferred tectonic setting for the sample under consideration. The inferred setting is the one for which the corresponding probability ($P1_s$, $P2_s$, or $P3_s$) is the highest. The actual value of the highest probability also indicates how far away from the tectonic field boundary the sample will actually plot in the field of the inferred tectonic setting. Thus, a simple comparison of the 3 probabilities will provide the inferred tectonic setting for a given sample or a set of samples, without any special need to plot the data in a discrimination diagram.

Nevertheless, these calculations must be carried out 5 times to obtain probabilities for all 5 discrimination diagrams of each set (Figures 1–3). Thus, probability

estimates can be obtained for a given set of samples analyzed from the area under study. Mean and standard deviation values, as well as total probabilities and the resulting total percent probabilities for the different tectonic settings, can be calculated and inferences made without the need of actually plotting the samples in diagrams. A similar procedure is valid for the other 2 sets of diagrams.

For actual applications, it is mandatory to use the highly precise centroid values (i.e. with many significant digits; Figures 1–3) in the probability calculations. Otherwise, the probability-based decisions of sample assignment to a group or class may not fully agree with the actual plotting of samples in the diagrams, particularly for samples that plot very close to the field boundaries.

To avoid excessive complication, we did not apply discordancy tests to the probability data and, therefore, we report only the initial mean probability values along with the respective standard deviation values; after all, these central tendency and dispersion estimates are for indication purposes only. The total probability and the respective total percent probability values are more important for the interpretation and inferences from these 15 diagrams, as recently documented by Verma (2012).

4.2. Evaluation of discrimination diagrams from samples of known tectonic settings

Independently of the database used for proposing new diagrams (Table S1), we compiled geochemical data for Neogene rock samples from known tectonic settings and separated those for the intermediate rocks to be used in our diagrams. More importantly, we present an innovative way to infer tectonic setting from probability calculations, particularly the total percent probability concept explained below in Section 4.2.1.

We did not process the $\log_e$-transformed data of the evaluation and application samples using the DODESSYS computer program (Verma & Díaz-González 2012), because such statistically censored data have generally increased the success rates and strengthened the inferences of the tectonic setting (see, e.g., Verma & Agrawal 2011; Verma *et al.* 2012). As seen below, the inferences from the 3 sets of diagrams are mutually consistent in most instances, and so there is no special need to identify discordant outliers in our applications. Furthermore, the concept of total probability values for the different tectonic settings is better applied to all samples without the identification and separation of samples representing discordant outlying observations.

Due to space limitations, we do not comment on the results of published sets of multidimensional diagrams for basic and ultrabasic (Verma *et al.* 2006; Agrawal *et al.* 2008; Verma & Agrawal 2011) or for acid magmas (Verma *et al.* 2012); such an application generally provided consistent results with those of the present work. Besides, only one set of plots is shown (Figures 4a–4e), but the results of all applicable diagrams (Figures 1–3) are summarized in Tables S12–S17. To familiarize the reader with this relatively new concept of using a set of 5 diagrams instead of just 1 diagram, especially the inferences based on probability calculations alone without the actual plotting of samples, the first example is described in greater detail than the remaining ones.

4.2.1. Samples from an island arc setting

Thirty rock samples of Pleistocene age from the Ijen volcanic complex, eastern Java, Indonesia (Handley *et al.* 2007) proved to be of intermediate magma types (Figure 4; Table S12). An island arc setting is known for this area (Handley *et al.* 2007).

For total probability estimates for a given tectonic setting in any diagram, we summed up the probability of only those samples that plotted in that particular tectonic setting. The smaller values of probability of these samples for the remaining 2 tectonic settings were not considered. For example, our first diagram (Figure 4a) discriminates 3 tectonic settings of IA+CA, CR+OI, and Col. Now, suppose that a sample plots in the IA+CA field and has the probability of 0.5010. Its remaining probability of 0.4990 (= 1 – 0.5010) will be divided for 2 other settings of CR+OI and Col. These 2 smaller probability values, which will add up to 0.4990, will actually depend on where exactly this sample plots in the combined arc (IA+CA) field. In the calculation of the total probability, we will assign the value of 0.5010 to the IA+CA field, but we will ignore the remaining 2 minor probability values corresponding to the other 2 fields, i.e. only the highest probability values are taken into account.

We could, of course, have used the other procedure to sum up all probabilities, irrespective of in which field the samples actually plot, but then the number of samples plotting in a given field and the total or mean probability values would have to be interpreted differently. As presented now, the mean probability values for a given field give us an idea of how far away from the boundaries the samples might be plotting in a tectonic field, without actually preparing and visually examining the plots.

Twenty-two samples (out of 30, with a success rate of about 73%) plotted in the combined arc (IA+CA) field, whereas the remaining 3 samples belonged to the within-plate and 5 to the collision field (Figure 4a). The probabilities for belonging to the field in which the samples plotted varied from 0.5010 to 0.9925 (p_{IA+CA}; n = 22 samples, with the mean $\overline{x}$ and standard deviation s values of 0.732 and 0.181, respectively, i.e. 0.732 ± 0.181) for the combined arc field, from 0.6157 to 0.8597 (p_{CR+OI}; n = 3, 0.743 ± 0.122) for the within-plate, and from 0.4832 to 0.8280 (p_{Col}; n = 5, 0.622 ± 0.131) for the collision setting. The 22 samples plotted more inside the combined arc

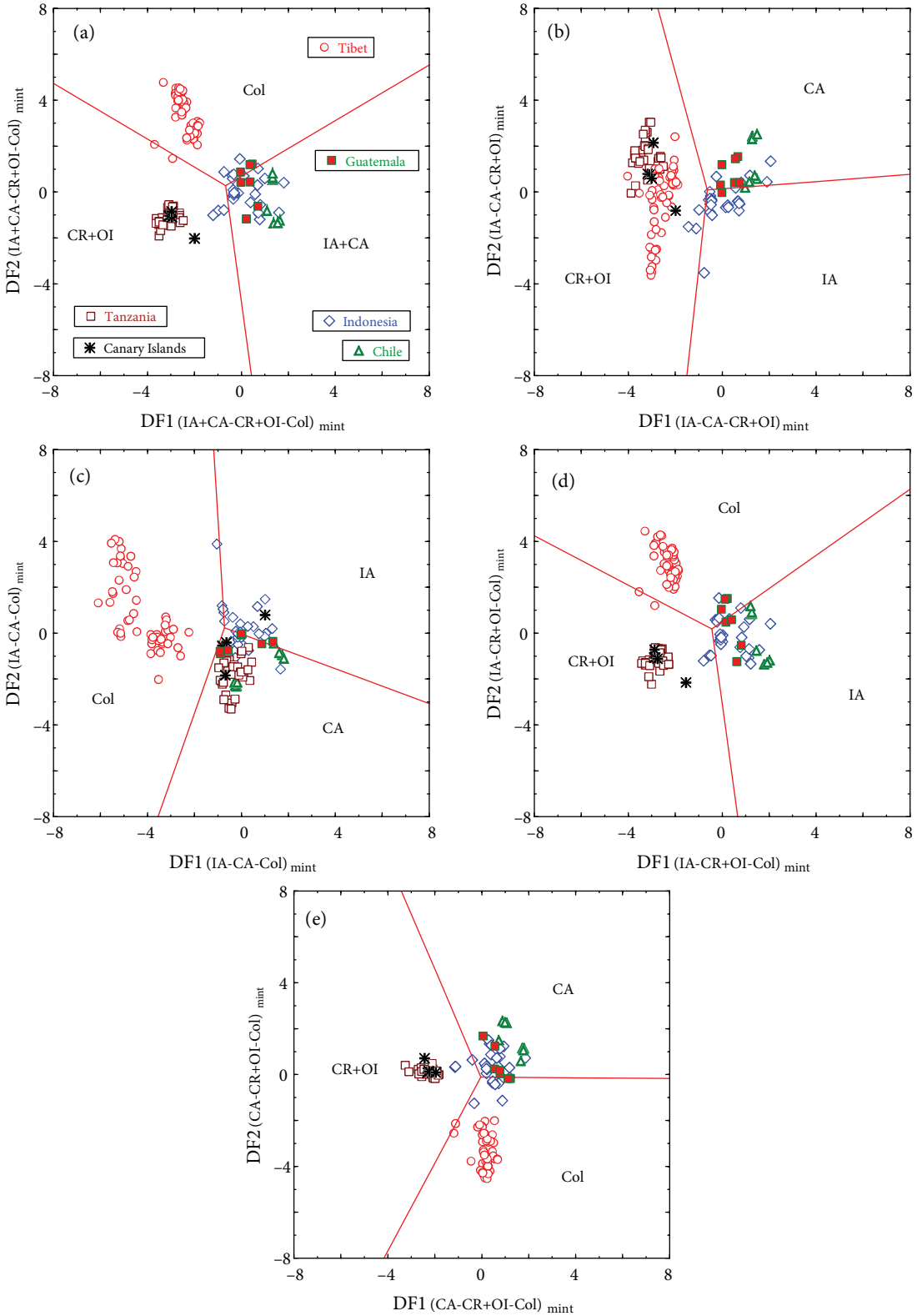

Figure 4. Evaluation of the first set of 5 discriminant-function multidimensional diagrams based on $\log_e$-transformed ratios of major elements for the discrimination of intermediate rocks from areas of known tectonic setting. The symbols are explained in the inset in Figure 4a. For more information, see Figure 1. **(a)** IA+CA-CR+OI-Col (1+2-3+4–5) diagram; **(b)** IA-CA-CR+OI (1-2-3+4) diagram; **(c)** IA-CA-Col (1-2-5) diagram; **(d)** IA-CR+OI-Col (1-3+4-5) diagram; and **(e)** CA-CR+OI-Col (2-3+4–5) diagram.

field, i.e. farther away from the field boundaries, and the 3 samples did more so in the within-plate field than the 5 samples of the collision field (qualitatively compare the mean values of 0.732 and 0.743 with 0.622; Table S12). Because most samples (22 out of 30) plotted in the arc field, the other diagrams of this set (Figures 4b–4e) can be used to discriminate the 2 types of arc setting (island and continental arcs).

A similarly high success rate of about 73% for the island arc field is obtained for the second diagram of this set (Figure 4b; Table S12), in which 22 samples out of 30 (with the mean p_{IA} value of about 0.547 for n = 22) plotted in the IA field. The remaining 8 samples were distributed between the continental arc (CA; 5 samples) and within-plate settings (3 samples; collision setting is absent from this diagram). This diagram (Figure 4b) indicates that the Indonesian samples likely represent an island arc setting rather than a continental arc.

The third diagram (Figure 4c), however, did not provide any decisive answer for the discrimination of these 2 very similar settings of IA and CA. Thirteen samples plotted in each of these 2 fields, with the remaining 4 in the collision field. The respective probabilities for the 2 fields (IA and CA) were also similar, although the mean value for IA was slightly greater (p_{IA} = 0.584 versus p_{CA} = 0.557) than that for the CA.

The fourth diagram (Figure 4d), from which the CA setting is missing, showed 21 samples in the IA field, whereas the fifth and final diagram (Figure 4e) showed 20 samples in the CA field. The respective mean probability values (p_{IA} = 0.763 for 21 samples of the IA field versus p_{CA} = 0.711 for 20 samples of the CA field) indicated that the Indonesian samples plotted somewhat more inside IA than CA (Figures 4d and 4e; Table S12).

From the consideration of all diagrams (Figures 4a–4e), the fifth diagram (Figure 4e), from which the island arc setting is absent, can be considered as the inapplicable diagram for these samples. An alternative way to interpret these results is to evaluate the overall picture of all 5 diagrams (Figures 4a–4e), without actually discarding any of them, in terms of the probability estimates (Table S12).

The overall picture of the number of samples plotting in different fields and the respective probabilities are then summarized in Table S12. Out of the total number of data points (150) in the 5 diagrams (Figures 4a–4e), 22 belonged to the combined arc, 56 to the island arc, 38 to the continental arc, 12 to the within-plate, and 22 to the collision field (Table S12). Although one can consider the percentage of these samples to infer the tectonic setting, this percentage does not take into account the relative distance from the tectonic field boundaries the samples plot in a given field. Therefore, it is advisable for the overall picture that the total probability for each field should be calculated for each tectonic field occupied in all 5 diagrams. Nevertheless, the total probability of samples that plotted in the combined arc field (Figure 4a) must be subdivided and assigned proportionately to the 2 types of arc fields IA and CA, according to the weighing factors of total probabilities for these 2 arc fields in all the remaining diagrams (Figures 4b–4e). When this was done and the total percent probability (% prob) values for the 4 tectonic settings (IA, CA, CR+OI, and Col) were calculated, the results (Table S12) showed that the rock samples from the Ijen volcanic complex gave 46.3% total percent probability for the IA, 31.8% for the CA, 8.8% for the within-plate, and 13.1% for the collision setting. Therefore, from the first set of major element-based diagrams (Figures 1a–1e) an island arc setting can be inferred for these samples.

The second set of diagrams (Figures 2a–2e: Indonesian data are not shown here, because no additional diagram is presented in this paper) based on relatively immobile major and trace elements confirmed the result of an island arc setting for the samples from Indonesia under study (Table S12), because a large number of samples (13 to 24 out of 28) plotted in the IA field and the overall total probability percentage of 47.3% was obtained for this setting. This highest value was followed by 38.7% for the competing very similar tectonic setting of continental arc, but it was much greater than that for the collision setting (14.0%). No samples plotted in the continental rift setting, which means that the total probability of samples for this tectonic setting was zero (Table S12).

The third set of diagrams (Figures 3a–3e: Indonesian data are not shown here) also based on relatively immobile elements (trace elements in this case) fully confirmed a successful test of these multidimensional diagrams (Table S12). Sixteen to 24 samples (out of 28; success rates of about 57%–86%) plotted in the IA or combined IA+CA field. In this case, the fifth diagram (Figure 3e) can be clearly declared as the inapplicable diagram, because the inferred (and expected) island arc field is absent from it. Alternatively, the overall picture of total percent probability values (% prob of 48.6% for IA followed by 37.5% for CA and 13.9% for Col) can be used to infer an island arc setting for these Pleistocene samples from eastern Java, Indonesia.

Satisfactory functioning of all 3 sets of diagrams (Figures 1–3) for the island arc setting is confirmed from this example.

4.2.2. Samples from a continental arc setting

The functioning of our diagrams for continental arc setting was tested using 9 intermediate rock samples of Pleistocene age reported for the Huiqui volcano, southern Chile, by Watt *et al.* (2011). A continental arc setting is clearly known for this area of Chile.

In the first set of diagrams based on major elements (Figures 4a–4e; see data identified as Chile), all 9 samples

plotted in the combined arc field and showed relatively high probability (p_{IA+CA}) values of 0.8008 to 0.9949 (Table S13), testifying that the samples plotted well inside the IA+CA field (Figure 4a). In the next 2 diagrams, 8 out of 9 samples plotted in the CA field, with the remaining sample in the IA field (Figures 4b and 4c). In the other 2 diagrams, in which only 1 type of arc field is present (IA in Figure 4d and CA in Figure 4e), all the 9 samples plotted in the arc field. None of the samples plotted in within-plate or collision field in any of the 5 diagrams (Figures 4a–4e). Therefore, the continental arc setting expected for these samples is confirmed and Figure 4d is declared as the inapplicable diagram. Alternatively, the total probability estimates presented in Table S13 can be used to infer the tectonic setting of a continental arc, because the total percent probability (% prob) for this setting is the highest (70.8%) and that for the island arc setting is the complementary smaller value of 29.2%.

Geochemical data were also available for the second set of major and trace element-based diagrams (Table S13). A complete data set was not reported for our third set of diagrams (Th was the missing element; Watt *et al.* 2011), which meant that this third set based on immobile trace elements could not be tested for its functioning for the continental arc setting. Nevertheless, our second set of diagrams (Figure 2) provided exactly the same result as the first set, i.e. a continental arc setting for the Huiqui volcano, because the highest total percent probability of 70.1% was obtained for this field and the remaining much lower percent probability (29.9%) was shared by the IA (26.9%) and collision (3.0%) settings. Thus, satisfactory functioning of 2 sets of diagrams (Figures 1 and 2) for the discrimination of continental arc setting is safely inferred from this example.

4.2.3. Samples from a continental rift setting

Thirty-four samples of Pliocene-Holocene intermediate magmas from the Kilimanjaro volcano, Tanzania (Nonnotte *et al.* 2011) were successfully used to test all 3 sets of diagrams (Figures 1–3) for the continental rift setting (Table S14) from this largest volcano in Africa.

Complete major element data available for all 34 samples showed that all of them plotted in the within-plate (CR+OI) setting in the 4 diagrams in which this setting is present (Figures 4a, 4b, 4d, and 4e). In the inapplicable diagram (Figure 4c) from which this setting is absent, all samples plotted in the continental arc (CA) setting. Note that in all applicable diagrams, the samples plotted well inside the tectonic field. The corresponding probability values were very high (0.9703–0.9998; Table S14). The total percent probability estimates gave a high value of 83.5% for the within-plate setting.

For the second set of diagrams (Figure 2), only 23 samples (out of 34) had a complete data set (Ni concentrations were missing for the remaining samples; Nonnotte *et al.* 2011). Nevertheless, these samples fully confirmed the expected continental rift setting for the Kilimanjaro volcano, because all 23 samples plotted in the within-plate field (Table S14). In the only diagram without the expected setting (Figure 2c), they belonged to the collision setting. The total percent probability of samples for the within-plate setting was high (79.9%).

All 34 samples from the Kilimanjaro volcano had complete data for the third set of trace element-based diagrams (Figure 3), which once again confirmed the within-plate setting (Table S14). All samples plotted in this field in all 4 applicable diagrams, whereas in the inapplicable diagram (Figure 3c), most of them plotted in the collision field, with a few samples belonging to the continental arc field. The total percent probability value for this setting was similarly high (80.3%).

Thus, we may conclude that all 3 sets of diagrams perform well for the continental rift setting discriminated as within-plate (CR+OI).

4.2.4. Samples from an ocean island setting

For evaluating our diagrams for the ocean island setting, samples of Pleistocene-Holocene rocks from the El Hierro and La Palma islands of the Canary Islands (Day *et al.* 2010) were compiled. Because most rocks from this setting are of ultrabasic and basic magmas, only 5 samples proved to be of intermediate magma type.

The first set of diagrams (Figure 4) successfully indicated a within-plate setting for these 5 samples (Table S15). The total percent probability (% prob) gave a very high value of 87.0%.

For the trace elements used in our second set of diagrams (Nb, Ni, V, Y, and Zr) based on the combination of immobile major and trace elements, Day *et al.* (2010) presented 2 sets of data by the analytical techniques used by them (X-ray fluorescence spectrometry [XRF} and inductively coupled plasma mass spectrometry [ICPMS]). Although the data for Nb, V, Y, and Zr generally showed only relatively small differences, those for Ni appeared to be drastically different (0–4 μg g^{-1} by XRF and 1.2–30.8 μg g^{-1} by ICPMS). These 2 sets of data (XRF and ICPMS) gave inconclusive and inconsistent results for the second set of diagrams (Figure 2). We report here only the results of our second diagram (Table S15) from the use of their ICPMS data. These results seem to be inconclusive because the samples are almost equally divided in within-plate and collision settings, with total percent probability (% prob) values of 48.2% and 51.8%, respectively.

Nevertheless, the third set of diagrams (Figure 3) provided conclusive results consistent with the first set of diagrams (Table S15). A within-plate setting was indicated for these ocean island samples with a high total percent probability of 79.6%, with the remaining probability of 20.4% for the collision setting.

4.2.5. Samples from a collision setting

For the evaluation of our diagrams (Figures 1–3) for the collision setting, Miocene ultrapotassic intermediate magmas from southern and southwestern Tibet, with 19 samples from Gao *et al.* (2007) and 35 from Zhao *et al.* (2009), clearly showed a collision setting in all 3 sets of diagrams. Most or all samples (52 to 54 out of 54 in the first set; Figures 4a and 4c–e; all 54 for the other 2 sets; Table S16) plotted in the collision field. When the collision field is absent in a diagram (Figure 4b; Table S16), the samples plotted in the within-plate field, except for the second set of diagrams (Figures 2a–2e; Table S16), in which some samples also plotted in the continental arc field. The total percent probability (% prob) values for the collision setting were therefore consistently high (78.8% to 84.1%; Table S16). Thus, all 3 sets of diagrams performed well for the collision tectonic setting.

4.2.6. Altered samples from the Central American Volcanic Arc

Seven samples of intermediate magma of corestone-shell complexes from Moyuta and Tecuamburro volcanoes of Guatemala (a part of the Central American Volcanic Arc; Patino *et al.* 2003) were used to evaluate the effects of spheroidal weathering in our multidimensional diagrams (Table S17). The samples from Tecuamburro are of Pliocene-Pleistocene age, whereas the age of the Moyuta samples may be Late Tertiary. A continental arc setting was still inferred for these highly altered rocks, because most of them (4 to 6 out of 7 samples; Figure 4; Table S17) plotted in the CA field. Although these authors did not report analyses of fresh rocks from these volcanoes, which might have helped to better understand the alteration effects in our multidimensional diagrams, we may hypothesize that these effects probably led some samples to plot in the collision field, with relatively high probabilities. Finally, from the total percent probability considerations, the samples showed 53.2% (% prob) total percent probability value for the continental arc setting, whereas the remaining probability (100 – 53.2 = 46.8%) was almost equally subdivided between the island arc and collision settings (23.7% and 23.1%, respectively; Table S17).

5. Application of discrimination diagrams to old terrains

We selected 7 case studies with ages varying from Archean to Phanerozoic to illustrate the application and excellent functioning of the multidimensional discrimination diagrams. The Archean to Proterozoic rocks were evaluated under the assumption of prevalence of plate tectonic processes and similar $\log_e$-ratio geochemical variables for Archean to present-day tectonic regimes. For these applications, the plotting of samples in diagrams (Figures 1–3) was replaced by probability calculations (Table S18).

5.1. Wawa greenstone belt (Canada)

For the Late Archean Wawa greenstone belt in Canada, the 3 sets of diagrams for intermediate magma (32 samples; 14 from Polat *et al.* 1999 and 18 from Polat 2009) could be applied. The results are summarized in Table S18. The first set based on major elements (Figure 1) provided indecisive results because the samples were divided between arc and collision settings. The total percent probability values for island arc and collision settings (39.8% and 41.8%, respectively; Table S18) were very similar. The other 2 sets of diagrams based on relatively immobile elements, however, showed an island arc setting for the samples from the Wawa greenstone belt. The total percent probability values for this tectonic field were about 54.5% and 58.3%, respectively, for the second (Figure 2) and third (Figure 3) sets of diagrams. Therefore, an island arc setting can be inferred for this belt. This application to the Wawa greenstone belt also implies that similar plate tectonic processes as today might have been operative during the Archean (at about 2700 Ma; Table S18).

5.2. Southwestern Sweden

From the first set of diagrams applied to 13 intermediate samples of Paleoproterozoic intrusive rocks (1870–1780 Ma) of south-central Sweden (Rutanen & Andersson 2009), an arc setting could be certainly inferred (Table S18), although the discrimination of an island or continental arc was not decisive. The total percent probability estimates for these 2 settings were very similar (42.6% and 42.2%, respectively, for island and continental arcs; Table S18). No trace element data were published for these rocks. It is likely that the immobile element-based second and third sets of diagrams might provide a decision of island or continental arc setting for this area.

5.3. Adola (Ethiopia)

Twelve Neoproterozoic (885–765 Ma) intermediate rock samples from Adola, southern Ethiopia (Wolde *et al.* 1996), with complete major element data showed an island arc setting, because 8 to 10 samples had the highest probability for this field and the total percent probability (% prob) was 57.2% (Table S18). Eight of these samples had complete data for immobile element-based diagrams (Figures 2 and 3). An arc setting can be certainly inferred from these diagrams, as well. However, the major and trace element-based diagrams (Figure 2) indicated a continental arc setting with 60.8% total percent probability, whereas the trace element-based ones (Figure 3) showed an island arc setting with 59.1% total percent probability (Table S18).

5.4. Malani igneous complex (India)

Twenty-one samples of Neoproterozoic intermediate magma from the Malani igneous complex, Rajasthan, India (Maheshwari *et al.* 1996; Bhushan & Chandrasekaran 2002; Sharma 2004; Singh & Vallinayagam 2004), showed a within-plate setting, because 16 to 18 samples were discriminated as this tectonic environment and the

respective total percent probability was about 69.9% (Table S18). Only 2 samples had complete major and trace element data for our second set of diagrams, which also indicated a within-plate setting (results of too few samples, only 2, are not included in Table S18).

5.5. Tasmania (Australia)

Thirty-nine samples of Cambrian intermediate magma from western Tasmania, Australia (Brown & Jenner 1989), with complete data for only major elements, were discriminated as an island arc setting, because most (33 to 38 out of 39) samples showed high probabilities for this field. Their total percent probability (% prob) value for an island arc setting was about 68.5% (Table S18).

5.6. The Alps (Europe)

Six samples of intermediate rocks of about 295 Ma from the Alps (France-Italy-Switzerland; Debon & Lemmet 1999) clearly showed a collision setting during the Late Carboniferous, because in the major element-based diagrams (Figure 1) all 6 samples plotted in this field with high probabilities (total percent probability of 83.1%; Table S18). This result was fully consistent with the other 2 sets of diagrams (Figures 2 and 3), in which all samples (5 out of 5 in Figure 2 and 6 out of 6 in Figure 3) plotted in the collision field (Table S18). The corresponding total percent probability values were very high (83.3% and 80.9%, respectively, for these 2 sets of diagrams based on immobile elements) for the Col setting.

5.7. Chichijima Island (Japan)

Finally, our last case study concerns the Bonin Archipelago, which represents an uplifted fore-arc area exposing the products of Eocene suprasubduction zone magmatism, with Chichijima Island being the type locality for boninite rocks (Taylor *et al.* 1994). An island arc setting was fully confirmed for the Chichijima Island during the Eocene, because all 35 intermediate rock samples plotted in the arc field with very high probabilities (0.6453–0.9998; Table S18). The total percent probability for the island arc field was also very high (77.3%; Table S18).

6. Evaluation of discrimination diagrams for element mobility and petrogenetic processes

We now briefly present the evaluation of our diagrams for compositional changes related to element mobility and petrogenetic processes of fractional crystallization (FC) and combined assimilation and fractional crystallization (AFC). Instead of plotting the data in diagrams (Figures 1–3), the probabilities for the 3 tectonic settings in a given diagram were calculated. The interpretation was based on these probability estimates.

6.1. Analytical errors, mobility of elements, and alteration effects

Extreme models of compositional changes were considered that may arise from analytical errors, mobility of elements caused by postemplacement processes such as weathering, Fe-oxidation, and low or even high temperature rock alteration. For simplicity and better understanding of the results, only changes (both gain and loss) of one element at a time were considered. From our 5-part database (see Tables S1 and S2), the mean compositions (centroid values) of compiled rocks for each tectonic setting were calculated and the models were evaluated for changes in these centroid compositions. For the first set of diagrams (Figure 1), these extreme models included ±10% changes for SiO_2; ±20% for TiO_2, Al_2O_3, Fe_2O_3, FeO, MgO, CaO, and P_2O_5; and ±40% for MnO, Na_2O, and K_2O. Similarly, for immobile element-based diagrams of the second and third sets (Figures 2 and 3), large gains or losses of ±20% were modeled for all corresponding major and trace elements. Greater than ±10% changes in SiO_2 were not considered realistic because the magma type may change to acid (from the gain of SiO_2) or basic (from the loss of SiO_2), which will render the present diagrams inapplicable to the modified or altered rocks. The results are summarized in Tables S19–S21 for the 3 sets of diagrams.

6.1.1. First set of diagrams

The first example of element mobility (SiO_2; Table S19) is described in detail. The probabilities for the expected tectonic field of the centroids (see the boldface probability values in the first row for the diagram type 1+2-3+4-5 in Table S19) for the IA discriminated as the combined arc (IA+CA) setting, the CA discriminated as IA+CA, the CR discriminated as within-plate, the OI discriminated as within-plate, and the Col discriminated as Col, were, respectively, 0.92046, 0.88378, 0.92458, 0.98888, and 0.94785. Although all centroids should plot well within the respective tectonic field (all probability values >> 0.5), the CA centroid (probability of 0.88378) would be somewhat closer to one of the tectonic field boundaries, whereas the OI centroid (probability of 0.98888) would be the much more inside the within-plate tectonic field, even more so than the CR centroid (probability of 0.92458) or the Col centroid (probability of 0.94785). For +10% change (gain) in SiO_2 (see the first value in all columns of the second row of Table S19), these probability values changed to about 0.8898, 0.8402, 0.8624, 0.9803, and 0.9710, respectively. Thus, the 10% increase in SiO_2 caused a probability change in the IA centroid of about (0.8898 – 0.92046) = –0.0306 (about –3.3%). For the other centroids, the probability changes were –0.0436 (–4.9%) for CA, –0.0622 (–6.7%) for CR, –0.0085 (–0.9%) for OI, and +0.0231 (+2.4%) for Col. All centroids remained within the original tectonic field, because the new probability values (range: 0.8402–0.9803; see the first value in each column of the second row of Table S19) for their respective fields were still very high (>>0.5). For 4 tectonic settings (IA, CA, CR, and OI) the centroid probability slightly decreased (by about

–0.0085 to –0.0622, amounting to about –0.9% to –6.7%). In other words, this SiO_2 mobility caused these centroids to move towards one of the boundaries (Figure 1a). For the Col setting, however, the centroid probability slightly increased from about 0.94785 to 0.9710 (about +0.0231; +2.4%), causing this centroid to plot still more inside this tectonic field.

Similarly, the –10% change (loss) in SiO_2 rendered the IA, CA, CR, OI, and Col centroid probabilities to become 0.9363, 0.9075, 0.9599, 0.9936, and 0.9005 (see the second value in each column of the second row of Table S19), i.e. the 10% decrease in SiO_2 caused probability changes of about +0.0158 (+1.7%), +0.0237 (+2.7%), +0.0353 (+3.8%), 0.0047 (+0.5%), and –0.0473 (–5.0%), respectively. These probability changes and the centroid movements are just in the opposite direction as compared to those for the SiO_2 gain, but the percent probability changes are not exactly the same. More importantly, for both SiO_2 gain as well as its loss, the centroids remained well within the respective tectonic fields and the percent probability changes (–6.7% to +3.8%) were much less than the changes of SiO_2 concentration (±10%).

For even larger changes in other major elements (±20% to ±40%; Table S19), none of the compositional changes caused any of the centroids in this first major element-based diagram (Figure 1a) to move outside the respective tectonic field. Therefore, we can safely conclude that the performance of this diagram (Figure 1a) is not seriously affected by element mobility from ±10% to ±40%. In other words, this diagram is particularly robust against such extreme concentration changes.

In the behavior of the second diagram of the first set (Figure 1b; see diagram type 1-2-3+4 in Table S19), in which both IA and CA fields are discriminated in the presence of the within-plate (CR+OI) field, the effects of compositional changes were less robust for these 2 very similar tectonic settings (IA and CA). The IA and CA centroids showed relatively low probabilities (0.61392 and 0.59320, respectively; see the second part of Table S19) and, consequently, would plot in Figure 1b closer to the tectonic field boundaries than the other 2 centroids (CR and OI, with probabilities of 0.95535 and 0.98472, respectively). The latter 2 centroid values obviously plotted well inside the within-plate field, away from the field boundaries (Figure 1b). The collision field is absent from this second diagram. The changes in SiO_2, TiO_2, Fe_2O_3, MgO, K_2O, and P_2O_5 were large, but did not cause any of the arc centroids to move outside their tectonic fields, whereas the changes modeled for the other elements (+20% for Al_2O_3, +40% for Na_2O, –40% for MnO, and –20% for CaO) led the IA centroid to move into the CA field (Table S19). Similarly, the CA centroid moved into the IA setting for +20% FeO, +40% MnO, +20% CaO, –20% Al_2O_3, and –40% Na_2O. For a given sample, however, there can be either a gain or a loss of an element. Therefore, misdiscrimination will occur only for a lower number of cases than those listed above. For example, if there were a gain of Al_2O_3 of about +20%, a sample from only the island arc setting is likely to be misdiscriminated in the continental arc setting, but not a sample from the continental arc setting; in fact, as a result of Al_2O_3 gain, this latter sample is likely to plot still more inside the continental arc field (the new probability value of 0.7344 is greater than the initial value of 0.59320 for the CA centroid; see Table S19). Nevertheless, because these 2 environments (IA and CA) are subduction-related settings, the misdiscrimination is not of too serious consequences. Note also that none of the compositional changes significantly affect the CR and OI centroids. All probability values remain consistently very high, 0.8115–0.9958; see the second part of Table S19.

In the third diagram of this set (Figure 1c; 1-2-5 type), the behavior of IA and CA was similar to the earlier diagram (Figure 1b), but for the Col setting, the discrimination results could be considered more robust against such compositional changes (Table S19). The misdiscrimination of the IA centroid as the CA setting was for Al_2O_3 gain (+20%), Na_2O gain (+40%), and MnO loss (–40%). Similarly, the CA centroid moved into the IA field for MnO gain (+40%), Al_2O_3 loss (–20%), and Na_2O loss (–40%). On the other hand, the Col centroid (Figure 1c) was little affected by any of the changes listed in Table S19; in all cases, it remained in the same tectonic field with high probability values of 0.7803–0.9949.

The fourth and fifth diagrams (Figures 1d and 1e; 1-3+4-5 and 2-3+4-5), in which both arc settings are not simultaneously present (Figure 1d has only IA whereas Figure 1e has only CA, along with the other 2 within-plate and Col settings), were observed to be totally immune to all the above-mentioned compositional changes. All centroids remained well within their respective fields and generally showed very high probability values (Table S19).

The major element-based diagrams perform well in spite of the large gains or losses modeled for any of these major elements. A possible explanation of such a good performance of our first set of diagrams may be related to the processing of the chemical data in SINCLAS and also the $\log_e$-ratio transformation that is involved in all of them; see Eqs. (1) through (10) above.

Simultaneous gains or losses of 2 or more elements will not really change our conclusions. In fact, because some $\log_e$-ratio terms in Eqs. (1) through (10) have positive signs, whereas the others have negative signs, simultaneous gains or losses of 2 elements may affect the final probability values even less; see Eqs. (31) through (39). For other cases, simultaneous gains and losses of 2 elements that appear in Eqs. (1) through (10) with the same sign may also keep the final probability changes to small values.

The simple oxidation process of FeO to Fe_2O_3, without any significant gain or loss of total Fe, will not affect our diagrams because all major element data are always readjusted from the SINCLAS computer program (Verma *et al.* 2002) to 100% on an anhydrous basis along with a prior adjustment of Fe_2O_3/FeO according to Middlemost's proposal (1989) for the least oxidized rock samples. The adjusted data should always be used for plotting the samples in Figures 1a–1e and calculating the respective probabilities in Eqs. (31) through (39).

6.1.2. Second and third sets of diagrams

Our results of element mobility in the remaining 2 sets of diagrams (Figures 2 and 3; Tables S20 and S21) are now briefly presented. Because both sets of diagrams are based on relatively immobile elements, the calculations for ±20% changes in the concentration of these elements probably represent extreme variations not likely to occur in most actual situations. The second set of diagrams based on 3 major and 5 trace elements was shown to be generally robust for all tectonic settings. The centroids remained in the expected field in practically all cases. The few exceptions were as follows (Table S20): MgO loss (–20%) caused the CR centroid to move to the Col setting in the first, fourth, and fifth diagrams (Figures 2a, 2d, and 2e); and P_2O_5 gain (+20%) and Y loss (–20%) caused the IA centroid to move to the within-plate (CR+OI) setting in the second and third diagrams (Figures 2b and 2c). However, the centroids remained rather close to the boundaries of the tectonic field to which they moved.

The third set of diagrams (Figures 3a–3e) based on immobile trace elements proved to be totally immune to these compositional changes (Table S21). The extremely large changes (gains or losses of ±20%) did not cause even a single centroid to move to a different tectonic field; all centroids remained well inside the original tectonic setting in all diagrams. Because concentration changes of only 1 element at a time were modeled, the probability values represent the highest changes compared to the simultaneous changes of 2 or more elements; see Eqs. (21) through (30) for DF1-DF2 functions and (31) through (39) for probability calculations. For example, because Yb was used as the common denominator, its gain or loss will affect most mathematical terms in Eqs. (21) through (30), and will probably cause more changes in the resulting probability values than the other elements. However, the probability changes caused by Yb gain or loss could be lower if other elements also changed simultaneously, which could be a more likely process to occur in nature. For the changes in other trace elements, the probability values of the IA, CA, CR, OI, and Col centroids (Figure 3a) changed respectively from 0.97541, 0.91223, 0.97804, 0.99661, and 0.98297 to about 0.9088–0.9899, 0.7884–0.9733, 0.9421–0.9933, 0.9908–0.9990, and 0.9523–0.9917. Similarly, small changes in probabilities were also observed in all other diagrams (Figures 3b–3e; Table S21).

The best performance of this set of diagrams as compared to the other 2 sets is an extremely important result of our modeling. This also implies that in case of inconsistency in the inferences of these 3 sets of diagrams for practical applications, this third set should be given more weight in decision making, i.e. in the case of inconsistent results, our decision can be based on this set of diagrams unless other independent geological, geochemical, or geophysical evidence were available to favor the results of other diagrams.

6.2. Petrogenetic process of bulk assimilation

Bulk assimilation of crust may be a petrogenetic process worth evaluating for its effects in our diagrams. For illustration purposes, we used the average upper continental crust (Taylor & McLennan 1995) and mixed 10% and 20% of this crust (UCC) with the centroids of our database. Still greater percentages of bulk assimilation were not modeled for 2 reasons: the magma type might change from intermediate to acid, in which case these diagrams should not be used; and the intermediate magma may not have a sufficient heat budget to assimilate greater proportions of crust. Other crustal compositions summarized by Taylor and McLennan 1995) could not be used because of the lack of P data for all of them.

In the first diagram (figure type 1+2-3+4-5; Table S22), UCC would plot well within the collision field (probability of 0.98306 for Col). From mixing of UCC, all centroids moved towards the boundary with the Col setting, but even with 20% UCC all of them remained in their respective fields (Table S22). As expected, the Col centroid showed only the smallest change in its probability. In the second diagram (figure type 1-2-3+4), UCC plotted in the within-plate field, whereas in all the remaining diagrams of this set, UCC plotted well within the Col setting. None of the centroids moved outside their fields in any of the major element-based diagrams (Table S22).

In the second set of diagrams, the results of bulk assimilation of UCC were practically similar, although for a few cases of 20% bulk assimilation the centroids moved to a different field. These include the following instances: the IA and CA moved to the Col setting in the first (figure type 1-2-3+4-5) and third (figure type 1-2-5) diagrams; the IA moved to Col in the fourth (figure type 1-3+4-5) diagram; and the CA moved to Col in the fifth (figure type 2-3+4-5) diagram.

In the third set of diagrams, the UCC plotted in the within-plate field except in diagram 1-2-5, where UCC plotted in the Col field. However, the centroids remained in their original fields (Table S22). Once again, this trace element-based diagram showed an excellent performance and robustness against the bulk assimilation process.

6.3. Petrogenetic process of fractional crystallization

Basic magma may undergo FC to produce intermediate magma. To model the effects of this process in our trace element-based diagrams (third set), the mean compositions of basic magma (see footnote of Table S23) from 3 tectonic settings (arc, continental rift, and ocean island) from the extensive database of Verma and Agrawal (2011) were estimated. For modeling the FC of common minerals (olivine, clinopyroxene [cpx], orthopyroxene [opx], and plagioclase [plg]), the partition coefficient data compiled by Torres-Alvarado *et al.* (2003) were used for extreme mineral fractionation of 50% (Table S23).

Verma and Agrawal (2011) had not made any distinction between island and continental arcs. The average composition (centroid) of arc basic rocks from their compilation plotted in the IA+CA field in diagram 1+2-3+4-5 (probability of 0.86271; Table S23); in the CA field in 1-2-3+4 (0.55888), 1-2-5 (0.48481) and 2-3+4-5 (0.88619) diagrams; and in the IA field in diagram 1-3+4-5 (0.80111). Similarly, the average composition of basic magma from the CR or OI setting plotted in the within-plate setting in all applicable diagrams (probability values of 0.97864–0.99620 for CR and 0.98237–0.99730 for OI). The initial probability for basic magma from the arc setting was distributed between the IA and CA settings in diagrams in which both IA and CA fields were present (0.42952 and 0.55888 in diagram 1-2-3+4, and 0.46586 and 0.48481 in diagram 1-2-5; Table S23).

The FC process generally did not drastically change the probability values for the basic magmas. For example, in the first diagram (1+2-3+4-5), the initial probability for the arc magma changed from 0.86271 to 0.8240, 0.5298, 0.9485, and 0.8598 for FC of olivine, cpx, opx, and plg, respectively. For the within-plate setting, the CR and OI basic magmas showed even much smaller changes. As an example, in the first diagram (1+2-3+4-5), the probability values for CR changed from 0.98273 to 0.9795–0.9847 and for OI from 0.98691 to 0.9845–0.9884.

In diagrams 1-2-3+4 and 1-2-5, in which both IA and CA settings are present as separate fields, the probabilities of arc basic magma after the FC process still showed that the evolved magma should plot in either of these 2 fields. For all basic magmas, thus, the evolved (probably intermediate) magmas obtained from the FC process remained within the expected field (Table S23). The only exception to this was in the fourth diagram (1-3+4-5) for the IA field, for which the evolved magma after 50% FC of cpx moved from the IA to Col setting (Table S23).

6.4. Petrogenetic process of assimilation coupled with fractional crystallization

The AFC process (DePaolo 1981) was also modeled for the basic magma compositions of the above section. More complex petrogenetic processes, such as those put forth by Spera and Bohrson (2004), were not considered because our aim was to understand the behavior of our complex diagrams for simple petrogenetic processes. Evaluation of more complex petrogenetic processes should constitute a separate study.

Two probably extreme models were considered and the results are presented in Table S24. The first model (r = 0.2 and F_{remain} = 0.7; Table S24) showed only a few cases in which the arc basic magma centroid moved to a different field. This took place for the arc centroid in diagram 1-3+4-5, where for the AFC process (A of UCC and FC of cpx) this centroid moved from the IA field to the collision setting, but only very close to the field boundary (the probabilities for IA and Col were about 0.4304 and 0.4355, respectively). For the second extreme model (r = 0.4 and F_{remain} = 0.5; Table S24), more cases of the arc centroid were misdiscriminated (Table S24). However, none of the 2 models affected the CR and OI centroids in any of the 5 diagrams. Nevertheless, the second AFC model should be considered as an extreme situation and less likely to occur in nature, because under such circumstances the evolved magma may even change to the acid type, rendering the present diagrams inapplicable to them.

7. Reasons for the good functioning of multidimensional diagrams

Why do the multidimensional diagrams based on LDA of $\log_e$-transformed ratios work so well? The high success rates documented above for all diagrams (Figures 1–3; Tables S5, S8, and S11); the excellent performance obtained for the 3 sets of diagrams from the testing examples (Figure 4; Tables S12–S17); the generally consistent inferences from the 7 application studies for Archean to Phanerozoic rocks (Table S18); and the overall best performance and minimal effects from compositional changes caused by analytical errors, element mobility, Fe-oxidation, and rock alteration (Tables S19–S21), as well as from bulk assimilation of crust (Table S22), fractional crystallization of common minerals (Table S23), and assimilation of upper crust coupled with fractional crystallization of common minerals (Table S24), are all worthy of mention. More important, however, would be the possible reasons for these favorable results.

There may be several reasons for such an excellent functioning of these diagrams. First, the basic condition of representativeness of the database is fulfilled when the samples from all over the world (Table S1) are compiled. All 5 tectonic groups are well chosen and represented (Table S2). Other reasons may be related to coherent statistical handling of compositional data (Verma 2012b; see also Aitchison 1986). Besides these reasons, the multivariate technique of LDA is centered around minimizing the effects of petrogenetic processes and maximizing the separation

among the different tectonic groups being discriminated (Verma 2012a). The complex multiplication factors with both positive and negative signs in Eqs. (1) through (30) may also be considered an asset rather than a disadvantage of these multidimensional diagrams. The probability-based boundaries further provide a better objective statistical method in comparison to the commonly used subjective method of determining the boundaries by eye judgment (Agrawal 1999; Agrawal & Verma 2007). Probability-based decisions in Eqs. (31) through (39) also constitute an important aspect of the new diagrams. The total percent probability calculations seem to provide an innovative way to interpret geochemical discrimination diagrams (Verma 2012a). Our interpretation in terms of these total percent probability estimates instead of simply counting the number of samples also seems helpful in this respect.

A computer program for efficiently processing the geochemical data for new applications is currently under preparation, which should be available in the future to potential users of our diagrams. In the meantime, we have developed a Statistica spreadsheet to facilitate such applications.

8. Conclusions

The 15 multidimensional diagrams with high success rates for intermediate magma, put forth in this work from correct statistical treatment of $\log_e$-ratio transformation, discordant outlier-free database, multivariate technique of LDA, probability-based boundaries, and associated sample probability and total percent probability calculations as a replacement for plotting samples, are shown to work well for relatively fresh to highly altered rocks of almost all ages from several areas around the world, and are therefore recommended to be used to decipher the tectonic settings of any area of interest. The robustness of all diagrams, especially those based on immobile trace elements, against the compositional changes from analytical errors and element mobility, as well as petrogenetic processes, is also well documented. This implies that these multidimensional diagrams can be safely used for deciphering the tectonic setting of old terrains as well as tectonically complex areas.

Acknowledgments

The second author (S.K.V.) thanks the Secretaría de Relaciones Exteriores (Mexico) for a doctoral fellowship. He is also grateful to the Fundação de Amparo à Pesquisa do Estado de São Paulo (FAPESP, Brazil) for his postdoctoral grant (2012/07243-3). This work was partly supported by DGAPA-UNAM PAPIIT project IN104813. We acknowledge Samuel Agostini for providing his compilation on Turkey to the first author, which was added to our database and updated in the present work. We also thank Mirna Guevara and Pandarinath Kailasa, both of whom participated during early stages of data compilation activity. We thank the editor, Dr Ercan Aldanmaz, and 2 anonymous reviewers for constructive comments to improve our paper

References

Agostini, S., Corti, G., Doglioni, C., Carminati, E., Innocenti, F., Tonarini, S., Manetti, P., Di Vincenzo, G. & Montanari, D. 2006. Tectonic and magmatic evolution of the active volcanic front in El Salvador: insight into the Berlín and Ahuachapán geothermal areas. *Geothermics* **35**, 368–408.

Agostini, S., Tokçaer, M. & Savaşçın, M.Y. 2010. Volcanic rocks from Foça-Karaburun and Ayvalik-Lesvos grabens (western Anatolia) and their petrogenetic-geodynamic significance. *Turkish Journal of Earth Sciences* **19**, 157–184.

Agrawal, S. 1999. Geochemical discrimination diagrams: a simple way of replacing eye-fitted boundaries with probability based classifier surfaces. *Journal of the Geological Society of India* **54**, 335–346.

Agrawal, S., Guevara, M. & Verma, S.P. 2004. Discriminant analysis applied to establish major-element field boundaries for tectonic varieties of basic rocks. *International Geology Review* **46**, 575–594.

Agrawal, S., Guevara, M. & Verma, S.P. 2008. Tectonic discrimination of basic and ultrabasic rocks through log-transformed ratios of immobile trace elements. *International Geology Review* **50**, 1057–1079.

Agrawal, S. & Verma, S.P. 2007. Comment on "Tectonic classification of basalts with classification trees" by Pieter Vermeesch (2006). *Geochimica et Cosmochimica Acta* **71**, 3388–3390.

Aitchison, J. 1986. *The Statistical Analysis of Compositional Data*. Chapman and Hall, London.

Alam, M.A., Chandrasekharam, D., Vaselli, O., Capaccioni, B., Manetti, P. & Santo, P.B. 2004. Petrology of the prehistoric lavas and dyke of the Barren island, Andaman sea, Indian ocean. *Proceedings of the Indian Academy of Sciences (Earth and Planetary Sciences)* **113**, 715–722.

Albarède, F., Luais, B., Fitton, G., Semet, M., Kaminski, E., Upton, B.G.J., Bachèlery, P. & Cheminée, J.L. 1997. The geochemical regimes of Piton de la Fournaise Volcano (Réunion) during the last 530 000 years. *Journal of Petrology* **38**, 171–201.

Albrecht, A. & Goldstein, S.L. 2000. Effects of basement composition and age on silicic magmas across an accreted terrane-Precambrian crust boundary, Sierra Madre Occidental, Mexico. *Journal of South American Earth Sciences* **13**, 255–273.

Aldanmaz, E., Pearce, J.A., Thirlwall, M.F. & Mitchell, J.G. 2000. Petrogenetic evolution of late Cenozoic, post-collision volcanism in western Anatolia, Turkey. *Journal of Volcanology and Geothermal Research* **102**, 67–95.

Alvarado, G.E., Soto, G.J., Schmincke, H.U., Bolge, L.L. & Sumita, M. 2006. The 1968 andesitic lateral blast eruption at Arenal volcano, Costa Rica. *Journal of Volcanology and Geothermal Research* **157**, 9–33.

Arnaud, N.O., Vidal, P., Tapponnier, P., Matte, P. & Deng, W.M. 1992. The high K20 volcanism of northwestern Tibet: geochemistry and tectonic implications. *Earth and Planetary Science Letters* **111**, 351–367.

Arpa, M.C.B., Patino, L.C. & Vogel, T.A. 2008. The basaltic to trachydacitic upper Diliman Tuff in Manila: Petrogenesis and comparison with deposits from Taal and Laguna Calderas. *Journal of Volcanology and Geothermal Research* **177**, 1020–1034.

Auchapt, A., Dupuy, C., Dostal, J. & Kanika, M. 1987. Geochemistry and petrogenesis of rift-related volcanic rocks from South Kivi (Zaire). *Journal of Volcanology and Geothermal Research* **31**, 33–46.

Ayalew, D., Ebinger, C., Bourdon, E., Wolfenden, E., Yirgu, G. & Grassineau, N. 2006. Temporal compositional variation of syn-rift rhyolites along the western margin of the southern Red Sea and northern Main Ethiopian Rift. *In:* Yirgu, G., Ebinger, C. & Maguire, P.K.H. (eds), *The Afar Volcanic Province within the East African Rift System*. Geological Society of London Special Publications, London, 121–130.

Aydar, E., Bayhan, H. & Gourgaud, A. 1998. Koroglu caldera, mid-west Anatolia, Turkey: volcanological and magmatological evolution. *Journal of Volcanology and Geothermal Research* **85**, 83–98.

Aydin, F., Karsli, O. & Chen, B. 2008. Petrogenesis of the Neogene alkaline volcanics with implications for post-collisional lithospheric thinning of the Eastern Pontides, NE Turkey. *Journal of Volcanology and Geothermal Research* **104**, 249–266.

Bachmann, O., Dungan, M.A. & Lipman, P.W. 2002. The Fish Canyon magma body, San Juan volcanic field, Colorado: rejuvenation and eruption of an upper-crustal batholith. *Journal of Petrology* **43**, 1469–1503.

Bailey, J.C. 1981. Geochemical criteria for a refined tectonic discrimination of orogenic andesites. *Chemical Geology* **32**, 139–154.

Ban, M., Hirotani, S., Wako, A., Suga, T., Iai, Y., Kagashima, S.I., Shuto, K. & Kagami, H. 2007. Origin of felsic magmas in a large-caldera-related stratovolcano in the central part of NE Japan — Petrogenesis of the Takamatsu volcano. *Journal of Volcanology and Geothermal Research* **167**, 100–118.

Barberi, F., Ferrara, G., Santacroce, R., Treuil, M. & Varet, J. 1975. A transitional basalt-pantellerite sequence of fractional crystallization, the Boina centre (Afar Rift, Ethiopia). *Journal of Petrology* **16**, 22–56.

Bardintzeff, J.M. & Deniel, C. 1992. Magmatic evolution of Pacaya and Cerro Chiquito volcanological complex, Guatemala. *Bulletin of Volcanology* **54**, 267–283.

Barling, J., Goldstein, S.L. & Nicholls, I.A. 1994. Geochemistry of Heard Island (Southern Indian Ocean): characterization of an enriched mantle component and implication for enrichment of the sub-Indian ocean mantle. *Journal of Petrology* **35**, 1017–1053.

Barnett, V. & Lewis, T. 1994. *Outliers in Statistical Data*. 3rd ed. John Wiley & Sons, Chichester.

Barsdell, M. 1988. Petrology and petrogenesis of clinopyroxene-rich tholeiitic lavas, Merelava volcano, Vanuatu. *Journal of Petrology* **29**, 927–964.

Barsdell, M. & Berry, R.F. 1990. Origin and evolution of primitive island arc ankaramites from western Epi, Vanuatu. *Journal of Petrology* **31**, 747–777.

Basu, A.R., Junwen, W., Wankang, H., Guanghong, X. & Tatsumoto, M. 1991. Major element, REE, and Pb, Nd and Sr isotopic geochemistry of Cenozoic volcanic rocks of eastern China: implications for their origin from suboceanic-type mantle reservoirs. *Earth and Planetary Science Letters* **105**, 149–169.

Bau, M. & Knittel, U. 1993. Significance of slab-derived partial melts and aqueous fluids for the genesis of tholeiitic and calc-alkaline island-arc basalts: evidence from Mt. Arayat, Philippines. *Chemical Geology* **105**, 233–251.

Beier, C., Haase, K.M. & Hansteen, T.H. 2006. Magma evolution of the Sete Cidades volcano, São Miguel, Azores. *Journal of Petrology* **47**, 1375–1411.

Bell, K. & Peterson, T. 1991. Nd and Sr isotopic systematics of Shombole volcano, East Africa, and the links between nephelinites, phonolites, and carbonatites. *Geology* **19**, 582–585.

Bellieni, G., Peccerillo, A. & Poli, G. 1981. The Vedrette di Ries (Rieserferner) plutonic complex: petrological and geochemical data bearing on its genesis. *Contributions to Mineralogy and Petrology* **78**, 145–156.

Bertrand, H. 1991. The Mesozoic tholeiitic province of northwest Africa: a volcano-tectonic record of the early opening of Central Atlantic. *In:* Kampunzu, A.B. & Lubala, R.T. (eds), *Magmatism in Extensional Structural Settings*. Springer Verlag, Berlin, 147–188.

Besang, C., Harre, W., Kreuzer, H., Lenz, H., Müller, P. & Wendt, I. 1977. Radiometrische datierung, geochemische und petrographische untersuchungen der fichtelgebirgsgranite. *Geologisches Jahrbuch* **8**, 3–71.

Bhushan, S.K. & Chandrasekaran, V. 2002. Geology and geochemistry of the magmatic rocks of the Malani igneous suite and Tertiary volcanic province of western Rajasthan. *Memoirs of the Geological Survey of India* **126**, 1–129.

Bloomer, S.H. 1987. Geochemical characteristics of boninite- and tholeiite-series volcanic rocks from the Mariana forearc and the role of an incompatible element enriched fluid in arc petrogenesis. *Geological Society of America Special Paper* **215**, 151–164.

Bloomer, S.H. & Hawkins, J.W. 1987. Petrology and geochemistry of boninite series volcanic rocks from the Mariana trench. *Contributions to Mineralogy and Petrology* **97**, 361–377.

Bloomer, S.H., Stern, R.J., Fisk, E. & Geschwind, C.H. 1989. Shoshonitic volcanism in the northern Mariana arc: 1. Mineralogic and major and trace element characteristics. *Journal of Geophysical Research* **94**, 4469–4496.

Blum, N., Halbach, P. & Münch, U. 1996. Geochemistry and mineralogy of alkali basalts from Tropic Seamount, central Atlantic Ocean. *Marine Geology* **136**, 1–19.

Bohrson, W.A. & Reid, M.R. 1995. Petrogenesis of alkaline basalts from Socorro Island, Mexico: trace element evidence for contamination of ocean island basalt in the shallow ocean crust. *Journal of Petrology* **100**, 24555–24576.

Bohrson, W.A. & Reid, M.R. 1997. Genesis of silicic peralkaline volcanic rocks in an ocean island setting by crustal melting and open-system processes: Socorro Island, Mexico. *Journal of Petrology* **38**, 1137–1166.

Bolge, L.L., Carr, M.J., Feigenson, M.D. & Alvarado, G.E. 2006. Geochemical stratigraphy and magmatic evolution at Arenal volcano, Costa Rica. *Journal of Volcanology and Geothermal Research* **157**, 34–48.

Booden, M.A., Smith, I.E.M., Black, P.M. & Mauk, J.L. 2011. Geochemistry of the Early Miocene volcanic succession of Northland, New Zealand, and implications for the evolution of subduction in the Southwest Pacific. *Journal of Volcanology and Geothermal Research* **199**, 25–37.

Borsi, S., Ferrara, G., Innocenti, F. & Mazzuoli, R. 1972. Geochronology and petrology of recent volcanics in the eastern Aegean Sea (West Anatolia and Lesvos Island. *Bulletin of Volcanology* **36**, 473–496.

Brophy, J.G. 1986. The Cold Bay volcanic center, Aleutian volcanic arc. I. Implications for the origin of hi-alumina arc basalt. *Contributions to Mineralogy and Petrology* **93**, 368–380.

Brown, A.V. & Jenner, G.A. 1989. Geological setting, petrology and chemistry of Cambrian boninite and low-Ti tholeiite lavas in western Tasmania. *In:* Crawford, A.J. (ed), *Boninites*. Unwin Hyman, London, 233–263.

Brown, G.M., Holland, J.G., Sigurdsson, H., Tomblin, J.F. & Arculus, R.J. 1977. Geochemistry of the Lesser Antilles volcanic island arc. *Geochimica et Cosmochimica Acta* **41**, 785–801.

Brueseke, M.E. & Hart, W.K. 2009. Intermediate composition magma production in an intracontinental setting: unusual andesites and dacites of the mid-Miocene Santa Rosa–Calico volcanic field, Northern Nevada. *Journal of Volcanology and Geothermal Research* **188**, 197–213.

Bruni, S., D'Orazio, M., Haller, M.J., Innocenti, F., Manetti, P., Pécskay, Z. & Tonarini, S. 2008. Time-evolution of magma sources in a continental back-arc setting: the Cenozoic basalts from Sierra de San Bernardo (Patagonia, Chubut, Argentina). *Geological Magazine* **145**, 714–732.

Bryan, S.E. 2006. Petrology and geochemistry of the Quaternary Caldera-forming, Phonolitic granadilla eruption, Tenerife (Canary Islands). *Journal of Petrology* **47**, 1557–1589.

Bryan, W.B., Stice, G.D. & Ewart, A. 1972. Geology petrography, and geochemistry of the volcanic islands of Tonga. *Journal of Geophysical Research* **77**, 1566–1585.

Bryant, J.A., Yogodzinski, G.M., Hall, M.L., Lewicki, J.L. & Bailey, D.G. 2006. Geochemical constraints on the origin of volcanic rocks from the Andean Northern volcanic zone, Ecuador. *Journal of Petrology* **47**, 1147–1175.

Cadoux, A. & Pinti, D.L. 2009. Hybrid character and pre-eruptive events of Mt Amiata volcano (Italy) inferred from geochronological petro-geochemical and isotopic data. *Journal of Volcanology and Geothermal Research* **179**, 169–190.

Cameron, B.I., Walker, J.A., Carr, M.J., Patino, L.C., Matías, O. & Feigenson, M.D. 2002. Flux versus decompression melting at stratovolcanoes in southeastern Guatemala. *Journal of Volcanology and Geothermal Research* **119**, 21–50.

Cameron, W.E. 1989. Contrasting boninite-tholeiite association from New Caledonia. *In:* Crawford, A.J. (ed), *Boninites*. Unwin Hyman, London, 314–338.

Camp, V.E., Roobol, M.J. & Hooper, P.R. 1991. The Arabian continental alkali basalt province: part II. Evolution of Harrats Khaybar, Ithnayn, and Kura, Kingdom of Saudi Arabia. *Geological Society of America Bulletin* **103**, 363–391.

Carr, M.J. 1984. Symmetrical and segmented variation of physical and geochemical characteristics of the Central American volcanic front. *Journal of Volcanology and Geothermal Research* **20**, 231–252.

Carr, M.J., Feigenson, M.D. & Bennett, E.A. 1990. Incompatible element and isotopic evidence for tectonic control of source mixing and melt extraction along the Central American arc. *Contributions to Mineralogy and Petrology* **105**, 369–380.

Castillo, P.R. & Newhall, C.G. 2004. Geochemical constraints on possible subduction components in lavas of Mayon and Taal volcanoes, southern Luzon, Philippines. *Journal of Petrology* **45**, 1089–1108.

Chadwick, J., Perfit, M., McInne, B., Kamenov, G. & Plank, T. 2009. Arc lavas on both sides of a trench: Slab window effects at the Solomon Islands triple junction, SW Pacific. *Earth and Planetary Science Letters* **279**, 293–302.

Chadwick, J.P., Troll, V.R., Ginibre, R.G., Morgan, D., Gertisser, R., Waight, T.E. & Davidson, J.P. 2007. Carbonate assimilation at Merapi Volcano, Java, Indonesia: insights from crystal isotope stratigraphy. *Journal of Petrology* **48**, 1793–1812.

Chan, L.H., Leeman, W.P. & You, C.F. 1999. Lithium isotopic composition of Central American Volcanic Arc lavas: implications for modification of subarc mantle by slab-derived fluids. *Chemical Geology* **160**, 255–280.

Chauvel, C. & Jahn, B.M. 1984. Nd-Sr isotope and REE geochemistry of alkali basalts from the Massif Central, France. *Geochimica et Cosmochimica Acta* **48**, 93–110.

Chen, J.L., Xu, J.F., Wang, B.D., Kang, Z.Q. & Jie, L. 2010. Origin of Cenozoic alkaline potassic volcanic rocks at KonglongXiang, Lhasa terrane, Tibetan Plateau: Products of partial melting of a mafic lower-crustal source? *Chemical Geology* **273**, 286–299.

Chung, S.L., Jahn, B.M., Chen, S.J., Lee, T. & Chen, C.H. 1995. Miocene basalts in northwestern Taiwan: evidence for EM-type mantle sources in the continental lithosphere. *Geochimica et Cosmochimica Acta* **59**, 549–555.

Churikova, T., Dorendorf, F. & Wörner, G. 2001. Sources and fluids in the mantle wedge below Kamchatka, evidence from across-arc geochemical variation. *Journal of Petrology* **42**, 1567–1593.

Cole, J.W. 1981. Genesis of lavas of the Taupo volcanic zone, North Island, New Zealand. *Journal of Volcanology and Geothermal Research* **10**, 317–337.

Cousens, B.L., Clague A.D. & Sharp, W.D. 2003. Chronology, chemistry, and origin of trachytes from Hualalai Volcano, Hawaii. *Geochemistry Geophysics Geosystems* **4**, 1078, doi: 1010.1029/2003GC000560.

Davidson, J.P., Ferguson, K.M., Colucci, M.T. & Dungan, M.A. 1988. The origin and evolution of magmas from the San Pedro-Pellado volcanic complex, S. Chile: multicomponent sources and open system evolution. *Contributions of Mineralogy and Petrology* **100**, 429–445.

Davidson, J.P. & Wilson, I.R. 1989. Evolution of an alkali basalt-trachyte suite from Jebel Marra volcano, Sudan, through assimilation and fractional crystallization. *Earth and Planetary Science Letters* **95**, 141–160.

Day, J.M.D., Pearson, D.G., Macpherson, C.G., Lowry, D. & Carracedo, J.C. 2010. Evidence for distinct proportions of subducted oceanic crust and lithosphere in HIMU-type mantle beneath El Hierro and La Palma, Canary Islands. *Geochimica et Cosmochimica Acta* **74**, 6565–6589.

De Mulder, M., Hertogen, J., Deutsch, S. & André, L. 1986. The role of crustal contamination in the potassic suite of the Karisimbi volcano (Virunga, African Rift Valley. *Chemical Geology* **57**, 117–136.

de Silva, S.L. 1991. Styles of zoning in central Andean ignimbrites: insights into magma chamber processes. *Geological Society of America Special Paper* **265**, 217–232.

Debon, F. & Lemmet, M. 1999. Evolution of Mg/Fe ratios in Late Variscan plutonic rocks from the external crystalline massifs of the Alps (France, Italy, Switzerland). *Journal of Petrology* **40**, 1151–1185.

Defant, M.J., Clark, L.F., Stewart, R.H., Drummond, M.S., De Boer, J.Z., Maury, R.C., Bellon, H., Jackson, T.E. & Restrepo, J.F. 1991a. Andesite and dacite genesis via contrasting processes: the geology and geochemistry of El Valle Volcano, Panama. *Contributions to Mineralogy and Petrology* **106**, 309–324.

Defant, M.J., Jacques, D., Maury, R.C., De Boer, J. & Joron, J.L. 1989. Geochemistry and tectonic setting of the Luzon arc, Philippines. *Geological Society of America Bulletin* **101**, 663–672.

Defant, M.J., Maury, R.C., Ripley, E.M., Feigenson, M.D. & Jacques, D. 1991b. An example of island-arc petrogenesis: geochemistry and petrology of the southern Luzon arc, Philippines. *Journal of Petrology* **32**, 455–500.

Defant, M.J., Richerson, P.M., De Boer, J.Z., Stewart, R.H., Maury, R.C., Bellon, H., Drummond, M.S., Feigenson, M.D. & Jackson, T.E. 1991c. Dacite genesis via both slab melting and differentiation: petrogenesis of La Yeguada volcanic complex, Panama. *Journal of Petrology* **32**, 1101–1142.

Defant, M.J., Sherman, S., Maury, R.C., Bellon, H., de Boer, J., Davidson, J. & Kepezhinskas, P. 2001. The geology, petrology, and petrogenesis of Saba Island, Lesser Antilles. *Journal of Volcanology and Geothermal Research* **107**, 87–111.

Delaloye, M. & Bingol, E. 2000. Granitoids from western and northwestern Anatolia: geochemistry and modeling of geodynamic evolution. *International Geology Review* **42**, 241–268.

Deniel, C., Vidal, P., Coulon, C., Vellutini, P. & Piguet, P. 1994. Temporal evolution of mantle sources during continental rifting: the volcanism of Djibouti (Afar). *Journal of Geophysical Research* **99**, 2853–2869.

DePaolo, D.J. 1981. Trace element and isotopic effects of combined wallrock assimilation and fractional crystallization. *Earth and Planetary Science Letters* **53**, 189–202.

Déruelle, B. 1982. Petrology of the Plio-Quaternary volcanism of the south-central and meridional Andes. *Journal of Volcanology and Geothermal Research* **14**, 77–124.

Dilek, Y., Imamverdiyev, N. & Altunkaynak, S. 2010. Geochemistry and tectonics of Cenozoic volcanism in the Lesser Caucasus (Azerbaijan) and the peri-Arabian region: collision-induced mantle dynamics and its magmatic fingerprint. *International Geology Review* **52**, 536–578.

Dini, A., Innocenti, F., Rocchi, S., Tonarini, S. & Westerman, D.S. 2002. The magmatic evolution of the late Miocene laccolith-pluton-dyke granitic complex of Elba Island, Italy. *Geological Magazine* **139**, 257–279.

Dorendorf, F., Churikova, T., Koloskov, A. & Wörner, G. 2000. Late Pleistocene to Holocene activity at Bakening volcano and surrounding monogenetic centers (Kamchatka): volcanic geology and geochemical evolution. *Journal of Volcanology and Geothermal Research* **104**, 131–151.

Duffield, W.A., Heiken, G.H., Wohletz, K.H., Maassen, L.W., Dengo, G., McKee, E.H. & Castañeda, O. 1992. Geology and geothermal potential of the Tecuamburro volcano area, Guatemala. *Geothemics* **21**, 425–446.

DuFrane, S.A., Asmerom, Y., Mukasa, S.B., Morris, J.D. & Dreyer, B.M. 2006. Subduction and melting processes inferred from U-series, Sr-Nd-Pb isotope, and trace element data, Bicol and Bataan arcs, Philippines. *Geochimica et Cosmochimica Acta* **70**, 3401–3420.

Duncker, K.E., Wolff, J.A., Harmon, R.S., Leat, P.T., Dickin, A.P. & Thompson, R.N. 1991. Diverse mantle and crustal components in lavas of the NW Cerros del Rio volcanic field, Rio Grande Rift, New Mexico. *Contributions to Mineralogy and Petrology* **108**, 331–345.

Dupuy, C., Dostal, J., Marcelot, G., Bougault, H., Joron, J.L. & Treuil, M. 1982. Geochemistry of basalts from central and southern New Hebrides arc: implication for their source rock composition. *Earth and Planetary Science Letters* **60**, 207–225.

Edwards, C.M.H., Menzies, M.A., Thirlwall, M.F., Morris, J.D., Leeman, W.P. & Harmon, R.S. 1994. The transition to potassic alkaline volcanism in island arcs: the Ringgit-Beser complex, east Java, Indonesia. *Journal of Petrology* **35**, 1557–1595.

Ekici, T., Alpaslan, M., Parlak, O. & Uçurum, A. 2009. Geochemistry of Middle Miocene collision-related Yamadağı (Eastern Anatolia) calc-alkaline volcanics, Turkey. *Turkish Journal of Earth Sciences* **18**, 511–528.

Elburg, M. & Foden, J. 1998. Temporal changes in arc magma geochemistry, northern Sulawesi, Indonesia. *Earth and Planetary Science Letters* **163**, 381–398.

Elburg, M. & Foden, J. 1999. Sources for magmatism in central Sulawesi: geochemical and Sr-Nd-Pb isotopic constraints. *Chemical Geology* **156**, 67–93.

Elburg, M.A., van Leeuwen, T., Foden, J. & Muhardjo. 2003. Spatial and temporal isotopic domains of contrasting igneous suites in Western and Northern Sulawesi, Indonesia. *Chemical Geology* **199**, 243–276.

Elliott, T., Plank, T., Zindler, A., White, W.M. & Bourdon, B. 1997. Element transport from slab to volcanic front at the Mariana arc. *Journal of Geophysical Research* **102**, 14991–15019.

Ercan, T., Dinçel, A. & Günay, E. 1979. Uşak volkanitlerinin petrolojisi ve plaka tektoniği açısından Ege Bölgesindeki yeri [Petrology of the Uşak volcanics and their place in the Aegean region according to plate tectonics]. *Türkiye Jeoloji Kurumu Bülteni* **22**, 185–198 (in Turkish with English abstract).

Ercan, T., Satır, M., Kreuzer, H., Türkecan, A., Günay, E., Çevikbaş, A., Ates, M. & Can, B. 1985. Batı Anadolu Senozoyik volkanitlerine ait yeni kimyasal, izotopik ve radyometrik verilerin yorumu [Interpretation of new chemical, isotopic and radiometric data on Cenozoic volcanics of western Anatolia]. *Türkiye Jeoloji Kurumu Bülteni* **28**, 121–136 [in Turkish with English abstract].

Ercan, T., Satır, M., Sevin, D. & Türkecan, A. 1997. Some new radiometric ages from Tertiary to Quaternary volcanic rocks from W. Anatolia (Turkey). *Maden Tetkik Arama Dergisi* **119**, 66.

Ertürk, O. 1990. *Petrology of the Cenozoic volcanics in the Biga Peninsula, NW Turkey*. PhD, Ankara University, Ankara.

Esder, T. 1992. The geology and petrology of the Neogene aged volcanic rocks of Aliağa (İzmir) area. *First International Symposium on Eastern Mediterranean Geology*, Adana, Turkey.

Ewart, A., Brothers, R.N. & Mateen, A. 1977. An outline of the geology and geochemistry, and the possible petrogenetic evolution of the volcanic rocks of the Tonga-Kermadec-New Zealand island arc. *Journal of Volcanology and Geothermal Research* **2**, 205–270.

Ewart, A. & Bryan, W.B. 1972. Petrography and geochemistry of the igneous rocks from EUA, Tongan islands. *Geological Society of America Bulletin* **83**, 3281–3298.

Fan, Q. & Hooper, P.R. 1991. The Cenozoic basaltic rocks of eastern China: petrology and chemical composition. *Journal of Petrology* **32**, 765–810.

Feigenson, M.D., Hofmann, A.W. & Spera, F.J. 1983. Case studies on the origin of basalt. II. The transition from tholeiitic to alkalic volcanism on Kohala volcano, Hawaii. *Contributions to Mineralogy and Petrology* **84**, 390–405.

Feuerbach, D.L., Smith, E.I., Walker, J.D. & Tangeman, J.A. 1993. The role of the mantle during crustal extension: constraints from geochemistry of volcanic rocks in the Lake Mead area, Nevada and Arizona. *Geological Society of America Bulletin* **105**, 1561–1575.

Fitton, J.G., James, D. & Leeman, W.P. 1991. Basic magmatism associated with Late Cenozoic extension in the western United States: compositional variations in space and time. *Journal of Geophysical Research* **96**, 13693–13711.

Foden, J.D. & Varne, R. 1980. The petrology and tectonic setting of Quaternary-Recent volcanic centres of Lombok and Sumbawa, Sunda arc. *Chemical Geology* **30**, 201–226.

Fontijn, K., Ernst, G.G.J., Elburg, M.A., Williamson, D., Abdallah, E., Kwelwa, S., Mbede, E. & Jacobs, P. 2010. Holocene explosive eruptions in the Rungwe Volcanic Province, Tanzania. *Journal of Volcanology and Geothermal Research* **196**, 91–110.

Frey, F.A., Garcia, M.O. & Roden, M.F. 1994. Geochemical characteristics of Koolau volcano: implications of intershield geochemical differences among Hawaiian volcanoes. *Geochimica et Cosmochimica Acta* **58**, 1441–1462.

Frey, F.A., Gerlach, D.C., Hickey, R.L., Lopez-Escobar, L. & Munizaga-Villavicencio, F. 1984. Petrogenesis of the Laguna del Maule volcanic complex, Chile. *Contributions to Mineralogy and Petrology* **88**, 133–149.

Frey, H.M., Lange, R.A., Hall, C.M., Delgado-Granados, H. & Carmichael, I.S.E. 2007. A Pliocene ignimbrite flare-up along the Tepic-Zacoalco rift: evidence for the initial stages of rifting between the Jalisco block (Mexico) and North America. *Geological Society of America Bulletin* **119**, 49–64.

Gamble, J.A., Smith, I.E.M., McCulloch, M.T., Graham, I.J. & Kokelaar, B.P. 1993. The geochemistry and petrogenesis of basalts from the Taupo volcanic zone and Kermadec Island arc, S.W. Pacific. *Journal of Volcanology and Geothermal Research* **54**, 265–290.

Gamble, J.A., Wright, I.C., Woodhead, J.D. & McCulloch, M.T. 1995. Arc and back-arc geochemistry in the southern Kermadec arc-Ngatoro basin and offshore Taupo volcanic zone, SW Pacific. *In:* Smellie, J.L. (ed), *Volcanism Associated with Extension at Consuming Plate Margins*. Geological Society Special Publication, London, 193–212.

Gao, Y., Hou, Z., Kamber, B.S., Wei, R., Meng, X. & Zhao, R. 2007. Lamproitic rocks from a continental collision zone: evidence for recycling of subducted Tethyan oceanic sediments in the mantle beneath southern Tibet. *Journal of Petrology* **48**, 729–752.

Geldmacher, J. & Hoernle, K. 2000. The 72 Ma geochemical evolution of the Medeira hotspot (eastern North Atlantic): recycling of Paleozoic (≤500 Ma) oceanic lithosphere. *Earth and Planetary Science Letters* **183**, 73–92.

Gerlach, D.C., Frey, F.A., Moreno-Roa, H. & Lopez-Escobar, L. 1988. Recent volcanism in the Puyehue-Cordon Caulle region, southern Andes, Chile (40.5°S): petrogenesis of evolved lavas. *Journal of Petrology* **29**, 333–382.

Gibson, S.A., Thompson, R.N., Leat, P.T., Dickin, A.P., Morrison, M.A., Hendry, G.L. & Mitchell, J.G. 1992. Asthenosphere-derived magmatism in the Rio Grande rift, western USA: implications for continental break-up. *In:* Storey, B.C., Alabaster, T. & Pankhurst, R.J. (eds), *Magmatism and the Causes of Continental Break-Up*. Geological Society Special Publication, London, 61–89.

González Partida, E., Torres Rodriguez, V. & Birkle, P. 1997. Plio-Pleistocene volcanic history of the Ahuachapan geothermal system, El Salvador: the Concepción de Ataco caldera. *Geothermics* **26**, 555–575.

Güleç, N. 1991. Crust-mantle interaction in western Turkey: implications from Sr and Nd isotope geochemistry of Tertiary and Quaternary volcanics. *Geological Magazine* **128**, 417–435.

Haase, K.M., Goldschmidt, B. & Garbe-Schönberg, C.D. 2004. Petrogenesis of Tertiary continental intra-plate lavas from the Westerwald region, Germany. *Journal of Petrology* **45**, 883–905.

Haase, K.M., Worthington, T.J., Stoffers, P., Garbe-Schönberg, D. & Wright, I. 2002. Mantle dynamics, element recycling, and magma genesis beneath the Kermadec arc-Havre Trough. *Geochemistry Geophysics Geosystems* **3**, 1071, doi: 1010.1029/2002GC00035.

Halama, R., Boudon, G., Villemant, B., Joron, J.L., Le Friant, A. & Komorowski, J.C. 2006. Pre-eruptive crystallization conditions of mafic and silicic magmas at the Plat Pays volcanic complex, Dominica (Lesser Antilles). *Journal of Volcanology and Geothermal Research* **153**, 200–220.

Han, B.F., Wang, S.G. & Kagami, H. 1999. Trace element and Nd-Sr isotope constraints on origin of the Chifeng flood basalts, North China. *Chemical Geology* **155**, 187–199.

Handley, H.K., Macpherson, C.G., Davidson, J.P., Berlo, K. & Lowry, D. 2007. Constraining fluid and sediment contributions to subduction-related magmatism in Indonesia: Ijen Volcanic Complex. *Journal of Petrology* **48**, 1155–1183.

Hart, W.K., WoldeGabriel, G., Walter, R.C. & Mertzman, S.A. 1989. Basaltic volcanism in Ethiopia: constraints on continental rifting and mantle interactions. *Journal of Geophysical Research* **94**, 7731–7748.

Hazlett, R.W. 1987. Geology of San Cristobal volcanic complex, Nicaragua. *Journal of Volcanology and Geothermal Research* **33**, 223–230.

Hekinian, R., Cheminée, J.L., Dubois, J., Stoffers, P., Scott, S., Guivel, C., Garbe-Schönberg, D., Devey, C., Bourdon, B., Lackschewitz, K., McMurtry, G. & Le Drezen, E. 2003. The Pitcairn hotspot in the South Pacific: distribution and composition of submarine volcanic sequences. *Journal of Volcanology and Geothermal Research* **121**, 219–245.

Hergt, J.M. & Woodhead, J.D. 2007. A critical evaluation of recent models for Lau–Tonga arc–backarc basin magmatic evolution. *Chemical Geology* **245**, 9–44.

Hickey, R.L. & Frey, F.A. 1982. Geochemical characteristics of boninite series volcanics: implications for their source. *Geochimica et Cosmochimica Acta* **46**, 2099–2115.

Hickey, R.L., Frey, F.A., Gerlach, D.C. & Lopez-Escobar, L. 1986. Multiple sources for basaltic arc rocks from the southern volcanic zone of the Andes (34°-41°S): trace element and isotopic evidence for contributions from subducted oceanic crust, mantle, and continental crust. *Journal of Geophysical Research* **91**, 5963–5983.

Hickey-Vargas, R., Moreno Roa, H., Lopez Escobar, L. & Frey, F.A. 1989. Geochemical variations in Andean basaltic and silicic lavas from the Villarrica-Lanin volcanic chain (39.5°S): an evaluation of source heterogeneity, fractional crystallization and crustal assimilation. *Contributions to Mineralogy and Petrology* **103**, 361–386.

Hidalgo, S., Monzier, M., Martin, H., Chazot, G., Eissen, J.P. & Cotten, J. 2007. Adakitic magmas in the Ecuadorian volcanic front: petrogenesis of the Iliniza volcanic complex (Ecuador). *Journal of Volcanology and Geothermal Research* **159**, 366–392.

Hildreth, W., Fierstein, J., Siems, D.F., Budahn, J.R. & Ruíz, J. 2004. Rear-arc vs. arc-front volcanoes in the Katmai reach of the Alaska peninsula: a critical appraisal of across-arc compositional variation. *Contributions to Mineralogy and Petrology* **147**, 243–275.

Hirotani, S. & Ban, M. 2006. Origin of silicic magma and magma feeding system of the Shirataka volcano, NE Japan. *Journal of Volcanology and Geothermal Research* **156**, 229–251.

Ho, K.S., Chen, J.C. & Juang, W.S. 2000. Geochronology and geochemistry of late Cenozoic basalts from Leiqiong area, southern China. *Journal of Asian Earth Sciences* **18**, 307–324.

Hoang, N., Itoh, J.I. & Miyagi, I. 2011. Subduction components in Pleistocene to recent Kurile arc magmas in NE Hokkaido, Japan. *Journal of Volcanology and Geothermal Research* **200**, 255–266.

Hole, M.J., Saunders, A.D., Marriner, G.F. & Tarney, J. 1984. Subduction of pelagic sediments: implications for the origin of Ce-Anomalous basalts from the Marianas Islands. *Journal of the Geological Society of London,* **141**, 453–472.

Holm, P.M., Wilson, J.R., Christensen, B.P., Hansen, L., Hansen, S.L., Hein, K.M., Mortensen, A.K., Pedersen, R., Plesner, S. & Runge, M.K. 2006. Sampling the Cape Verde mantle plume: evolution of melt compositions on Santo Antão, Cape Verde Islands. *Journal of Petrology* **47**, 145–189.

Hoogewerff, J.A., van Bergen, M.J., Vroon, P.Z., Hertogen, J., Wordel, R., Sneyers, A., Nasution, A., Varekamp, J.C., Moens, H.L.E. & Mouchel, D. 1997. U-series, Sr-Nd-Pb isotope and trace-element systematics across an active island arc-continent collision zone: implications for element transfer at the slab-wedge interface. *Geochimica et Cosmochimica Acta* **61**, 1057–1072.

Hsu, C.N., Chen, J.C. & Ho, K.S. 2000. Geochemistry of Cenozoic volcanic rocks from Kirin Province, northeast China. *Geochemical Journal* **34**, 33–58.

Huang, Y., Hawkesworth, C., Smith, I., van Calsteren, P. & Black, P. 2000. Geochemistry of late Cenozoic basaltic volcanism in Northland and Coromandel, New Zealand: implications for mantle enrichment processes. *Chemical Geology* **164**, 219–238.

Huijsmans, J.P.P., Barton, M. & Salters, V.J.M. 1988. Geochemistry and evolution of the calc-alkaline volcanic complex of Santorini, Aegean Sea, Greece. *Journal of Volcanology and Geothermal Research* **34**, 283–306.

Ilbeyli, N., Pearce, J.A., Thirlwall, M.F. & Mitchell, J.G. 2004. Petrogenesis of collision-related plutonics in Central Anatolia, Turkey. *Lithos* **72**, 163–182.

Innocenti, F., Agostini, S., Di Vincenzo, G., Doglioni, C., Manetti, P., Savaşçin, M.Y. & Tonarini, S. 2005. Neogene and Quaternary volcanism in western Anatolia: magma sources and geodynamic evolution. *Marine Geology* **221**, 397–421.

Innocenti, F. & Mazzuoli, R. 1972. Petrology of the Izmir-Karaburun Volcanic Area, West Turkey. *Bulletin of Volcanology* **36**, 83–104.

Ishikawa, T., Tera, F. & Nakazawa, T. 2001. Boron isotope and trace element systematics of the 3 volcanic zones in the Kamchatka arc. *Geochimica et Cosmochimica Acta* **65**, 4523–4537.

Ishizuka, O., Taylor, R.N., Milton, T.J. & Nesbitt, R. 2003. Fluid mantle interaction in an intra-oceanic arc: constraints from high-precision Pb isotopes. *Earth and Planetary Science Letters* **211**, 221–236.

Ishizuka, O., Taylor, R.N., Milton, J.A., Nesbitt, R.W., Yuasa, M. & Sakamoto, I. 2006. Variation in the mantle sources of the northern Izu arc with time and space — constraints from high-precision Pb isotopes. *Journal of Volcanology and Geothermal Research* **156**, 266–290.

Izbekov, P.E., Eichelberger, J.C. & Ivanov, B.V. 2004. The 1996 eruption of Karymsky volcano, Kamchatka: historical record of basaltic replenishment of an andesite reservoir. *Journal of Petrology* **45**, 2325–2345.

Johnson, C.M. & Lipman, P.W. 1988. Origin of metaluminous and alkaline volcanic rocks of the Latir volcanic field, northern Rio Grande rift, New Mexico. *Contributions to Mineralogy and Petrology* **100**, 107–128.

Johnson, R.W., Knutson, J. & Taylor, S.R. 1989. *Intraplate Volcanism in Eastern Australia and New Zealand*. Australian Academy of Science and Cambridge University Press, Cambridge.

Jutzeler, M., Schmincke, H.U. & Sumita, M. 2010. The incrementally zoned Miocene Ayagaures ignimbrite (Gran Canaria, Canary Islands). *Journal of Volcanology and Geothermal Research* **196**, 1–19.

Kabeto, K., Sawada, Y., Iizumi, S. & Wakatsuki, T. 2001. Mantle sources and magma-crust interactions in volcanic rocks from northern Kenya rift: geochemical evidence. *Lithos* **56**, 111–136.

Kampunzu, A.B. & Mohr, P. 1991. Magmatic evolution and petrogenesis in the East African rift system. *In:* Kampunzu, A.B. & Lubala, R.T. (eds), *Magmatism in Extensional Structural Settings*. Springer Verlag, Berlin, 85–136.

Karsli, O., Chen, B., Uysal, I., Aydin, F., Wijbrans, J.R. & Kandemir, R. 2008. Elemental and Sr-Nd-Pb isotopic geochemistry of the most recent Quaternary volcanism in the Erzincan basin, Eastern Turkey: framework for the evaluation of basalt-lower crust interaction. *Lithos* **106**, 55–70.

Kay, S.M. & Kay, R.W. 1994. Aleutian magmas in space and time. *In:* Plafker, G. & Berg, H.C. (eds), *The Geology of North America*. Geological Society of America, Boulder, CO, USA, 687–722.

Kay, S.M., Kay, R.W. & Citron, G.P. 1982. Tectonic controls on tholeiitic and calc-alkaline magmatism in the Aleutian arc. *Journal of Geophysical Research* **87**, 4051–4072.

Kay, S.M., Maksaev, V., Moscoso, R., Mpodozis, C. & Nasi, C. 1987. Probing the evolving Andean lithosphere: mid-late Tertiary magmatism in Chile (29°30'30'S) over the modern zone of subhorizontal subduction. *Journal of Geophysical Research* **92**, 6173–6189.

Kay, S.M., Maksaev, V., Moscoso, R., Mpodozis, C., Nasi, C. & Gordillo, C.E. 1988. Tertiary Andean magmatism in Chile and Argentina between 28°S and 33°S: correlation of magmatic chemistry with a changing Benioff zone. *Journal of South American Earth Sciences* **1**, 21–38.

Kelly, P.J., Kyle, P.R., Dunbar, N.W. & Sims, K.W.W. 2008. Geochemistry and mineralogy of the phonolite lava lake, Erebus volcano, Antarctica: 1972-2004 and comparison with older lavas. *Journal of Volcanology and Geothermal Research* **177**, 589–605.

Kempton, P.D., Fitton, J.G., Hawkesworth, C.J. & Ormerod, D.S. 1991. Isotopic and trace element constraints on the composition and evolution of the lithosphere beneath the Southwestern United States. *Journal of Geophysical Research* **96**, 13713–13735.

Kepezhinskas, P., McDermott, F., Defant, M.J., Hochstaedter, A., Drummond, M.S., Hawkesworth, C.J., Koloskov, A., Maury, R.C. & Bellon, H. 1997. Trace element and Sr-Nd-Pb isotopic constraints on a three-component model of Kamchatka arc petrogenesis. *Geochimica et Cosmochimica Acta* **61**, 577–600.

Keskin, M., Pearce, J.A. & Mitchell, J.G. 1998. Volcano-stratigraphy and geochemistry of collision-related volcanism on the Erzurum-Kars Plateau, northeastern Turkey. *Journal of Volcanology and Geothermal Research* **85**, 355–404.

Kimura, J.I., Manton, W.I., Sun, C.H., Iizumi, S., Yoshida, T. & Stern, R.J. 2002. Chemical diversity of the Ueno basalts, Central Japan: identification of mantle and crustal contributions to arc basalts. *Journal of Petrology* **43**, 1923–1946.

Kimura, J.I. & Yoshida, T. 2006. Contributions of slab fluid, mantle wedge and crust to the origin of Quaternary lavas in the NE Japan arc. *Journal of Petrology* **47**, 2185–2232.

Kita, I., Yamamoto, M., Asakawa, Y., Nakagawa, M., Taguchi, S. & Hasegawa, H. 2001. Contemporaneous ascent of within-plate type and island-arc type magmas in the Beppu-Shimabara graben system, Kyushu island, Japan. *Journal of Volcanology and Geothermal Research* **111**, 99–109.

Knittel, U., Hegner, E., Bau, M. & Satir, M. 1997. Enrichment processes in the sub-arc mantle: a Sr-Nd-Pb isotopic and REE study of primitive arc basalts from the Philippines. *The Canadian Mineralogist* **35**, 327–346.

Kuritani, T., Kitagawa, H. & Nakamura, E. 2005. Assimilation and fractional crystallization controlled by transport process of crustal melt: implications from an alkali basalt–dacite suite from Rishiri Volcano, Japan. *Journal of Petrology* **46**, 1421–1442.

Kuritani, T., Yokoyama, T. & Nakamura, E. 2008. Generation of rear-arc magmas induced by influx of slab-derived supercritical liquids: implications from alkali basalt lavas from Rishiri volcano, Kurile arc. *Journal of Petrology* **49**, 1319–1342.

Lai, Y.M., Song, S.R. & Iizuka, Y. 2008. Magma mingling in the Tungho area, Coastal Range of eastern Taiwan. *Journal of Volcanology and Geothermal Research* **178**, 608–623.

Le Bas, M.J., Le Maitre, R.W., Streckeisen, A. & Zanettin, B. 1986. A chemical classification of volcanic rocks based on the total alkali-silica diagram. *Journal of Petrology* **27**, 745–750.

Le Roex, A.P., Späth, A. & Zartman, R.E. 2001. Lithospheric thickness beneath the southern Kenya rift: implications from basalt geochemistry. *Contributions to Mineralogy and Petrology* **142**, 89–106.

Lindsay, J.M., Trumbull, R.B. & Siebel, W. 2005. Geochemistry and petrogenesis of late Pleistocene to Recent volcanism in southern Dominica, Lesser Antilles. *Journal of Volcanology and Geothermal Research* **148**, 253–394.

Lipman, P.W., Rhodes, R.M. & Dalrymple, G.B. 1990. The Ninole Basalt - Implications for the structural evolution of Mauna Loa volcano, Hawaii. *Bulletin of Volcanology* **53**, 1–19.

Liu, C.Q., Masuda, A. & Xie, G.H. 1992. Isotope and trace-element geochemistry of alkali basalts and associated megacrysts from the Huangyishan volcano, Kuandian, Liaoning, NE China. *Chemical Geology* **97**, 219–231.

Lloyd, F.E., Huntingdon, A.T., Davies, G.R. & Nixon, P.H. 1991. Phanerozoic volcanism of southern Uganda: a case for regional K and LILE enrichment of the lithosphere beneath a domed and rifted continental plate. *In:* Kampunzu, A.B. & Lubala, R.T. (eds), *Magmatism in Extensional Structural Settings*. Springer Verlag, Berlin, 23–72.

López-Escobar, L., Kilian, R., Kempton, P.D. & Tagiri, M. 1993. Petrography and geochemistry of Quaternary rocks from the southern volcanic zone of the Andes between 41°30′ and 46°00′ S, Chile. *Revista Geológica de Chile* **20**, 33–35.

López-Escobar, L., Tagiri, M. & Vergara, M. 1991. Geochemical features of southern Andes Quaternary volcanics between 41º5' and 43º00'S. *Geological Society of America Special Paper* **265**, 45–56.

Lopez-Escobar, L., Vergara, M. & Frey, F.A. 1981. Petrology and geochemistry of lavas from Antuco volcano, a basaltic volcano of the southern Andes (37°25'). *Journal of Volcanology and Geothermal Research* **11**, 329–352.

Luhr, J.F. & Haldar, D. 2006. Barren island volcano (NE Indian ocean): island-arc high-alumina basalts produced by troctolite contamination. *Journal of Volcanology and Geothermal Research* **149**, 177–212.

Macdonald, R., Belkin, H.E., Fitton, J.G., Rogers, N.W., Nejbert, K., Tindle, A.G. & Marshall, A.S. 2008. The roles of fractional crystallization, magma mixing, crystal mush remobilization, and volatile-melt interactions in the genesis of young basalt-peralkaline rhyolite suite, the Greater Olkaria Volcanic Complex, Kenya Rift Valley. *Journal of Petrology* **49**, 1515–1547.

Macdonald, R., Davies, G.R., Upton, B.G.J., Denkley, P.N., Smith, M. & Leat, P.T. 1995. Petrogenesis of Silali volcano, Gregory rift, Kenya. *Journal of the Geological Society of London*, **152**, 703–720.

Mahéo, G., Blichert-Toft, J., Pin, C., Guillot, S. & Pecher, A. 2009. Partial melting of mantle and crustal sources beneath south Karakorum, Pakistan: implications for the Miocene geodynamic evolution of the India-Asia convergence zone. *Journal of Petrology* **30**, 427–449.

Maheshwari, A., Coltorti, M., Sial, A.N. & Mariano, G. 1996. Crustal influences in the petrogenesis of the Malani rhyolites, southwestern Rajasthan: combined trace element and oxygen isotope constraints. *Journal of Geological Society of India* **47**, 611–619.

Maldonado, F., Budahn, J.R., Peters, L. & Unruh, D.M. 2006. Geology geochronology, and geochemistry of basaltic flows of the Cat Hills, Cat Mesa, Wind Mesa, Cerro Verde, and Mesita Negra central New Mexico. *Canadian Journal of Earth Sciences* **43**, 1251–1268.

McDermott, F., Delfin F.G. Jr, Defant, M.J., Turner, S. & Maury, R. 2005. The petrogenesis of volcanics from Mt. Bulusan and Mt. Mayon in the Bicol arc, the Philippines. *Contributions to Mineralogy and Petrology* **150**, 652–670.

McMillan, N.J., Dickin, A.P. & Haag, D. 2000. Evolution of magma source regions in the Rio Grande rift, southern New Mexico. *Geological Society of America Bulletin* **112**, 1582–1593.

Meschede, M. 1986. A method of discriminating between different types of mid-ocean ridge basalts and continental tholeiites with the Nb-Zr-Y diagram. *Chemical Geology* **56**, 207–218.

Middlemost, E.A.K. 1989. Iron oxidation ratios, norms, and the classification of volcanic rocks. *Chemical Geology* **77**, 19–26.

Mitropoulos, P., Tarney, J., Saunders, A.D. & Marsh, N.G. 1987. Petrogenesis of Cenozoic volcanic rocks from the Aegean island arc. *Journal of Volcanology and Geothermal Research* **32**, 177–193.

Mollel, G.F., Swisher C.C. 3rd, Feigenson, M.D. & Carr, M.J. 2008. Geochemical evolution of Ngorongoro Caldera, Northern Tanzania: implications for crust–magma interaction. *Earth and Planetary Science Letters* **271**, 337–347.

Monzier, M., Danyushevsky, L.V., Crawford, A.J., Bellon, H. & Cotten, J. 1993. High-Mg andesites from the southern termination of the New Hebrides island arc (SW Pacific). *Journal of Volcanology and Geothermal Research* **57**, 193–217.

Monzier, M., Robin, C., Eissen, J.P. & Cotten, J. 1997. Geochemistry vs. seismo-tectonics along the volcanic New Hebrides Central Chain (Southwest Pacific). *Journal of Volcanology and Geothermal Research* **78**, 1–29.

Moriguti, T., Shibata, T. & Nakamura, E. 2004. Lithium, boron and lead isotope and trace element systematics of Quaternary basaltic volcanic rocks in northeastern Japan: mineralogical controls on slab-derived fluid composition. *Chemical Geology* **212**, 81–100.

Morrison, D.F. 1990. *Multivariate Statistical Methods*. 3rd ed. McGraw-Hill, New York.

Moyer, T.C. & Esperança, S. 1989. Geochemical and isotopic variations in a bimodal magma system: the Kaiser Spring volcanic field, Arizona. *Journal of Geophysical Research* **94**, 7841–8759.

Myers, J.D., Marsh, B.D., Frost, C.D. & Linton, J.A. 2002. Petrologic constraints on the spatial distribution of crustal magma chambers, Atka volcanic center, central Aleutian arc. *Contributions to Mineralogy and Petrology* **143**, 567–586.

Myers, J.D., Marsh, B.D. & Sinha, A.K. 1985. Strontium isotopic and selected trace element variations between two Aleutian volcanic centers (Adak and Atka): implications for the development of arc volcanic plumbing systems. *Contributions to Mineralogy and Petrology* **91**, 221–234.

Nakagawa, M., Ishizuka, Y., Kudo, T., Yoshimoto, M., Hirose, W., Ishizaki, Y., Gouchi, N., Katsui, Y., Solovyow, A.W., Steinberg, G.S. & Abdurakhmanov, A.I. 2002. Tyatya volcano, southwestern Kuril arc: recent eruptive activity inferred from widespread tephra. *The Island Arc* **11**, 236–254.

Nick, K. 1988. *Mineralogische, Geochemische und Petrographische Untersuchungen in der Sierra de San Carlos, Mexiko*. PhD, Universitaet (TH) Fridericiana Karlsruhe, Karlsruhe, Germany.

Nonnotte, P., Benoit, M., Le Gall, B., Hémond, C., Rolet, J. & Cotten, J. 2011. Petrology and geochemistry of alkaline lava series, Kilimanjaro, Tanzania: new constraints on petrogenetic processes. *Geological Society of America Special Paper* **478**, 127–158.

Nye, C.J. & Reid, M.R. 1986. Geochemistry of primary and least fractionated lavas from Okmok volcano, central Aleutians: implications for arc magma genesis. *Journal of Geophysical Research* **91**, 10271–10287.

Ohara, Y., Fujioka, K., Ishizuka, O. & Ishii, T. 2002. Peridotites and volcanics from the Yap arc system: implications for tectonics of the southern Philippine Sea plate. *Chemical Geology* **189**, 35–53.

Ohba, T., Kimura, Y. & Fujimaki, H. 2007. High-magnesian andesite produced by two-stage magma mixing: a case study from Hachimantai, northern Honshu, Japan. *Journal of Petrology* **48**, 627–645.

Ohba, T., Matsuoka, K., Kimura, Y., Ishikawa, H. & Fujimaki, H. 2009. Deep crystallization differentiation of arc tholeiite basalt magmas from Northern Honshu Arc, Japan. *Journal of Petrology* **50**, 1025–1046.

Omrani, J., Agard, P.H.W., Benoit, M., Prouteau, G. & Jolivet, L. 2008. Arc-magmatism and subduction history beneath the Zagros Mountains, Iran: a new report of adakites and geodynamics consequences. *Lithos* **106**, 380–398.

Palacz, Z.A. & Saunders, A.D. 1986. Coupled trace element and isotope enrichment in the Cook-Austral-Samoa islands, southwest pacific. *Earth and Planetary Science Letters* **79**, 270–280.

Palacz, Z.A. & Wolff, J.A. 1989. Strontium, neodymium, and lead isotope characteristics of the Granadilla Pumice, Tenerife: a study of the causes of strontium isotope disequilibrium in felsic pyroclastic deposits. *Geological Society of London Special Publications* **42**, 147–159.

Parat, F., Dungan, M.A. & Lipman, P.W. 2005. Contemporaneous trachyandesitic and calc-alkaline volcanism of the Huerto andesite, San Juan Volcanic Field, Colorado, USA. *Journal of Petroleum Geology* **46**, 859–891.

Pardo, N., Avellán, D.R., Macías, J.L., Scolamacchia, T. & Rodríguez, D. 2008. The ~1245 yr BP Asososca maar: new advances on recent volcanic stratigraphy of Managua (Nicaragua) and hazard implications. *Journal of Volcanology and Geothermal Research* **176**, 493–512.

Paslick, C., Halliday, A., James, D. & Dawson, J.B. 1995. Enrichment of the continental lithosphere by OIB melts: isotopic evidence from the volcanic province of northern Tanzania. *Earth and Planetary Science Letters* **130**, 109–126.

Patino, L.C., Velbel, M.A., Price, J.R. & Wade, J.A. 2003. Trace element mobility during spheroidal weathering of basalts and andesites in Hawaii and Guatemala. *Chemical Geology* **202**, 343–364.

Pearce, J.A. & Cann, J.R. 1971. Ophiolite origin investigated by discriminant analysis using Ti, Zr and Y. *Earth and Planetary Science Letters* **12**, 339–349.

Pearce, J.A. & Cann, J.R. 1973. Tectonic setting of basic volcanic rocks determined using trace element analyses. *Earth and Planetary Science Letters* **19**, 290–300.

Pearce, J.A., Harris, N.B.W. & Tindle, A.G. 1984. Trace element discrimination diagrams for the tectonic interpretation of granitic rocks. *Journal of Petrology* **25**, 956–983.

Peate, D.W., Pearce, J.A., Hawkesworth, C.J., Colley, H., Edwards, C.M.H. & Hirose, K. 1997. Geochemical variations in Vanuatu arc lavas: the role of subducted material and a variable mantle wedge composition. *Journal of Petrology* **38**, 1331–1358.

Peccerillo, A., Barberio, M.R., Yirgu, G., Ayalew, D., Barbieri, M. & Wu, T.W. 2003. Relationships between mafic and peralkaline silicic magmatism in continental rift settings: a petrological, geochemical and isotopic study of the Gedemsa volcano, central Ethiopian rift. *Journal of Petrology* **44**, 2003–2032.

Peccerillo, A., Donati, C., Santo, A.P., Orlando, A., Yirgu, G. & Ayalew, D. 2007. Petrogenesis of silicic peralkaline rocks in the Ethiopian Rift: geochemical evidence and volcanological implications. *Journal of African Earth Sciences* **48**, 161–173.

Peng, Z.C., Zartman, R.E., Futa, K. & Chen, D.G. 1986. Pb-, Sr- and Nd-isotopic systematics and chemical characteristics of Cenozoic basalts, eastern China. *Chemical Geology* **59**, 3–33.

Pe-Piper, G. & Moulton, B. 2008. Magma evolution in the Pliocene-Pleistocene of Kos, South Aegean arc (Greece). *Lithos* **106**, 110–124.

Perry, F.V., Baldridge, W.S., DePaolo, D.J. & Shafiqullah, M. 1990. Evolution of a magmatic system during continental extension: the mount Taylor volcanic field, New Mexico. *Journal of Geophysical Research* **95**, 19327–19348.

Polat, A. 2009. The geochemistry of Neoarchean (ca. 2700 Ma) tholeiitic basalts, transitional to alkaline basalts, and gabbros, Wawa Subprovince, Canada: implications for petrogenetic and geodynamic processes. *Precambrian Research* **168**, 83–105.

Polat, A., Kerrich, R. & Wyman, D.A. 1999. Geochemical diversity in oceanic komatiites and basalts from the late Archean Wawa greenstone belts, Superior Province, Canada: trace element and Nd isotope evidence for a heterogeneous mantle. *Precambrian Research* **94**, 139–173.

Potter, L.S. 1996. Chemical variation along strike in feldspathoidal rocks of the Eastern Alkalic Belt, Trans-Pecos magmatic province, Texas and New Mexico. *Canadian Mineralogist* **34**, 241–264.

Prægel, N.O. & Holm, P.M. 2006. Lithospheric contributions to high-MgO basanites from the Cumbre Vieja volcano, La Palma, Canary Islands and evidence for temporal variation in plume influence. *Journal of Volcanology and Geothermal Research* **149**, 213–239.

Price, R.C., Gray, C.M. & Frey, F.A. 1997. Strontium isotopic and trace element heterogeneity in the plains basalts of the Newer Volcanic Province, Victoria, Australia. *Geochimica et Cosmochimica Acta* **61**, 171–192.

Reagan, M.K. & Gill, J.B. 1989. Coexisting calcalkaline and high-niobium basalts from Turrialba volcano, Costa Rica: implications for residual titanates in arc magma sources. *Journal of Geophysical Research* **94**, 4619–4633.

Reagan, M.K., Hanan, B.B., Heizler, M.T., Hartman, B.S. & Hickey-Vargas, R. 2008. Petrogenesis of volcanic rocks from Saipan and Rota, Mariana Islands, and implications for evolution of Nascent Island Arcs. *Journal of Petrology* **49**, 441–464.

Reagan, M.K. & Meijer, A. 1984. Geology and geochemistry of early arc-volcanic rocks from Guam. *Geological Society of America Bulletin* **95**, 701–713.

Reagan, M.K., Sims, K.W.W., Erich, J., Thomas, R.B., Cheng, H., Edwards, R.L., Layne, G. & Ball, L. 2003. Time-scales of differentiation from mafic parents to rhyolite in North American continental arcs. *Journal of Petrology* **44**, 1703–1726.

Reichardt, H., Weinberg, R.F., Andersen, U.B. & Fanning, C.M. 2010. Hybridization of granitic magmas in the source: the origin of the Karakoram Batholith, Ladakh, NW India. *Lithos* **116**, 249–272.

Robin, C., Eissen, J.P., Samaniego, P., Martin, H., Hall, M. & Cotten, J. 2009. Evolution of the late Pleistocene Mojanda-Fuya Fuya volcanic complex (Ecuador), by progressive adakitic involvement in mantle magma sources. *Bulletin of Volcanology* **71**, 233–258.

Rodríguez, C., Sellés, D., Dungan, M., Langmuir, C. & Leeman, W. 2007. Adakitic dacites formed by intracrustal crystal fractionation of water-rich parent magmas at Nevado de Longaví volcano (36.2°S) Andean southern volcanic zone, central Chile. *Journal of Petrology* **18**, 2033–2061.

Rogers, N.W., Evans, P.J., Blake, S., Scott, S.C. & Hawkesworth, C.J. 2004. Rates and timescales of fractional crystallization from ^{238}U–^{230}Th–^{226}Ra disequilibria in trachyte lavas from Longonot Volcano, Kenya. *Journal of Petrology* **45**, 1747–1776.

Rollinson, H.R. 1993. Discriminating between tectonic environments using geochemical data. *In:* Rollinson, H.R. (ed), *Using Geochemical Data: Evaluation, Presentation, Interpretation*. Longman Scientific & Technical, Essex, UK, 171–214.

Romick, J.D., Perfit, M.R., Swanson, S.E. & Shuster, R.D. 1990. Magmatism in the eastern Aleutian arc: temporal characteristic of igneous activity on Akutan Island. *Contributions to Mineralogy and Petrology* **104**, 700–721.

Ronga, F., Lustrino, M., Marzoli, A. & Melluso, L. 2010. Petrogenesis of a basalt-comendite-pantellerite rock suite: the Boseti Volcanic Complex (Main Ethiopian Rift. *Mineralogy and Petrology* **98**, 227–243.

Rooney, T., Furman, T., Bastow, I., Ayalew, D. & Yirgu, G. 2007. Lithospheric modification during crustal extension in the Main Ethiopian Rift. *Journal of Geophysical Research* **112**, doi:10210.11029/12006JB004916.

Rotolo, S.G. & Castorina, F. 1998. Transition from midly-tholeiitic to calc-alkaline suite: the case of Chicontepec volcanic centre, El Salvador, Central America. *Journal of Volcanology and Geothermal Research* **86**, 117–136.

Rutanen, H. & Andersson, U.B. 2009. Mafic plutonic rocks in a continental-arc setting: geochemistry of 1.87-1.78 Ga rocks from south-central Sweden and models of their palaeotectonic setting. *Geological Journal,* **44**, DOI: 10.1002/gj.1133.

Ryder, C.H., Gill, J.B., Tepley F. 3rd, Ramos, F. & Reagan, M. 2006. Closed- to open-system differentiation at Arenal volcano 1968-2003. *Journal of Volcanology and Geothermal Research* **157**, 75–93.

Sakuyama, M. & Nesbitt, R.W. 1986. Geochemistry of the Quaternary volcanic rocks of the Northeast Japan arc. *Journal of Volcanology and Geothermal Research* **29**, 413–450.

Sakuyama, T., Ozawa, K., Sumino, H. & Nagao, K. 2009. Progressive melt extraction from upwelling mantle constrained by the Kita-Matsuura basalts in NW Kyushu, SW Japan. *Journal of Petrology* **50**, 725–779.

Samaniego, P., Barba, D., Robin, C., Fornari, M. & Bernard, B. 2012. Eruptive history of Chimborazo volcano (Ecuador): a large, ice-capped and hazardous compound volcano in the Northern Andes. *Journal of Volcanology and Geothermal Research* **221–222**, 35–51.

Sano, T., Hasenaka, T., Shimaoka, A., Yonesawa, C. & Fukuoka, T. 2001. Boron contents of Japan trench sediments and Iwate basaltic lavas, northeast Japan arc: estimation of sediment-derived fluid contribution in mantle wedge. *Earth and Planetary Science Letters* **186**, 187–198.

Sato, M., Shuto, K. & Yagi, M. 2007. Mixing of asthenospheric and lithospheric mantle-derived basalt magmas as shown by along-arc variation in Sr and Nd isotopic compositions of Early Miocene basalts from back-arc margin of the NE Japan arc. *Lithos* **96**, 453–474.

Saunders, A.D., Tarney, J., Stern, C.R. & Dalziel, I.W.D. 1979. Geochemistry of Mesozoic marginal basin floor igneous rocks from southern Chile. *Geological Society of America Bulletin* **90**, 237–258.

Schmitz, M.D. & Smith, I.E.M. 2004. The petrology of the Rotoiti eruption sequence, Taupo Volcanic Zone: an example of fractionation and mixing in a rhyolitic system. *Journal of Petrology* **45**, 2045–2066.

Sendjaja, Y.A., Kimura, J.I. & Sunardi, E. 2009. Across-arc geochemical variation of Quaternary lavas in west Java, Indonesia: mass-balance elucidation using arc basalt simulator model. *Island Arc* **18**, 201–224.

Seyitoglu, G., Anderson, D., Nowell, G. & Scott, B. 1997. The evolution from Miocene potassic to Quaternary sodic magmatism in western Turkey: implications for enrichment processes in the lithospheric mantle. *Journal of Volcanology and Geothermal Research* **76**, 127–147.

Seymour, K.S. & Vlassopoulos, D. 1992. Magma mixing at Nisyros volcano, as inferred from incompatible trace-element systematics. *Journal of Volcanology and Geothermal Research* **50**, 273–299.

Sharma, K.K. 2004. The Neoproterozoic Malani magmatism of the northwestern Indian shield: implications for crust-building processes. *Proceedings of the Indian Academy of Sciences (Earth and Planetary Sciences)* **113**, 795–807.

Shervais, J.W. 1982. Ti-V plots and the petrogenesis of modern and ophiolitic lavas. *Earth and Planetary Science Letters* **59**, 101–118.

Shinjo, R. 1998. Petrochemistry and tectonic significance of the emerged late Cenozoic basalts behind the Okinawa Trough Ryukyu arc system. *Journal of Volcanology and Geothermal Research* **80**, 39–53.

Shinjo, R. 1999. Geochemistry of high Mg andesites and the tectonic evolution of the Okinawa Trough-Ryukyu arc system. *Chemical Geology* **157**, 69–88.

Shinjo, R., Woodhead, J.D. & Hergt, J.M. 2000. Geochemical variation within the northern Ryukyu: magma source compositions and geodynamic implications. *Contributions to Mineralogy and Petrology* **140**, 263–282.

Shukuno, H., Tamura, Y., Tani, K., Chang, Q., Suzuki, T. & Fiske, R.S. 2006. Origin of silicic magmas and the compositional gap at Sumisu submarine caldera, Izu-Bonin arc, Japan. *Journal of Volcanology and Geothermal Research* **156**, 187–216.

Shuto, K., Hirahara, Y., Ishimoto, H., Aoki, A., Jinbo, A. & Goto, Y. 2004. Sr and Nd isotopic compositions of the magma source beneath north Hokkaido, Japan: comparison with the back-arc side in the NE Japan arc. *Journal of Volcanology and Geothermal Research* **134**, 57–75.

Shuto, K., Ishimoto, H., Hirahara, Y., Sato, M., Matsui, K., Fujibayashi, N., Takazawa, E., Yabuki, K., Sekine, M., Kato, M. & Rezanov, A.I. 2006. Geochemical secular variation of magma source during Early to Middle Miocene time in the Niigata area, NE Japan: asthenospheric mantle upwelling during back-arc basin opening. *Lithos* **86**, 1–33.

Singer, B.S. & Kudo, A.M. 1986. Assimilation-fractional crystallization of Polvadera Group rocks in the northwestern Jemez volcanic field, New Mexico. *Contributions to Mineralogy and Petrology* **94**, 374–386.

Singer, B.S., Myers, J.D. & Frost, C.D. 1992. Mid-Pleistocene lavas from the Seguam volcanic center, central Aleutian arc: closed-system fractional crystallization of a basalt to rhyodacite eruptive suite. *Contributions to Mineralogy and Petrology* **110**, 87–112.

Singh, A.K. & Vallinayagam, G. 2004. Geochemistry and petrogenesis of anorogenic basic volcanic-plutonic rocks of the Kundal area, Malani igneous suite, western Rajasthan, India. *Proceedings of the Indian Academy of Sciences (Earth and Planetary Sciences)* **113**, 667–681.

Smellie, J.L. 1983. A geochemical overview of subduction-related igneous activity in the South Shetland Islands, Lesser Antarctica. *In:* Oliver, R.L., James, P.R. & Jago, J.B. (eds), *Antarctic Earth Science*. Australian Academy of Sciences and Cambridge University Press, Cambridge, 352–356.

Smith, I.E.M., Stewart, R.B. & Price, R.C. 2003. The petrology of a large intra-oceanic silicic eruption: the Sandy Bay tephra, Kermadec arc, southwest Pacific. *Journal of Volcanology and Geothermal Research* **124**, 173–194.

Smith, T.E., Thirlwall, M.F. & MacPherson, C. 1996. Trace element and isotope geochemistry of the volcanic rocks of Bequia, Grenadine Islands, Lesser Antilles Arc: a study of subduction enrichment and intra-crustal contamination. *Journal of Petrology* **37**, 117–143.

Spengler, S.R. & Garcia, M.O. 1988. Geochemistry of the Hawi lavas, Kohala Volcano, Hawaii. *Contributions to Mineralogy and Petrology* **99**, 90–104.

Spera, F.J. & Bohrson, W.A. 2004. Open-system magma chamber evolution: an energy-constrained geochemical model incorporating the effects of concurrent eruption, recharge, variable assimilation and fractional crystallization (EC-E'RAcFC). *Journal of Petrology* **45**, 2459–2480.

Sruoga, P., Llambías, E.J., Fauqué, L., Schonwandt, D. & Repol, D.G. 2005. Volcanological and geochemical evolution of the Diamante caldera-Maipo volcano complex in the southern Andes of Argentina (34°10'S). *Journal of South American Earth Sciences* **19**, 399–414.

Stephenson, D. & Marshall, T.R. 1984. The petrology and mineralogy of Mt. Popa volcano and the nature of the late-Cenozoic Burma volcanic arc. *Journal of the Geological Society of London* **141**, 747–762.

Stolz, A.J., Varne, R., Davies, G.R., Wheller, G.E. & Fodon, J.D. 1990. Magma source components in an arc-continent collision zone: the Flores-Lembata sector, Sunda arc, Indonesia. *Contributions to Mineralogy and Petrology* **105**, 585–601.

Sussman, D. 1985. Apoyo caldera, Nicaragua: a major Quaternary silicic eruptive center. *Journal of Volcanology and Geothermal Research* **24**, 249–282.

Suzuki, Y. & Nakada, S. 2007. Remobilization of highly crystalline felsic magma by injection of mafic magma: constraints from the middle sixth century eruption at Haruna volcano, Honshu, Japan. *Journal of Petrology* **48**, 1543–1567.

Takanashi, K., Shuto, K. & Sato, M. 2011. Origin of Late Paleogene to Neogene basalts and associated coeval felsic volcanic rocks in Southwest Hokkaido, northern NE Japan arc: constraints from Sr and Nd isotopes and major- and trace-element chemistry. *Lithos* **125**, 368–392.

Tamura, Y. 1994. Genesis of island arc magmas by mantle derived bimodal magmatism: evidence from the Shiraham group, Japan. *Journal of Petrology* **35**, 619–645.

Tamura, Y., Tani, K., Chang, Q., Shukuno, H., Kawabata, H., Ishizuka, O. & Fiske, R.S. 2007. Wet and dry basalt magma evolution at Torishima Volcano, Izu-Bonin Arc, Japan: the possible role of phengite in the downgoing slab. *Journal of Petrology* **48**, 1999–2031.

Tamura, Y., Yuhara, M., Ishii, T., Irino, N. & Shukuno, H. 2003. Andesites and dacites from Daisen volcano, Japan: partial-to-total remelting of an andesite magma body. *Journal of Petrology* **44**, 2243–2260.

Tatsumi, Y., Murasaki, M., Arsadi, E.M. & Nohda, S. 1991. Geochemistry of Quaternary lavas from NE Sulawesi: transfer of subduction components into the mantle wedge. *Contributions to Mineralogy and Petrology* **107**, 137–149.

Tatsumi, Y., Murasaki, M. & Nohda, S. 1992. Across-arc variation of lava chemistry in the Izu-Bonin arc: identification of subduction components. *Journal of Volcanology and Geothermal Research* **49**, 179–190.

Taylor, R.N. & Nesbitt, R.W. 1998. Isotopic characteristics of subduction fluids in an intra-oceanic setting, Izu-Bonin Arc, Japan. *Earth and Planetary Science Letters* **164**, 79–98.

Taylor, R.N., Nesbitt, R.W., Vidal, P., Harmon, R.S., Auvray, B. & Croudace, I.W. 1994. Mineralogy, chemistry, and genesis of the boninite series volcanics, Chichijima, Bonin Islands, Japan. *Journal of Petrology* **35**, 577–617.

Taylor, S.R. & McLennan, S.M. 1995. The geochemical evolution of the continental crust. *Review in Geophysics* **33**, 241–265.

Temel, A., Gündoğdu, M.N. & Gourgaud, A. 1998. Petrological and geochemical characteristics of Cenozoic high-K calc-alkaline volcanism in Konya, Central Anatolia, Turkey. *Journal of Volcanology and Geothermal Research* **85**, 327–354.

Thirlwall, M.F. & Graham, A.M. 1984. Evolution of high-Ca, high-Sr C-series basalts from Grenada, Lesser Antilles: the effects of intra-crustal contamination. *Journal of the Geological Society of London* **141**, 427–445.

Thirlwall, M.F., Graham, A.M., Arculus, R.J., Harmon, R.S. & Macpherson, C.G. 1996. Resolution of the effects of crustal assimilation, sediment subduction, and fluid transport in island arc magmas: Pb-Sr-Nd-O isotope geochemistry of Grenada, Lesser Antilles. *Geochimica et Cosmochimica Acta* **60**, 4785–4810.

Tian, L., Castillo, P.R., Hawkins, J.W., Hilton, D.R., Hanan, B.B. & Pietruszka, A.J. 2008. Major and trace element and Sr-Nd isotope signatures of lava from the central Lau Basin: implications for the nature and influence of subduction components in the back-arc mantle. *Journal of Volcanology and Geothermal Research* **178**, 657–670.

Timm, C., Hoernle, K., Bogaard, P.V.D., Bindeman, I. & Weaver, S. 2009. Geochemical evolution of intraplate volcanism at Banks Peninsula, New Zealand: interaction between asthenospheric and lithospheric melts. *Journal of Petrology* **50**, 989–1023.

Togashi, S., Tanaka, T., Yoshida, T., Ishikawa, K.I., Fujinawa, A. & Kurasawa, H. 1992. Trace elements and Nd-Sr isotopes of island arc tholeiites from frontal arc of northeast Japan. *Geochemical Journal* **26**, 261–277.

Tormey, D.R., Hickey-Vargas, R., Frey, F.A. & López-Escobar, L. 1991. Recent lavas from the Andean volcanic front (33 to 42°S); interpretations of along-arc compositional variations. *In:* Harmon, R.S. & Rapela, C.W. (eds), *Andean Magmatism and Its Tectonic Setting, Geological Society of America Special Paper*. Geological Society of America, Boulder, CO, USA, 57–77.

Torres-Alvarado, I.S., Verma, S.P., Palacios-Berruete, H., Guevara, M. & González-Castillo, O.Y. 2003. DC_Base: a database system to manage Nernst distribution coefficients and its application to partial melting modeling. *Computers & Geosciences* **29**, 1191–1198.

Toya, N., Ban, M. & Shinjo, R. 2005. Petrology of Aoso volcano, northeast Japan arc: temporal variation of the magma feeding system and nature of low-K amphibole andesite in the Aoso-Osore volcanic zone. *Contributions to Mineralogy and Petrology* **148**, 566–581.

Trua, T., Deniel, C. & Mazzuoli, R. 1999. Crustal control in the genesis of Plio-Quaternary bimodal magmatism of the Main Ethiopian Rift (MER): geochemical and isotopic (Sr, Nd, Pb) evidence. *Chemical Geology* **155**, 201–231.

Turner, S. & Foden, J. 2001. U, Th and Ra disequilibria, Sr, Nd, and Pb isotope and trace element variations in Sunda arc lavas: predominance of a subducted sediment component. *Contributions to Mineralogy and Petrology* **142**, 43–57.

Turner, S., Hawkesworth, C., Rogers, N. & King, P. 1997. U-Th isotope disequilibria and ocean island basalt generation in the Azores. *Chemical Geology* **139**, 145–164.

Turner, S., Hawkesworth, C.J., Calsteren, P.V., Heath, E., Macdonald, R. & Black, S. 1996. U-series isotopes and destructive plate margin magma genesis in the Lesser Antilles. *Earth and Planetary Science Letters* **142**, 191–207.

Ujike, O. & Stix, J. 2000. Geochemistry and origins of Ueno and Ontake basaltic to andesitic rocks (<3 Ma) produced by distinct contributions of subduction components, central Japan. *Journal of Volcanology and Geothermal Research* **95**, 49–64.

van Bergen, M.J., Vroon, P.Z., Varekamp, J.C. & Poorter, R.P.E. 1992. The origin of the potassic rock suite from Batu Tara volano (East Sunda Arc, Indonesia). *Lithos* **28**, 261–282.

Vergara, M., López-Escobar, L., Cancino, A. & Levi, B. 1991. The Pichidangui formation; some geochemical characteristics and tectonic implications of the Triassic marine volcanism in central Chile (31°55'S to 32°20'S). *Geological Society of America Special Paper* **265**, 93–98.

Vergara, M., López-Escobar, L., Palma, J.L., Hickey-Vargas, R. & Roeschmann, C. 2004. Late Tertiary volcanic episodes in the area of the city of Santiago de Chile: new geochronological and geochemical data. *Journal of South American Earth Sciences* **17**, 227–238.

Verma, S.K., Pandarinath, K. & Verma, S.P. 2012. Statistical evaluation of tectonomagmatic discrimination diagrams for granitic rocks and proposal of new discriminant-function-based multi-dimensional diagrams for acid rocks. *International Geology Review* **54**, 325–347.

Verma, S.P. 2005. *Estadística básica para el manejo de datos experimentales: aplicación en la Geoquímica (Geoquimiometría)*. Universidad Nacional Autónoma de México, México, Mexico City.

Verma, S.P. 2010. Statistical evaluation of bivariate, ternary, and discriminant function tectonomagmatic discrimination diagrams. *Turkish Journal of Earth Sciences* **19**, 185–238.

Verma, S.P. 2012a. Application of multi-dimensional discrimination diagrams and probability calculations to acid rocks from Portugal and Spain. *Comunicações Geológicas* **99**, 79–93.

Verma, S.P. 2012b. Geochemometrics. *Revista Mexicana de Ciencias Geológicas* **29**, 276–298.

Verma, S.P. & Agrawal, S. 2011. New tectonic discrimination diagrams for basic and ultrabasic volcanic rocks through log-transformed ratios of high field strength elements and implications for petrogenetic processes. *Revista Mexicana de Ciencias Geológicas* **28**, 24–44.

Verma, S.P. & Díaz-González, L. 2012. Application of the discordant outlier detection and separation system in the geosciences. *International Geology Review* **54**, 593–614.

Verma, S.P., Guevara, M. & Agrawal, S. 2006. Discriminating four tectonic settings: five new geochemical diagrams for basic and ultrabasic volcanic rocks based on log-ratio transformation of major-element data. *Journal of Earth System Science* **115**, 485–528.

Verma, S.P., Torres-Alvarado, I.S. & Sotelo-Rodríguez, Z.T. 2002. SINCLAS: standard igneous norm and volcanic rock classification system. *Computers & Geosciences* **28**, 711–715.

Verwoerd, W.J., Erlank, A.J. & Kable, E.J.D. 1976. Geology and geochemistry of Bouvet Island. *Proceedings of the Symposium on Andean and Antarctic Volcanology Problems*, Santiago, Chile, 201–207.

Vespa, M., Keller, K. & Gertisser, R. 2006. Interplinian explosive activity of Santorini volcano (Greece) during the past 150,000 years. *Journal of Volcanology and Geothermal Research* **153**, 262–286.

Vezzoli, L., Tibaldi, A., Renzulli, A., Menna, M. & Flude, S. 2008. Faulting-assisted lateral collapses and influence on shallow magma feeding system at Ollague volcano (Central Volcanic Zone, Chile-Bolivia Andes). *Journal of Volcanology and Geothermal Research* **171**, 137–159.

Wade, J.A., Plank, T., Stern, R.J., Tollstrup, D.L., Gill, J.B., O'Leary, J.C., Eiler, J.M., Moore, R.B., Woodhead, J.D., Trusdell, F., Fischer, T.P. & Hilton, D.R. 2005. The May 2003 eruption of Anatahan volcano, Mariana Islands: geochemical evolution of a silicic island-arc volcano. *Journal of Volcanology and Geothermal Research* **146**, 139–170.

Walker, J.A., Moulds, T.N., Zentilli, M. & Feigenson, M.D. 1991. Spatial and temporal variations in volcanics of the Andean Central volcanic zone (26 to 28°S). *Geological Society of America Special Paper* **265**, 139–156.

Walker, J.A., Patino, L.C., Cameron, B.I. & Carr, M.J. 2000. Petrogenetic insights provided by compositional transects across the Central American arc: southeastern Guatemala and Honduras. *Journal of Geophysical Research* **105**, 18949–18963.

Walker, J.A., Patino, L.C., Carr, M.J. & Feigenson, M.D. 2001. Slab control over HFSE depletions in central Nicaragua. *Earth and Planetary Science Letters* **192**, 533–543.

Watt, S.F.L., Pyle, D.M. & Mather, T.A. 2011. Geología, petrología y geoquímica de los domos volcánicos del volcán Huequi, Chile meridional. *Andean Geology* **38**, 335–348.

Weis, D., Frey, F.A., Leyrit, H. & Gautier, I. 1993. Kerguelen archipelago revisited: geochemical and isotopic study of the southeast province lavas. *Earth and Planetary Science Letters* **118**, 101–119.

West, H.B., Garcia, M.O., Gerlach, D.C. & Romero, J. 1992. Geochemistry of tholeiites from Lanai, Hawaii. *Contributions to Mineralogy and Petrology* **112**, 520–542.

Wheller, G.E., Varne, R., Foden, J.D. & Abbott, M.J. 1987. Geochemistry of Quaternary volcanism in the Sunda-Banda arc, Indonesia, and three-component genesis of island-arc basaltic magmas. *Journal of Volcanology and Geothermal Research* **32**, 137–160.

Wolde, B., Asres, Z., Desta, Z. & Gonzalez, J.J. 1996. Neoproterozoic zirconium-depleted boninite and tholeitic series rocks from Adola, southern Ethiopia. *Precambrian Research* **80**, 261–279.

Wood, D.A. 1980. The application of a Th-Hf-Ta diagram to problems of tectonomagmatic classification and to establishing the nature of crustal contamination of basaltic lavas of the British Tertiary volcanic province. *Earth and Planetary Science Letters* **50**, 11–30.

Woodhead, J.D. 1988. The origin of geochemical variations in Mariana lavas: a general model for petrogenesis in intra-oceanic island arcs. *Journal of Petrology* **29**, 805–830.

Woodhead, J.D., Eggins, S.M. & Johnson, R.W. 1998. Magma genesis in the New Britain Island Arc: further insights into melting and mass transfer processes. *Journal of Petrology* **39**, 1641–1668.

Woodhead, J.D. & Johnson, R.W. 1993. Isotopic and trace-element profiles across the New Britain island arc, Papua New Guinea. *Contributions to Mineralogy and Petrology* **113**, 479–491.

Wright, I.C., Worthington, T.J. & Gamble, J.A. 2006. New multibeam and geochemistry of the 30°-35°S sector, and overview of southern Kermadec arc volcanism. *Journal of Volcanology and Geothermal Research* **149**, 263–296.

Xu, G., Frey, F.A., Clague, D.A., Abouchami, W., Blichert-Toft, J., Cousens, B. & Weisler, M. 2007. Geochemical characteristics of West Molokai shield- and postshield-stage lavas: constraints on Hawaiian plume models. *Geochemistry Geophysics Geosystems* **8**, 1–40.

Xu, G., Frey, F.A., Clague, D.A., Weis, D. & Beeson, M.H. 2005. East Molokai and other Kea-trend volcanoes: magmatic processes and sources as they migrate away from the Hawaiian hot spot. *Geochemistry Geophysics Geosystems* **6**, doi: 05010.01029/02004GC000830.

Xu, Y.G., Ma, J.L., Frey, F.A., Feigenson, M.D. & Liu, J.F. 2005. Role of lithosphere-asthenosphere interaction in the genesis of Quaternary alkali and tholeiitic basalts from Datong, western North China Craton. *Chemical Geology* **224**, 247–271.

Zellmer, G., Turner, S. & Hawkesworth, C. 2000. Timescales of destructive plate margin magmatism: new insights from Santorini, Aegean volcanic arc. *Earth and Planetary Science Letters* **174**, 265–281.

Zellmer, G.F., Hawkesworth, C.J., Sparks, R.S.J., Thomas, L.E., Harford, C.L., Brewer, T.S. & Loughlin, S.C. 2003. Geochemical evolution of the Soufrière Hills volcano, Montserrat, Lesser Antilles volcanic arc. *Journal of Petrology* **44**, 1349–1374.

Zhang, M., Suddaby, P., Thompson, R.N., Thirlwall, M.F. & Menzies, M.A. 1995. Potassic volcanic rocks in NE China: geochemical constraints on mantle source and magma genesis. *Journal of Petrology* **36**, 1275–1303.

Zhao, Z., Mo, X., Dilek, Y., Niu, Y., DePaolo, D.J., Robinson, P., Zhu, D., Sun, C., Dong, G., Zhou, S., Luo, Z. & Hou, Z. 2009. Geochemical and Sr-Nd-O isotopic compositions of the post-collisional ultrapotassic magmatism in SW Tibet: petrogenesis and implications for India intra-continental subduction beneath southern Tibet. *Lithos* **113**, 190–212.

Zhi, X., Song, Y., Frey, F.A., Feng, J. & Zhai, M. 1990. Geochemistry of Hannuoba basalts, eastern China: constraints on the origin of continental alkalic and tholeiitic basalt. *Chemical Geology* **88**, 1–33.

Zhuravlev, D.Z., Tsvetkov, A.A., Zhuravlev, A.Z., Gladkov, N.G. & Chernysheva, I.V. 1987. $^{143}Nd/^{144}Nd$ and $^{87}Sr/^{86}Sr$ ratios in recent magmatic rocks of the Kurile Island Arc. *Chemical Geology* **66**, 227–243.

Zou, H., Zindler, A., Xisheng, X. & Qi, Q. 2000. Major, trace element, and Nd, Sr and Pb isotope studies of Cenozoic basalts in SE China: mantle sources, regional variations and tectonic significance. *Chemical Geology* **171**, 33–47.

Table S1. Locations and literature sources for the 5-part database.

Region	References, arranged chronologically
	Island arcs
Aegean	Huijsmans *et al.* 1988; Mitropoulos *et al.* 1987; Zellmer *et al.* 2000; Vespa *et al.* 2006
Alaskan peninsula	Hildreth *et al.* 2004
Aleutians	Kay *et al.* 1982; Myers *et al.* 1985, 2002; Brophy 1986; Nye & Reid 1986; Romick *et al.* 1990; Singer *et al.* 1992; Kay & Kay 1994
Barren Islands	Alam *et al.* 2004; Luhr & Haldar 2006
Burma	Stephenson & Marshall 1984
Indonesian islands (Java, Sangihe, Sua, Sulawesi, Sunda-Banda)	Foden & Varne 1980; Wheller *et al.* 1987; Stolz *et al.* 1990; Tatsumi *et al.* 1991; van Bergen *et al.* 1992; Edwards *et al.* 1994; Hoogewerff *et al.* 1997; Elburg & Foden 1998; Turner & Foden 2001; Elburg *et al.* 2003; Toya *et al.* 2005; Chadwick *et al.* 2007; Sendjaja *et al.* 2009; Takanashi *et al.* 2011
Izu-Bonin	Tatsumi *et al.* 1992; Taylor & Nesbitt 1998; Ishizuka et al. 2003, 2006; Shukuno *et al.* 2006; Tamura *et al.* 2007
Japan	Hickey & Frey 1982; Sakuyama & Nesbitt 1986; Togashi *et al.* 1992; Tamura 1994; Taylor *et al.* 1994; Ujike & Stix 2000; Kita *et al.* 2001; Sano *et al.* 2001; Kimura *et al.* 2002; Tamura *et al.* 2003; Moriguti *et al.* 2004; Toya *et al.* 2005; Shuto *et al.* 2004, 2006; Kuritani *et al.* 2005, 2008; Hirotani & Ban 2006; Kimura & Yoshida 2006; Ban *et al.* 2007; Ohba *et al.* 2007, 2009; Sato *et al.* 2007; Suzuki & Nakada 2007; Hoang *et al.* 2011; Takanashi *et al.* 2011
Kamchatka	Kepezhinskas *et al.* 1997; Dorendorf *et al.* 2000; Churikova *et al.* 2001; Ishikawa *et al.* 2001; Izbekov *et al.* 2004
Kuril	Zhuravlev *et al.* 1987; Nakagawa *et al.* 2002
Lau	Tian *et al.* 2008
Lesser Antilles	Brown *et al.* 1977; Thirlwall & Graham 1984; Smith *et al.* 1996; Thirlwall *et al.* 1996; Turner *et al.* 1996; Defant *et al.* 2001; Zellmer *et al.* 2003; Lindsay *et al.* 2005; Halama et al. 2006
Marianas	Hickey & Frey 1982; Hole *et al.* 1984; Reagan & Meijer 1984; Woodhead 1988; Bloomer 1987; Bloomer & Hawkins 1987; Bloomer *et al.* 1989; Elliott *et al.* 1997; Wade *et al.* 2005; Reagan *et al.* 2008
New Britain	Woodhead *et al.* 1998; Woodhead & Johnson 1993
New Caledonia	Cameron 1989
New Hebrides	Dupuy *et al.* 1982; Monzier *et al. 19*93, 1997
New Zealand (Northland, Taupo)	Cole 1981; Gamble *et al.* 1993; Huang *et al.* 2000; Schmitz & Smith 2004; Booden *et al.* 2011
Papua New Guinea	Hickey & Frey 1982
Philippines (Arayat, Bataan, Bicol, Luzon)	Defant *et al.* 1989, 1991b; Bau & Knittel 1993; Knittel *et al.* 1997; Castillo & Newhall 2004; McDermott *et al.* 2005; DuFrane *et al.* 2006
Ryukyu	Shinjo 1998, 1999; Shinjo *et al.* 2000
Solomon	Chadwick *et al.* 2009
South Shetland	Smellie 1983
Taiwan	Lai *et al.* 2008
Tonga-Kermadec	Bryan *et al.* 1972; Ewart & Bryan 1972; Ewart *et al.* 1977; Gamble *et al.* 1993, 1995; Haase *et al.* 2002; Smith *et al.* 2003; Wright *et al.* 2006; Hergt & Woodhead 2007
Vanuatu	Barsdell 1988; Barsdell & Berry 1990; Peate *et al.* 1997
Yap arc system	Ohara *et al.* 2002
	Continental arcs
Argentina	Déruelle 1982; Sruoga *et al.* 2005; Bruni *et al.* 2008
Antarctica	Kelly *et al.* 2008
Bolivia	Vezzoli *et al.* 2008
Chile	Saunders *et al.* 1979; López-Escobar *et al.* 1981, 1991, 1993; Déruelle 1982; Frey *et al.* 1984; Hickey *et al.* 1986; Kay *et al.* 1987, 1988; Davidson *et al.* 1988; Gerlach *et al.* 1988; Hickey-Vargas *et al.* 1989; de Silva 1991; Tormey *et al.* 1991; Vergara *et al.* 1991, 2004; Walker *et al.* 1991; Rodríguez *et al.* 2007; Vezzoli *et al.* 2008
Costa Rica	Reagan & Gill 1989; Chan *et al.* 1999; Alvarado *et al.* 2006; Bolge *et al.* 2006; Ryder *et al.* 2006
Ecuador	Bryant *et al.* 2006; Hidalgo *et al.* 2007; Robin *et al.* 2009; Samaniego *et al.* 2012

Table S1. (continued).

El Salvador	Carr 1984; González Partida *et al.* 1997; Rotolo & Castorina 1998; Chan *et al.* 1999; Agostini *et al.* 2006
Guatemala	Bardintzeff & Deniel 1992; Duffield *et al.* 1992; Chan *et al.* 1999; Walker *et al.* 2000; Cameron *et al.* 2002
Honduras	Walker *et al.* 2000
Mexico (Sierra Madre Occidental)	Albrecht & Goldstein 2000
Nicaragua	Sussman 1985; Hazlett 1987; Carr *et al.* 1990; Chan *et al.* 1999; Walker *et al.* 2001; Pardo *et al.* 2008
Panama	Defant *et al.* 1991a, 1991c
USA (Alaska, California, Oregon)	Reagan *et al.* 2003
	Continental rifts and break-up regions
Afar	Barberi *et al.* 1975; Deniel *et al.* 1994
Australia	Johnson *et al.* 1989; Price *et al.* 1997
China	Peng *et al.* 1986; Zhi *et al.* 1990; Basu *et al.* 1991; Fan & Hooper 1991; Liu *et al.* 1992; Chung *et al.* 1995; Zhang *et al.* 1995; Han *et al.* 1999; Ho *et al.* 2000; Hsu *et al.* 2000; Zou *et al.* 2000; Y.G. Xu *et al.* 2005
Ethiopia	Hart *et al.* 1989; Trua *et al.* 1999; Peccerillo *et al.* 2003, 2007; Ayalew *et al.* 2006; Rooney *et al.* 2007; Ronga *et al.* 2010
France	Chauvel & Jahn 1984
Germany	Haase *et al.* 2004
Kenya	Bell & Peterson 1991; Kampunzu & Mohr 1991; Macdonald *et al.* 1995, 2008; Kabeto *et al.* 2001; Le Roex *et al.* 2001; Rogers *et al.* 2004
Japan (Beppu-Shimbara graben)	Kita *et al.* 2001; Sakuyama *et al.* 2009
Mali and Morocco	Bertrand 1991
Mexico (Eastern Alkaline Province, Tepic-Zacoalco rift)	Nick 1988; Frey *et al.* 2007
New Zealand	Timm *et al.* 2009
Philippines	Arpa *et al.* 2008
Republic of Congo	de Mulder *et al.* 1986
Saudi Arabia	Camp *et al.* 1991
Sudan	Davidson & Wilson 1989
Tanzania	Paslick *et al.* 1995; Mollel *et al.* 2008; Fontijn *et al.* 2010
Turkey	Besang *et al.* 1977; Karsli *et al.* 2008
Uganda	Llyod *et al.* 1991
USA (Basin and Range, Colorado, Fish Canyon, Nevada, Rio Grande Rift)	Singer & Kudo 1986; Johnson & Lipman 1988; Moyer & Esperança 1989; Perry *et al.* 1990; Duncker *et al.* 1991; Fitton *et al.* 1991; Kempton *et al.* 1991; Gibson *et al.* 1992; Feuerbach *et al.* 1993; Potter 1996; Bachmann *et al.* 2002; McMillan *et al.* 2000; Parat *et al.* 2005; Maldonado *et al.* 2006; Brueseke & Hart 2009
Zaire	Auchapt *et al.* 1987
	Ocean islands
Atlantic (Tropic seamount)	Blum *et al.* 1996
Azores (Sao Miguel)	Turner *et al.* 1997; Beier *et al.* 2006
Bouvet	Verwoerd *et al.* 1976
Canary Islands (Granadilla, Gran Canaria, La Palma, Tenerife)	Palacz & Wolff 1989; Bryan 2006; Praegel & Holm 2006; Jutzeler *et al.* 2010
Cape Verde	Holm *et al.* 2006
French Polynesia (Cook-Austral)	Palacz & Saunders 1986

Table S1. (continued).

Hawaiian Islands	Feigenson *et al.* 1983; Spengler & Garcia 1988; Lipman *et al.* 1990; West *et al.* 1992; Frey *et al.* 1994; Cousens *et al.* 2003; G. Xu *et al.* 2005, 2007
Heard	Barling *et al.* 1994
Kerguelen	Weis *et al.* 1993
Madeira	Geldmacher & Hoernle 2000
Pitcairn	Hekinian *et al.* 2003
Réunion	Albarède *et al.* 1997
Socorro	Bohrson & Reid 1995, 1997
Collision	
Azerbaijan	Dilek *et al.* 2010
Greece	Seymore & Vlassopoulos 1992; Pe-Piper & Moulton 2008
India (Himalayas)	Reichardt *et al.* 2010
Indonesia (Sulawesi)	Elburg & Foden 1999; Elburg *et al.* 2003
Iran	Omrani *et al.* 2008
Italy	Bellieni *et al.* 1981; Dini *et al.* 2002; Cadoux & Pinti 2009
Pakistan (Karakorum)	Mahéo *et al.* 2009
Tibet	Arnaud *et al.* 1992; Chen *et al.* 2010
Turkey	Borsi *et al.* 1972; Innocenti & Mazzuoli 1972; Besang *et al.* 1977; Ercan *et al.* 1979, 1985, 1997; Ertürk 1990; Esder 1992; Güleç 1991; Seyitoglu *et al.* 1997; Aydar *et al.* 1998; Keskin *et al.* 1998; Temel *et al.* 1998; Aldanmaz *et al.* 2000; Delaloye & Bingol 2000; Ilbeyli *et al.* 2004; Innocenti *et al.* 2005; Aydin *et al.* 2008; Ekici *et al.* 2009; Agostini *et al.* 2010

Table S2. Number of samples in the training set of normally distributed discordant outlier-free database.

		Total number of samples		
Tectonic setting §	Group number §	Major elements	Major and trace elements	Trace elements
IA	1	1552	873	671
CA	2	726	340	301
CR	3	517	221	241
OI	4	277	77	136
Col	5	592	357	163
Sum	1–5	3664	1868	1512

§ IA = island arc (group number 1); CA = continental arc (group number 2); CR = continental rift (group number 3); OI = ocean island (group number 4); Col = collision (group number 5).

Table S3. Mean and standard deviation of adjusted major elements and log-transformed ratios for the 5 tectonic settings (IA, CA, CR, OI, and Col) for discordant outlier-free samples.

Original (wt.% or μg g^{-1}) or log_e-transformed ratio variable	IA (1) (n = 1552)		CA (2) (n = 726)		CR (3) (n = 517)		OI (4) (n = 277)		Col (5) (n = 592)	
	$\bar{x}$	s	$\bar{x}$	s	$\bar{x}$	s	$\bar{x}$	s	$\bar{x}$	s
$(SiO_2)_{adj}$	56.23	3.17	56.39	3.17	56.55	3.55	56.69	3.66	58.45	3.00
$(TiO_2)_{adj}$	0.838	0.217	0.862	0.276	1.48	0.66	1.46	0.77	0.938	0.317
$(Al_2O_3)_{adj}$	17.52	1.38	18.16	1.41	16.19	1.91	17.57	2.63	16.76	1.55
$(Fe_2O_3)_{adj}$	1.960	0.301	1.860	0.281	2.18	0.50	1.94	0.64	1.637	0.281
$(FeO_2)_{adj}$	6.15	1.15	5.81	1.10	6.03	1.78	5.19	2.48	4.47	0.92
$(MnO)_{adj}$	0.1664	0.0291	0.1489	0.0325	0.174	0.066	0.206	0.071	0.1135	0.0312
$(MgO)_{adj}$	4.41	1.76	4.02	1.30	3.69	2.41	2.74	2.61	3.84	1.74
$(CaO)_{adj}$	8.33	1.59	7.89	1.51	6.09	2.64	4.76	3.23	6.73	1.44
$(Na_2O)_{adj}$	3.15	0.65	3.50	0.57	4.27	1.50	5.50	2.08	3.43	0.74
$(K_2O)_{adj}$	1.06	0.65	1.14	0.66	2.89	1.89	3.57	2.25	3.25	1.63
$(P_2O_5)_{adj}$	0.189	0.102	0.220	0.077	0.438	0.321	0.379	0.350	0.383	0.256
$\ln(TiO_2/SiO_2)_{adj}$	−4.237	0.276	−4.227	0.328	−3.75	0.55	−3.85	0.72	−4.180	0.338
$\ln(Al_2O_3/SiO_2)_{adj}$	−1.168	0.108	−1.135	0.111	−1.256	0.120	−1.181	0.128	−1.252	0.107
$\ln(Fe_2O_3/SiO_2)_{adj}$	−3.367	0.180	−3.421	0.184	−3.285	0.283	−3.436	0.417	−3.588	0.197
$\ln(FeO_2/SiO_2)_{adj}$	−2.229	0.231	−2.289	0.239	−2.289	0.390	−2.52	0.60	−2.589	0.238
$\ln(MnO/SiO_2)_{adj}$	−5.836	0.190	−5.961	0.263	−5.843	0.350	−5.668	0.293	−6.278	0.291
$\ln(MgO/SiO_2)_{adj}$	−2.620	0.429	−2.696	0.388	−3.06	1.00	−3.55	1.14	−2.81	0.46
$\ln(CaO/SiO_2)_{adj}$	−1.928	0.252	−1.986	0.254	−2.38	0.69	−2.81	0.98	−2.183	0.257
$\ln(Na_2O/SiO_2)_{adj}$	−2.901	0.188	−2.790	0.139	−2.635	0.294	−2.415	0.394	−2.860	0.227
$\ln(K_2O/SiO_2)_{adj}$	−4.15	0.59	−4.04	0.50	−3.21	0.71	−3.14	1.02	−3.01	0.50
$\ln(P_2O_5/SiO_2)_{adj}$	−5.82	0.50	−5.598	0.326	−5.12	0.80	−5.49	1.12	−5.19	0.58

$\bar{x}$ = mean; s = standard deviation. The data are presented as rounded values obtained from the flexible rules summarized by Verma (2005).

Table S4. Test of equality of group means for 10 log_e-transformed major element ratio variables in the discordant outlier-free samples summarized in Table S3.

Variable	Wilks' lambda	F-ratio	Significance
$\ln(TiO_2/SiO_2)_{adj}$	0.2522	247.53	0.000000
$\ln(Al_2O_3/SiO_2)_{adj}$	0.2053	31.97	0.000000
$\ln(Fe_2O_3/SiO_2)_{adj}$	0.2016	14.75	0.000000
$\ln(FeO/SiO_2)_{adj}$	0.2061	35.77	0.000000
$\ln(MnO/SiO_2)_{adj}$	0.2240	118.15	0.000000
$\ln(MgO/SiO_2)_{adj}$	0.2002	8.43	0.000001
$\ln(CaO/SiO_2)_{adj}$	0.2121	63.20	0.000000
$\ln(Na_2O/SiO_2)_{adj}$	0.2096	51.75	0.000000
$\ln(K_2O/SiO_2)_{adj}$	0.2159	80.81	0.000000
$\ln(P_2O_5/SiO_2)_{adj}$	0.2053	31.83	0.000000

Wilks' lambda (U-statistic) and F-ratio with degree of freedom df1 = v1 = g – 1 = 5 – 1 = 4 and df2 = v2 = n – g = 3664 – 5 = 3659, where g is the number of groups and n is total number of samples.

Table S5. Assessment of correct discrimination (success rate %) of 4 tectonic settings from the set of 5 diagrams based on major elements.

Actual affinity	Discrimination diagram (Figures 1a–1e) §	Total no. of samples	Predicted tectonic affinity and number of discriminated samples (%)				
			IA+CA (1+2)	IA (1)	CA (2)	CR+OI (3+4)	Col (5)
IA (1)	1+2-3+4-5	1552	***1398*** (90.1)	---	---	61 (3.9)	93 (6.0)
IA (1)	1-2-3+4	1552	---	***1106*** (71.3)	380 (24.5)	66 (4.2)	---
IA (1)	1-2-5	1552	---	***1072*** (69.1)	407 (26.2)	---	73 (4.7)
IA (1)	1-3+4-5	1552	---	***1383*** (89.1)	---	71 (4.6)	98 (6.3)
IA (1)	2-3+4-5*	1552	---	---	1311 (84.5)	117 (7.5)	124 (8.0)
CA (2)	1+2-3+4-5	726	***576*** (79.3)	---	---	50 (6.9)	100 (13.8)
CA (2)	1-2-3+4	726	---	148 (20.4)	***526*** (72.5)	52 (7.1)	---
CA (2)	1-2-5	726	---	158 (21.8)	***502*** (69.1)	---	66 (9.1)
CA (2)	1-3+4-5*	726	---	530 (73.0)	---	61 (8.4)	135 (18.6)
CA (2)	2-3+4-5	726	---	---	***581*** (80.0)	57 (7.9)	88 (12.1)
CR (3)	1+2-3+4-5	517	62 (12.0)	---	---	***371*** (72.1)	82 (15.9)
CR (3)	1-2-3+4	517	---	51 (9.9)	70 (13.5)	***396*** (76.6)	---
CR (3)	1-2-5*	517	---	206 (39.8)	128 (24.8)	---	183 (35.4)
CR (3)	1-3+4-5	517	---	53 (10.3)	---	***388*** (75.0)	76 (14.7)
CR (3)	2-3+4-5	517	---	---	64 (12.4)	***368*** (71.2)	85 (16.4)
OI (4)	1+2-3+4-5	277	7 (2.5)	---	---	***267*** (96.4)	3 (1.1)
OI (4)	1-2-3+4	277	---	6 (2.1)	11 (4.0)	***260*** (93.9)	---
OI (4)	1-2-5*	277	---	149 (53.8)	82 (29.6)	---	46 (16.6)
OI (4)	1-3+4-5	277	---	9 (3.2)	---	***263*** (95.0)	5 (1.8)
OI (4)	2-3+4-5	277	---	---	7 (2.5)	***266*** (96.0)	4 (1.5)
Col (5)	1+2-3+4-5	592	54 (9.1)	---	---	24 (4.1)	***514*** (86.8)
Col (5)	1-2-3+4*	592	---	147 (24.8)	273 (46.1)	172 (29.1)	---
Col (5)	1-2-5	592	---	30 (5.1)	57 (9.6)	---	***505*** (85.3)
Col (5)	1-3+4-5	592	---	51 (8.6)	---	28 (4.7)	***513*** (86.7)
Col (5)	2-3+4-5	592	---	---	59 (10.0)	26 (4.4)	***507*** (85.6)

§ The groups discriminated in discriminant-function-based multidimensional diagrams are as follows: island arc (group 1–IA), continental arc (group 2–CA), continental rift (group 3–CR), ocean island (group 4–OI), and collision (group 5–Col); the numbers in the parentheses are the percentages of samples plotting in a given field and the correct discrimination can be seen in the column with italic boldface numbers; *: inapplicable diagram.

Table S6. Mean and standard deviation of major and trace elements as well as log-transformed ratios for the 5 tectonic settings (IA, CA, CR, OI, and Col) for discordant outlier-free samples.

Original (wt.% or μg g^{-1}) or log_e-transformed ratio variable	IA (1) (n = 873)		CA (2) (n = 340)		CR (3) (n = 221)		OI (4) (n = 77)		Col (5) (n = 357)	
	$\bar{x}$	s	$\bar{x}$	s	$\bar{x}$	s	$\bar{x}$	s	$\bar{x}$	s
$(TiO_2)_{adj}$	0.846	0.249	0.808	0.278	1.64	0.50	2.134	0.256	0.971	0.329
$(MgO)_{adj}$	4.58	1.81	4.386	1.203	5.14	2.10	6.26	2.00	3.95	1.76
$(P_2O_5)_{adj}$	0.188	0.108	0.210	0.072	0.455	0.276	0.376	0.227	0.380	0.249
Nb	4.19	3.54	4.04	2.85	23.9	17.8	27.1	35.5	17.1	9.0
Ni	36	58	33.0	23.9	81	64	111	64	56	72
V	211	73	176	51	165	62	216	63	142.2	37.5
Y	23.6	7.6	18.2	5.1	30.1	11.5	27.1	10.8	24.5	7.5
Zr	96	47	89.7	38.1	220	111	231	173	254	198
$ln(MgO/TiO_2)_{adj}$	1.65	0.48	1.703	0.316	1.08	0.54	1.00	0.47	1.368	0.396
$ln(P_2O_5/TiO_2)_{adj}$	–1.598	0.435	–1.341	0.254	–1.39	0.48	–1.86	0.47	–1.045	0.383
$ln(Nb/(TiO_2)_{adj})$	–7.89	0.82	–7.66	0.49	–6.71	0.53	–7.25	0.94	–6.410	0.367
$ln(Ni/(TiO_2)_{adj})$	–6.12	1.27	–5.81	0.93	–5.84	1.30	–5.67	1.27	–5.67	0.99
$ln(V/(TiO_2)_{adj})$	–3.713	0.356	–3.822	0.251	–4.62	0.46	–4.651	0.408	–4.208	0.290
$ln(Y/(TiO_2)_{adj})$	–5.894	0.291	–6.078	0.272	–6.319	0.403	–6.715	0.293	–5.967	0.356
$ln(Zr/(TiO_2)_{adj})$	–4.541	0.432	–4.538	0.342	–4.38	0.48	–4.71	0.55	–3.770	0.403

$\bar{x}$ = mean; s = standard deviation. The data are presented as rounded values obtained from the flexible rules summarized by Verma (2005).

Table S7. Test of equality of group means for 7 log_e-transformed major and trace element ratio variables in the discordant outlier-free samples summarized in Table S6.

Element	Wilks' lambda	F-ratio	Significance
$ln(MgO/TiO_2)_{adj}$	0.2119	25.1	0.000000
$ln(P_2O_5/TiO_2)_{adj}$	0.2268	59.5	0.000000
$ln(Nb/(TiO_2)_{adj})$	0.2354	79.4	0.000000
$ln(Ni/(TiO_2)_{adj})$	0.2156	33.7	0.000000
$ln(V/(TiO_2)_{adj})$	0.2391	88.0	0.000000
$ln(Y/(TiO_2)_{adj})$	0.2139	29.8	0.000000
$ln(Zr/(TiO_2)_{adj})$	0.2298	66.4	0.000000

Wilks' lambda (U-statistic) and F-ratio with degree of freedom df1 = ν1 = g – 1 = 5 – 1 = 4 and df2 = ν2 = n – g = 1868 – 5 = 1863, where g is the number of groups and n is total number of samples.

Table S8. Assessment of correct discrimination (success rate %) of 4 tectonic settings from the set of 5 diagrams based on immobile major and trace elements.

Actual affinity	Discrimination diagram (Figures 2a–2e) §	Total no. of samples	Predicted tectonic affinity and number of discriminated samples (%)				
			IA+CA (1+2)	IA (1)	CA (2)	CR+OI (3+4)	Col (5)
IA (1)	1+2-3+4-5	873	***753*** (86.3)	---	---	17 (1.9)	103 (11.8)
IA (1)	1-2-3+4	873	---	***615*** (70.4)	156 (17.9)	102 (11.7)	---
IA (1)	1-2-5	873	---	***548*** (62.8)	220 (25.2)	---	105 (12.0)
IA (1)	1-3+4-5	873	---	***746*** (85.5)	---	15 (1.7)	112 (12.8)
IA (1)	2-3+4-5*	873	---	---	727 (83.3)	22 (2.5)	124 (14.2)
CA (2)	1+2-3+4-5	340	***301*** (88.5)	---	---	7 (2.1)	32 (9.4)
CA (2)	1-2-3+4	340	---	54 (15.9)	***278*** (81.8)	8 (2.3)	---
CA (2)	1-2-5	340	---	60 (17.6)	***259*** (76.2)	---	21 (6.2)
CA (2)	1-3+4-5*	340	---	284 (83.5)	---	13 (3.9)	43 (12.6)
CA (2)	2-3+4-5	340	---	---	***322*** (94.7)	4 (1.2)	14 (4.1)
CR (3)	1+2-3+4-5	221	20 (9.0)	---	---	***161*** (72.9)	40 (18.1)
CR (3)	1-2-3+4	221	---	14 (6.3)	32 (14.5)	***175*** (79.2)	---
CR (3)	1-2-5*	221	---	11 (4.9)	47 (21.3)	---	163 (73.8)
CR (3)	1-3+4-5	221	---	19 (8.6)	---	***164*** (74.2)	38 (17.2)
CR (3)	2-3+4-5	221	---	---	21 (9.5)	***161*** (72.9)	39 (17.6)
OI (4)	1+2-3+4-5	77	0 (0.0)	---	---	***77*** (100.0)	0 (0.0)
OI (4)	1-2-3+4	77	---	0 (0.0)	0 (0.0)	***77*** (100.0)	---
OI (4)	1-2-5*	77	---	4 (5.2)	54 (70.3)	---	19 (24.5)
OI (4)	1-3+4-5	77	---	0 (0.0)	---	***76*** (98.7)	1 (0.3)
OI (4)	2-3+4-5	77	---	0 (0.0)	---	***76*** (98.7)	1 (0.3)
Col (5)	1+2-3+4-5	357	16 (4.5)	---	---	19 (5.3)	***322*** (90.2)
Col (5)	1-2-3+4*	357	---	100 (28.0)	154 (43.1)	103 (28.9)	---
Col (5)	1-2-5	357	---	11 (3.1)	15 (4.2)	---	***331*** (92.7)
Col (5)	1-3+4-5	357	---	16 (4.5)	---	19 (5.3)	***322*** (90.2)
Col (5)	2-3+4-5	357	---	---	14 (3.9)	19 (5.3)	***324*** (90.8)

For more explanation, see footnote of Table S5.

Table S9. Mean and standard deviation of trace elements and log-transformed ratios for discordant outlier-free samples.

Original (μg g^{-1}) or $\log_e$-transformed ratio variable	IA (1) (n = 671)		CA (2) (n = 301)		CR (3) (n = 241)		OI (4) (n = 136)		Col (5) (n = 163)	
	$\bar{x}$	s	$\bar{x}$	s	$\bar{x}$	s	$\bar{x}$	s	$\bar{x}$	s
Yb	2.40	0.81	1.90	0.66	3.93	3.01	3.71	2.11	2.14	0.75
La	9.9	6.5	11.5	4.8	59	57	82	63	48.2	29.6
Ce	21.8	12.7	25.0	9.9	111	105	150	105	92	53
Sm	3.40	1.27	3.47	1.07	9.2	5.7	10.5	5.9	6.90	3.23
Nb	3.36	2.68	3.92	2.74	71	97	135	124	16.4	10.7
Th	2.28	2.42	1.67	1.20	10.7	11.0	13.0	14.1	18.0	18.0
Y	23.8	8.0	19.5	6.5	45.8	37.6	43.2	22.2	24.9	8.2
Zr	89.9	43.4	86.0	41.3	363	355	680	499	208	113
ln(La/Yb)	1.27	0.60	1.787	0.381	2.51	0.56	2.76	0.80	2.97	0.63
ln(Ce/Yb)	2.10	0.52	2.571	0.328	3.18	0.56	3.48	0.63	3.63	0.61
ln(Sm/Yb)	0.332	0.253	0.613	0.180	0.897	0.324	1.030	0.333	1.113	0.437
ln(Nb/Yb)	0.09	0.80	0.66	0.49	2.30	0.98	3.02	1.05	1.89	0.63
ln(Th/Yb)	–0.45	0.93	–0.25	0.48	0.77	0.64	0.42	1.40	1.76	0.90
ln(Y/Yb)	2.291	0.115	2.333	0.093	2.476	0.195	2.480	0.169	2.451	0.156
ln(Zr/Yb)	3.568	0.387	3.767	0.309	4.38	0.57	5.02	0.58	4.50	0.49

$\bar{x}$ = mean; s = standard deviation. The data are presented as rounded values obtained from the flexible rules summarized by Verma (2005).

Table S10. Test of equality of group means for 10 $\log_e$-transformed trace element ratio variables in the discordant outlier-free samples summarized in Table S9.

Element	Wilks' lambda	F-ratio	Significance
ln(La/Yb)	0.1466	5.0	0.000490
ln(Ce/Yb)	0.1475	7.3	0.000008
ln(Sm/Yb)	0.1496	12.7	0.000000
ln(Nb/Yb)	0.1986	140.0	0.000000
ln(Th/Yb)	0.1892	115.6	0.000000
ln(Y/Yb)	0.1515	17.8	0.000000
ln(Y/Yb)	0.1691	63.5	0.000000

Wilks' lambda (U-statistic) and univariate-ratio with degree of freedom df1 = ν1 = g – 1 = 5 – 1 = 4 and df2 = ν2 = n – g = 1512 – 5 = 1507, where g is the number of groups and n is total number of samples.

Table S11. Assessment of correct discrimination (success rate %) of 4 tectonic settings from the set of 5 diagrams based on immobile trace elements.

Actual affinity	Discrimination diagram (Figures 3a–3e) §	Total no. of samples	Predicted tectonic affinity and number of discriminated samples (%)				
			IA+CA (1+2)	IA (1)	CA (2)	CR+OI (3+4)	Col (5)
IA (1)	1+2-3+4-5	671	***613*** (91.4)	---	---	33 (4.9)	25 (3.7)
IA (1)	1-2-3+4	671	---	***508*** (75.7)	144 (21.5)	19 (2.8)	---
IA (1)	1-2-5	671	---	***488*** (72.7)	163 (24.3)	---	20 (3.0)
IA (1)	1-3+4-5	671	---	***606*** (90.3)	---	37 (5.5)	28 (4.2)
IA (1)	2-3+4-5*	671	---	---	623 (92.8)	26 (3.9)	22 (3.3)
CA (2)	1+2-3+4-5	301	***272*** (90.4)	---	---	10 (3.3)	19 (6.3)
CA (2)	1-2-3+4	301	---	95 (31.6)	***198*** (65.8)	8 (2.6)	---
CA (2)	1-2-5	301	---	95 (31.6)	***194*** (64.5)	---	12 (3.9)
CA (2)	1-3+4-5*	301	---	262 (87.0)	---	15 (5.0)	24 (8.0)
CA (2)	2-3+4-5	301	---	---	***288*** (95.7)	9 (3.0)	4 (1.3)
CR (3)	1+2-3+4-5	241	16 (6.6)	---	---	***179*** (74.3)	46 (19.1)
CR (3)	1-2-3+4	241	---	7 (2.9)	40 (16.6)	***194*** (80.5)	---
CR (3)	1-2-5*	241	---	19 (7.9)	61 (25.3)	---	161 (66.8)
CR (3)	1-3+4-5	241	---	17 (7.0)	---	***180*** (74.7)	44 (18.3)
CR (3)	2-3+4-5	241	---	---	24 (9.9)	***179*** (74.3)	38 (15.8)
OI (4)	1+2-3+4-5	136	0 (0.0)	---	---	***136*** (100.0)	0 (0.0)
OI (4)	1-2-3+4	136	---	0 (0.0)	0 (0.0)	***136*** (100.0)	---
OI (4)	1-2-5*	136	---	1 (0.7)	54 (39.7)	---	81 (59.6)
OI (4)	1-3+4-5	136	---	0 (0.0)	0 (0.0)	***136*** (100.0)	---
OI (4)	2-3+4-5	136	---	7 (5.1)	---	***128*** (94.1)	1 (0.8)
Col (5)	1+2-3+4-5	163	17 (10.4)	---	---	14 (8.6)	***132*** (81.0)
Col (5)	1-2-3+4*	163	---	13 (8.0)	76 (46.6)	74 (45.4)	---
Col (5)	1-2-5	163	---	11 (6.8)	15 (9.2)	---	***137*** (84.0)
Col (5)	1-3+4-5	163	---	12 (7.3)	---	13 (8.0)	***138*** (84.7)
Col (5)	2-3+4-5	163	---	---	17 (10.4)	14 (8.6)	***132*** (81.0)

For more explanation, see footnote of Table S5.

Table S12. Evaluation of the new multidimensional diagrams from Pleistocene (Quaternary) intermediate magmas from the Ijen volcanic complex, eastern Java, Indonesia (island arc setting).

Figure name §	Figure type §	Total number of samples	Number of discriminated samples				
			Arc			Within-plate	Collision
			IA+CA [$\overline{x} \pm s$] (p_{IA+CA}) Θ	IA [$\overline{x} \pm s$] [p_{IA}] Θ	CA [$\overline{x} \pm s$] [p_{CA}] Θ	CR+OI [$\overline{x} \pm s$] [p_{CR+OI}] Θ	Col [$\overline{x} \pm s$] [p_{Col}] Θ
Major elements	1+2-3+4-5	30	***22*** [0.732 ± 0.181] (0.5010–0.9925)	---	---	3 [0.743 ± 0.122] (0.6157–0.8597)	5 [0.622 ± 0.131] (0.4832–0.8280)
	1-2-3+4	30	---	***22*** [0.547 ± 0.108] (0.3754–0.7278)	5 [0.603 ± 0.086] (0.5403–0.7452)	3 [0.694 ± 0.125] (0.5914–0.8333)	---
	1-2-5	30	---	***13*** [0.584 ± 0.134] (0.3636–0.8590)	13 [0.557 ± 0.083] (0.4594–0.7058)	---	4 [0.457 ± 0.076] (0.3956–0.5657)
	1-3+4-5	30	---	***21*** [0.763 ± 0.174] (0.5218–0.9884)	---	3 [0.690 ± 0.106] (0.6089–0.8096)	6 [0.588 ± 0.152] (0.4853–0.8943)
	2-3+4-5 *	30	---	---	20 [0.711 ± 0.153] (0.4570–0.9278)	3 [0.738 ± 0.214] (0.4917–0.8649)	7 [0.611 ± 0.129] (0.4887–0.8799)
All major element-based diagrams	**{Σn} {Σprob} [%prob]**	**{150}**	**{22} {16.1099} [---]**	**{56} {35.6611} [46.3%]**	**{38} {24.5093} [31.8%]**	**{12} {8.5942} [8.8%]**	**{22} {12.7441} [13.1%]**
Major and trace elements	1+2-3+4-5	28	***23*** [0.780 ± 0.156] (0.5001–0.9935)	---	---	0	5 [0.687 ± 0.134] (0.5519–0.9047)
	1-2-3+4	28	---	***19*** [0.628 ± 0.125] (0.5013–0.9463)	9 [0.581 ± 0.045] (0.4916–0.6405)	0	---
	1-2-5	28	---	***13*** [0.462 ± 0.055] (0.4062–0.5810)	9 [0.550 ± 0.059] (0.4579–0.6339)	---	6 [0.569 ±0.135] (0.4345–0.7984)
	1-3+4-5	28	---	***24*** [0.755 ± 0.146] (0.5251–0.9496)	---	0	4 [0.648 ± 0.124] (0.5270–0.7958)
	2-3+4-5 *	28	---	---	22 [0.879 ± 0.134] (0.5296–0.9972)	0	6 [0.697 ± 0.179] (0.5256–0.9818)
All major and trace element-based diagrams	**{Σn} {Σprob} [%prob]**	**{140}**	**{23} {17.9474} [---]**	**{56} {36.0589} [47.3%]**	**{40} {29.5188} [38.7%]**	**{0} {0.0} [0%]**	**{21} {13.6219} [14.0%]**
Trace elements	1+2-3+4-5	28	***21*** [0.601 ± 0.121] (0.4595–0.8424)	---	---	0	7 [0.4975 ± 0.0281] (0.5519–0.9047)
	1-2-3+4	28	---	***17*** [0.534 ± 0.047] (0.4616–0.6314)	10 [0.588 ± 0.091] (0.4500–0.6973)	0	---
	1-2-5	28	---	***16*** [0.441 ± 0.046] (0.3730–0.5461)	10 [0.501 ± 0.068] (0.4011–0.6168)	---	2 [0.406 ± 0.067] (0.3581–0.4535)
	1-3+4-5	28	---	***24*** [0.575 ± 0.080] (0.4795–0.7795)	---	0	4 [0.4888 ± 0.0111] (0.4752–0.5021)
	2-3+4-5 *	28	---	---	19 [0.612 ± 0.137] (0.4348–0.9021)	0	9 [0.483 ± 0.050] (0.4424–0.6001)
All trace element-based diagrams	**{Σn} {Σprob} [%prob]**	**{140}**	**{21} {12.6207} [---]**	**{57} {29.9301} [48.6%]**	**{40} {23.1159} [37.5%]**	**{0} {0.0} [0%]**	**{22} {10.5924} [13.9%]**

§ "Figure name" corresponds to 1 of the 3 sets of diagrams based on major elements, immobile major and trace elements, and immobile trace elements, respectively, whereas "Figure type" gives the tectonic fields being discriminated where the tectonic group numbers are as follows: 1–IA (island arc), 2–CA (continental arc), 3–CR (continental rift) and 4–OI (ocean island) together as within-plate, and 5–Col (collision); $\overline{x} \pm s$ = mean ± 1 standard deviation of the probability estimates for all samples discriminated in a given tectonic setting reported in square brackets; Θ = probability estimates for different tectonic groups are summarized after the number of discriminated samples as follows: [p_{IA+CA}]–range of probability values estimated for IA+CA combined setting, [p_{IA}]–for IA, [p_{CA}]–for CA, [p_{CR+OI}]–for CR+OI, and [p_{Col}]–for Col. Boldface italic font shows the expected or more probable tectonic setting; *: inapplicable diagram identified whenever it is clearly established, although this diagram is used in the overall total number of samples and probability estimates (see the next explanation); the final row gives a synthesis of results as **{Σn} {Σprob} [%prob]** where **{Σn}** = number of samples plotting in all 5 diagrams reported in the column of total number of samples, whereas the sum of samples plotting in a given tectonic field are reported in the respective tectonic field column; **{Σprob}** = sum of probability values for all samples plotting in a given tectonic field reported in the respective tectonic field column; **[%prob]** = total probability of a given tectonic setting expressed in percent after assigning the probability of IA+CA to IA and CA (using weighing factors explained in the text).

Table S13. Evaluation of the new multidimensional diagrams from Pleistocene (Quaternary) intermediate magmas from the Huequi volcano, Chile (continental arc setting).

Figure name §	Figure type §	Total number of samples	Number of discriminated samples				
			Arc			Within-plate	Collision
			IA+CA [$\overline{x} \pm s$] (p_{IA+CA}) Θ	IA [$\overline{x} \pm s$] [p_{IA}] Θ	CA [$\overline{x} \pm s$] [p_{CA}] Θ	CR+OI [$\overline{x} \pm s$] [p_{CR+OI}] Θ	Col [$\overline{x} \pm s$] [p_{Col}] Θ
Major elements	1+2-3+4-5	9	***9*** [0.915 ± 0.075] (0.8008–0.9949)	---	---	0	0
	1-2-3+4	9	---	1 [---] (0.4989)	***8*** [0.785 ± 0.165] (0.5573–0.9111)	0	---
	1-2-5	9	---	1 [---] (0.5286)	***8*** [0.756 ± 0.157] (0.5491–0.8787)	---	0
	1-3+4-5 *	9	---	9 [0.839 ± 0.156] (0.5850–0.9970)	---	0	0
	2-3+4-5	9	---	---	***9*** [0.942 ± 0.050] (0.8244–0.9877)	0	0
All major element-based diagrams	**{Σn} {Σprob} [%prob]**	**{45}**	**{9} {8.2361} [---]**	**{11} {8.5774} [29.2%]**	**{25} {20.8001} [70.8%]**	**{0} {0} [0%]**	**{0} {0} [0%]**
Major and trace elements	1+2-3+4-5	9	***8*** [0.805 ± 0.115] (0.6486–0.9461)	---	---	0	1 [---] (0.4585)
	1-2-3+4	9	---	0	***9*** [0.587 ± 0.054] (0.5035–0.7050)	0	---
	1-2-5	9	---	0	***8*** [0.534 ± 0.095] (0.4081–0.7075)	---	1 [---] (0.4952)
	1-3+4-5 *	9	---	9 [0.737 ± 0.150] (0.4444–0.9169)	---	0	0
	2-3+4-5	9	---	---	***9*** [0.859 ± 0.150] (0.5246–0.9832)	0	0
All major and trace element-based diagrams	**{Σn} {Σprob} [%prob]**	**{45}**	**{8} {6.4391} [---]**	**{9} {6.6362} [26.9%]**	**{26} {17.2886} [70.1%]**	**{0} {0} [0%]**	**{2} {0.9537} [3.0%]**

For more explanation, see footnote of Table S12.

Table S14. Evaluation of the new multidimensional diagrams from Pliocene-Holocene (Quaternary) intermediate magmas from the Kilimanjaro volcano, Tanzania (continental rift setting).

Figure name §	Figure type §	Total number of samples	Number of discriminated samples				
			Arc			Within-plate	Collision
			IA+CA [$\overline{x} \pm s$] (p_{IA+CA}) Θ	IA [$\overline{x} \pm s$] [p_{IA}] Θ	CA [$\overline{x} \pm s$] [p_{CA}] Θ	CR+OI [$\overline{x} \pm s$] [p_{CR+OI}] Θ	Col [$\overline{x} \pm s$] [p_{Col}] Θ
Major elements	1+2-3+4-5	34	0	---	---	***34*** [0.9974 ± 0.0018] (0.9943–0.9998)	0
	1-2-3+4	34	---	0	0	***34*** [0.9948 ± 0.0049] (0.9838–0.9998)	---
	1-2-5 *	34	---	0	***34*** [0.787 ± 0.092] (0.5999–0.9409)	---	0
	1-3+4-5	34	---	0	---	***34*** [0.9965 ± 0.0024] (0.9910–0.9996)	0
	2-3+4-5	34	---	---	0	***34*** [0.9874 ± 0.0076] (0.9703–0.9989)	0
All major element-based diagrams	**{Σn} {Σprob} [%prob]**	**{170}**	**{0} {0} [0%]**	**{0} {0} [0%]**	**{34} {26.7449} [16.5%]**	**{136} {135.1858} [83.5%]**	**{0} {0} [0%]**
Major and trace elements	1+2-3+4-5	23	0	---	---	***23*** [0.9968 ± 0.0060] (0.9756–1.0000)	0
	1-2-3+4	23	---	0	0	***23*** [1.0000 ± 0.0000] (1.0000–1.0000)	---
	1-2-5 *	23	---	0	0	---	***23*** [0.9998 ± 0.0002] (0.9992–1.0000)
	1-3+4-5	23	---	0	---	***23*** [0.9949 ± 0.0092] (0.9635–1.0000)	0
	2-3+4-5	23	---	---	0	***23*** [0.9874 ± 0.0234] (0.9093–1.0000)	0
All major and trace element-based diagrams	**{Σn} {Σprob} [%prob]**	**{115}**	**{0} {0} [0%]**	**{0} {0} [0%]**	**{0} {0} [0%]**	**{92} {91.5175} [79.9%]**	**{23} {22.9961} [20.1%]**
Trace elements	1+2-3+4-5	34	0	---	---	***34*** [0.9908 ± 0.0139] (0.9358–0.9999)	0
	1-2-3+4	34	---	0	0	***34*** [0.9988 ± 0.0025] (0.9870–1.0000)	---
	1-2-5 *	34	---	0	4 [0.863 ± 0.142] (0.6653–0.9756)	---	30 [0.965 ± 0.048] (0.8178–0.9978)
	1-3+4-5	34	---	0	---	***34*** [0.9868 ± 0.0174] (0.9189–1.0000)	0
	2-3+4-5	34	---	---	0	***34*** [0.9842 ± 0.0185] (0.9097–0.9985)	0
All trace element-based diagrams	**{Σn} {Σprob} [%prob]**	**{170}**	**{0} {0} [0%]**	**{0} {0} [0%]**	**{4} {3.4522} [2.1%]**	**{133} {131.7091} [80.3%]**	**{30} {28.9438} [17.6%]**

For more explanation, see footnote of Table S12.

Table S15. Evaluation of the new multidimensional diagrams from Pleistocene-Holocene (Quaternary) intermediate magmas from the Canary Islands (ocean island setting).

Figure name §	Figure type §	Total number of samples	Number of discriminated samples				
			Arc			Within-plate	Collision
			IA+CA [$\overline{x} \pm s$] (p_{IA+CA}) Θ	IA [$\overline{x} \pm s$] [p_{IA}] Θ	CA [$\overline{x} \pm s$] [p_{CA}] Θ	CR+OI [$\overline{x} \pm s$] [p_{CR+OI}] Θ	Col [$\overline{x} \pm s$] [p_{Col}] Θ
Major elements	1+2-3+4-5	5	0	---	---	***5*** [0.9959 ± 0.0041] (0.9886–0.9982)	0
	1-2-3+4	5	---	0	0	***5*** [0.9883 ± 0.0168] (0.9586–0.9977)	---
	1-2-5 *	5	---	1 [---] (0.7600)	4 [0.554 ± 0.143] (0.4737–0.7683)	---	0
	1-3+4-5	5	---	0	---	***5*** [0.9937 ± 0.0070] (0.9813–0.9976)	0
	2-3+4-5	5	---	---	0	***5*** [0.9878 ±0.0051] (0.9788–0.9911)	0
All major element-based diagrams	**{Σn} {Σprob} [%prob]**	**{25}**	**{0} {0} [0%]**	**{1} {0.7600} [3.3%]**	**{4} {2.2165} [9.7%]**	**{20} {19.8285} [87.0%]**	**{0} {0} [0%]**
Major and trace elements	1+2-3+4-5	5	0	---	---	4 [0.679 ± 0.196] (0.5381–0.9633)	1 [---] (0.9859)
	1-2-3+4	5	---	0	0	***5*** [1.0000 ± 0.0000] (1.0000–1.0000)	---
	1-2-5	5	---	0	0	---	5 [1.0000 ± 0.0000] (1.0000–1.0000)
	1-3+4-5	5	---	0	---	2 [0.726 ± 0.293] (0.5183–0.9331)	3 [0.711 ± 0.243] (0.5545–0.9901)
	2-3+4-5	5	---	---	0	1 [---] (0.9344)	4 [0.689 ± 0.209] (0.5178–0.9938)
All major and trace element-based diagrams	**{Σn} {Σprob} [%prob]**	**{25}**	**{0} {0} [0%]**	**{0} {0} [0%]**	**{0} {0} [0%]**	**{12} {10.1008} [48.2%]**	**{13} {10.8758} [51.8%]**
Trace elements	1+2-3+4-5	5	0	---	---	***5*** [0.9745 ± 0.0106] (0.9639–0.9908)	0
	1-2-3+4	5	---	0	0	***5*** [0.9986 ± 0.0011] (0.9976–0.9998)	---
	1-2-5 *	5	---	0	0	---	5 [0.9871 ± 0.0066] (0.9817–0.9983)
	1-3+4-5	5	---	0	---	***5*** [0.9639 ± 0.0137] (0.9509–0.9851)	0
	2-3+4-5	5	---	---	0	***5*** [0.9167 ± 0.0394] (0.8875–0.9852)	0
All trace element-based diagrams	**{Σn} {Σprob} [%prob]**	**{25}**	**{0} {0} [0%]**	**{0} {0} [0%]**	**{0} {0} [0%]**	**{20} {19.2690} [79.6%]**	**{5} {4.9356} [20.4%]**

For more explanation, see footnote of Table S12.

Table S16. Evaluation of the new multidimensional diagrams from Miocene (Neogene) ultrapotassic intermediate magmas from southern and southwestern Tibet (collision setting).

Figure name §	Figure type §	Total number of samples	Number of discriminated samples				
			Arc			Within-plate	Collision
			IA+CA [$\overline{x} \pm s$] (p_{IA+CA}) Θ	IA [$\overline{x} \pm s$] [p_{IA}] Θ	CA [$\overline{x} \pm s$] [p_{CA}] Θ	CR+OI [$\overline{x} \pm s$] [p_{CR+OI}] Θ	Col [$\overline{x} \pm s$] [p_{Col}] Θ
	1+2-3+4-5	54	0	---	---	2 [0.571 ± 0.061] (0.5281–0.6145)	***52*** [0.9858 ± 0.0200] (0.9180–0.9995)
	1-2-3+4 *	54	---	0	0	54 [0.9809 ± 0.0229] (0.8785–0.9998)	---
Major elements	1-2-5	54	---	0	0	---	***54*** [0.9965 ± 0.0083] (0.9547–1.0000)
	1-3+4-5	54	---	0	---	2 [0.595 ± 0.098] (0.5256–0.6642)	***52*** [0.9780 ± 0.0286] (0.8842–0.9993)
	2-3+4-5	54	---	---	0	1 [---] (0.5017)	***53*** [0.971 ± 0.060] (0.5749–0.9976)
All major element-based diagrams	**{Σn} {Σprob} [%prob]**	**{270}**	**{0} {0} [0%]**	**{0} {0} [0%]**	**{0} {0} [0%]**	**{59} {55.8040} [21.2%]**	**{211} {207.3658} [78.8%]**
	1+2-3+4-5	54	0	---	---	0	***54*** [0.9819 ± 0.0240] (0.8759–0.9996)
	1-2-3+4 *	54	---	0	11 [0.635 ± 0.071] (0.5163–0.7466)	43 [0.769 ± 0.155] (0.4964–0.9902)	---
Major and trace elements	1-2-5	54	---	0	0	---	***54*** [0.9901 ± 0.0125] (0.9536–1.0000)
	1-3+4-5	54	---	0	---	0	***54*** [0.9753 ± 0.0330] (0.8366–0.9995)
	2-3+4-5	54	---	---	0	0	***54*** [0.9819 ± 0.0263] (0.8598–0.9996)
All major and trace element-based diagrams	**{Σn} {Σprob} [%prob]**	**{270}**	**{0} {0} [0%]**	**{0} {0} [0%]**	**{11} {6.9832} [2.8%]**	**{43} {33.0767} [13.1%]**	**{216} {212.1850} [84.1%]**
	1+2-3+4-5	54	0	---	---	0	***54*** [0.9973 ± 0.0046] (0.9818–1.0000)
	1-2-3+4 *	54	---	0	0	54 [0.9997 ± 0.0006] (0.9963–1.0000)	---
Trace elements	1-2-5	54	---	0	0	---	***54*** [1.0000 ± 0.0000] (1.0000–1.0000)
	1-3+4-5	54	---	0	---	0	***54*** [0.9942 ± 0.0095] (0.9679–1.0000)
	2-3+4-5	54	---	---	0	0	***54*** [0.9939 ± 0.0099] (0.9634–1.0000)
All trace element-based diagrams	**{Σn} {Σprob} [%prob]**	**{270}**	**{0} {0} [0%]**	**{0} {0} [0%]**	**{0} {0} [0%]**	**{54} {53.9838} [20.1%]**	**{216} {215.2133} [79.9%]**

For more explanation, see footnote of Table S12.

Table S17. Evaluation and testing of one set of new multidimensional diagrams from Late Tertiary to Quaternary altered intermediate magmas from the Central American Volcanic Arc (continental arc setting).

Figure name	Figure type §	Total number of samples	Number of discriminated samples				
			Arc			Within-plate	Collision
			IA+CA [$\overline{x} \pm s$] (p_{IA+CA}) Θ	IA [$\overline{x} \pm s$] [p_{IA}] Θ	CA [$\overline{x} \pm s$] [p_{CA}] Θ	CR+OI [$\overline{x} \pm s$] [p_{CR+OI}] Θ	Col [$\overline{x} \pm s$] [p_{Col}] Θ
Major elements	1+2-3+4-5	7	***4*** [0.773 ± 0.165] (0.5746–0.9468)	---	---	0	3 [0.6091 ± 0.0320] (0.5733–0.6349)
	1-2-3+4	7	---	1 [---] (0.4997)	***6*** [0.645 ± 0.129] (0.4947–0.5423)	0	---
	1-2-5	7	---	2 [0.507 ± 0.050] (0.4711–0.5423)	***5*** [0.5226 ± 0.0433] (0.4768–0.5900)	---	0
	1-3+4-5*	7	---	4 [0.736 ± 0.219] (0.5185–0.9339)	---	0	3 [0.807 ± 0.071] (0.7244–0.8512)
	2-3+4-5	7	---	---	***5*** [0.707 ± 0.161] (0.5429–0.8961)	0	2 [0.5155 ± 0.0026] (0.5136–0.5173)
All major element-based diagrams	**{Σn} {Σprob} [%prob]**	**{35}**	**{4} {3.0921} [---]**	**{7} {4.4555} [23.7%]**	**{16} {10.0154} [53.2%]**	**{0} {0} [0%]**	**{8} {5.2782} [23.1%]**

For more explanation, see footnote of Table S12.

Table S18. Application of the new multidimensional diagrams to Archean to Phanerozoic igneous rocks.

Area, country (reference); age; figure name	Figure type	Total number of samples	Number of discriminated samples				
			Arc			Within-plate	Collision
			IA+CA [$\overline{x} \pm s$] (p_{IA+CA}) Θ	IA [$\overline{x} \pm s$] [p_{IA}] Θ	CA [$\overline{x} \pm s$] [p_{CA}] Θ	CR+OI [$\overline{x} \pm s$] [p_{CR+OI}] Θ	Col [$\overline{x} \pm s$] [p_{Col}] Θ
Wawa greenstone belt, Canada (Polat *et al*., 1999; Polat, 2009); Late Archean, 2700 Ma; major elements	1+2-3+4-5	32	10 [0.920 ± 0.090] (0.7113–0.9952)	---	---	4 [0.870 ± 0.231] (0.5249–0.9986)	18 [0.962 ± 0.072] (0.6977–0.9995)
	1-2-3+4	32	---	25 [0.898 ± 0.116] (0.5729–0.9988)	0	7 [0.837 ± 0.202] (0.4539–0.9979)	---
	1-2-5	32	---	18 [0.856 ± 0.150] (0.5272–0.9981)	1 [---] (0.7845)	---	13 [0.903 ±0.124] (0.6264–0.9997)
	1-3+4-5	32	---	12 [0.910 ±0.117] (0.6257–0.9982)	---	4 [0.887 ± 0.203] (0.5829–0.9994)	16 [0.812 ± 0.143] (0.5118–0.9933)
	2-3+4-5	32	---	---	9 [0.849 ± 0.147] (0.5696–0.9824)	4 [0.869 ± 0.237] (0.5133–0.9971)	19 [0.925 ± 0.124] (0.5378–0.9994)
All major element-based diagrams	**{Σn} {Σprob} [%prob]**	**{160}**	**{10} {9.1982} [---]**	**{55} {48.7725} [39.8%]**	**{10} {8.4248} [6.9%]**	**{19} {16.3630} [11.5%]**	**{66} {59.6018} [41.8%]**
Wawa greenstone belt, Canada (Polat *et al*., 1999; Polat, 2009); Late Archean, 2700 Ma; major and trace elements	1+2-3+4-5	32	***22*** [0.808 ± 0.163] (0.4463–0.9905)	---	---	10 [0.943 ± 0.068] (0.7796–0.9983)	0
	1-2-3+4	32	---	***22*** [0.810 ± 0.103] (0.6564–0.9386)	0	10 [0.920 ± 0.127] (0.6000–0.9998)	---
	1-2-5	32	---	***27*** [0.775 ± 0.120] (0.4438–0.9142)	0	---	5 [0.756 ± 0.174] (0.5252–0.9589)
	1-3+4-5	32	---	***22*** [0.854 ± 0.126] (0.5555–0.9877)	---	10 [0.914 ± 0.095] (0.7053–0.9973)	0
	2-3+4-5 *	32	---	---	18 [0.739 ± 0.207] (0.4326–0.9981)	14 [0.842 ± 0.184] (0.5217–0.9988)	0
All major and trace element-based diagrams	**{Σn} {Σprob} [%prob]**	**{160}**	**{22} {17.7694} [---]**	**{71} {57.5270} [54.5%]**	**{18} {13.3033} [12.6%]**	**{44} {39.5541} [30.0%]**	**{5} {3.7792} [2.9%]**
Wawa greenstone belt, Canada (Polat *et al*., 1999; Polat, 2009); Late Archean, 2700 Ma; trace elements	1+2-3+4-5	32	***27*** [0.9412 ± 0.0431] (0.8536–0.9978)	---	---	5 [0.680 ± 0.053] (0.6324–0.7564)	0
	1-2-3+4	32	---	***24*** [0.793 ± 0.068] (0.6401–0.9285)	6 [0.563 ± 0.063] (0.4770–0.6429)	2 [0.509 ± 0.033] (0.4854–0.5324)	---
	1-2-5	32	---	***24*** [0.722 ± 0.076] (0.5552–0.8928)	8 [0.811 ± 0.116] (0.6587–0.9384)	---	0
	1-3+4-5	32	---	***27*** [0.9499 ± 0.0409] (0.8233–0.9977)	---	5 [0.779 ± 0.067] (0.6755–0.8423)	0
	2-3+4-5 *	32	---	---	30 [0.903 ± 0.071] (0.5612–0.9983)	2 [0.548 ± 0.071] (0.4979–0.5978)	0
All trace element-based diagrams	**{Σn} {Σprob} [%prob]**	**{160}**	**{27} {25.4114} [---]**	**{75} {62.0089} [58.3%]**	**{44} {36.9603} [34.7%]**	**{14} {39.5541} [7.2%]**	**{0} {0} [0%]**
South-central Sweden (Rutanen & Andersson, 2009); Paleoproterozoic, 1870–1780 Ma; major elements	1+2-3+4-5	13	***11*** [0.796 ± 0.114] (0.5903–0.9700)	---	---	0	2 [0.809 ± 0.178] (0.6831–0.9350)
	1-2-3+4	13	---	5 [0.741 ± 0.120] (0.6376–0.9412)	8 [0.579 ± 0.115] (0.3494–0.7459)	0	---
	1-2-5	13	---	5 [0.642 ± 0.156] (0.5008–0.9007)	7 [0.602 ± 0.078] (0.4885–0.7290)	---	1 [---] (0.8784)
	1-3+4-5	13	---	11 [0.789 ± 0.127] (0.6035–0.9670)	---	0	2 [0.839 ± 0.142] (0.7390–0.9399)
	2-3+4-5	13	---	---	9 [0.736 ± 0.155] (0.5250–0.9367)	0	4 [0.735 ± 0.138] (0.5546–0.8908)

Table S18. (continued).

All major element-based diagrams	**{Σn} {Σprob} [%prob]**	**{65}**	**{11} {8.7553} [---]**	**{21} {15.5963} [42.6%]**	**{24} {15.4717} [42.2%]**	**{0} {0} [0%]**	**{9} {7.1160} [15.2%]**
Adola, southern Ethiopia (Wolde *et al*., 1996); Neoproterozoic, 885–765 Ma; major elements	1+2-3+4-5	12	***7*** [0.9967 ± 0.0065] (0.9824–1.0000)	---	---	0	5 [0.644 ± 0.234] (0.3928–0.9997)
	1-2-3+4	12	---	***9*** [0.899 ± 0.131] (0.6498–1.0000)	2 [0.785 ± 0.121] (0.6992–0.8706)	1 [---] (0.5881)	---
	1-2-5	12	---	***10*** [0.882 ± 0.136] (0.6590–1.0000)	2 [0.664 ± 0.142] (0.5641–0.7645)	---	0
	1-3+4-5	12	---	***8*** [0.9968 ± 0.0077] (0.9780–1.0000)	---	1 [---] (0.3879)	3 [0.765 ± 0.208] (0.5813–0.9900)
	2-3+4-5 *	12	---	---	7 [0.9701 ± 0.0425] (0.8842–1.0000)	0	5 [0.842 ± 0.250] (0.4036–1.0000)
All major element-based diagrams	**{Σn} {Σprob} [%prob]**	**{60}**	**{7} {6.9770} [---]**	**{27} {24.8922} [57.2%]**	**{11} {9.6890} [22.3%]**	**{2} {0.9760} [1.9%]**	**{13} {9.7239} [18.6%]**
Adola, southern Ethiopia (Wolde *et al*., 1996); Neoproterozoic, 885–765 Ma; major and trace elements	1+2-3+4-5	8	***7*** [0.884 ± 0.172] (0.5379–0.9945)	---	---	1 [---] (0.9992)	0
	1-2-3+4	8	---	0	***7*** [0.738 ± 0.098] (0.5406–0.8256)	1 [---] (0.9981)	---
	1-2-5	8	---	0	***8*** [0.742 ± 0.096] (0.5452–0.8277)	---	0
	1-3+4-5 *	8	---	***6*** [0.888 ± 0.135] (0.6276–0.9856)	---	1 [---] (0.9991)	1 [---] (0.5164)
	2-3+4-5	8	---	---	***5*** [0.879 ± 0.174] (0.5879–0.9909)	0	2 [0.78 ± 0.31] (0.5563–0.9962)
All major and trace element-based diagrams	**{Σn} {Σprob} [%prob]**	**{40}**	**{7} {6.1921} [---]**	**{6} {5.3295} [20.9%]**	**{20} {15.5044} [60.8%]**	**{4} {3.9930} [12.1%]**	**{3} {2.0689} [6.2%]**
Adola, southern Ethiopia (Wolde *et al*., 1996); Neoproterozoic, 885–765 Ma; trace elements	1+2-3+4-5	8	***7*** [0.9916 ± 0.0144] (0.9601–0.9998)	---	---	1 [---] (0.9521)	0
	1-2-3+4	8	---	***6*** [0.810 ± 0.115] (0.6251–0.9664)	1 [---] (0.5023)	1 [---] (0.8820)	---
	1-2-5	8	---	***6*** [0.759 ± 0.129] (0.5568–0.9283)	2 [0.674 ± 0.199] (0.5329–0.8142)	---	0
	1-3+4-5	8	---	***7*** [0.9904 ± 0.0170] (0.9527–0.9997)	---	1 [---] (0.9647)	0
	2-3+4-5 *	8	---	---	***7*** [0.933 ±0.097] (0.7566–0.9989)	1 [---] (0.9503)	0
All trace element-based diagrams	**{Σn} {Σprob} [%prob]**	**{40}**	**{7} {6.9411} [---]**	**{19} {16.3458} [59.1%]**	**{10} {8.3815} [30.3%]**	**{4} {3.7491} [10.6%]**	**{0} {0} [0%]**
Malani igneous complex, Rajasthan, India (Maheshwari *et al*., 1996; Bhushan & Chandrasekharam, 2002; Singh & Vallinanyagam, 2004); Neoproterozoic, 750 Ma; major elements	1+2-3+4-5	21	3 [0.618 ± 0.231] (0.4442–0.8799)	---	---	***18*** [0.883 ± 0.171] (0.4683–1.0000)	0
	1-2-3+4	21	---	0	3 [0.745 ± 0.247] (0.5057–0.9985)	***18*** [0.831 ± 0.185] (0.4611–0.9999)	---
	1-2-5 *	21	---	3 [0.831 ± 0.213] (0.5871–0.9825)	17 [0.783 ± 0.213] (0.3816–0.9977)	---	1 [---] (0.5083)
	1-3+4-5	21	---	4 [0.660 ± 0.135] (0.5195–0.8428)	---	***17*** [0.910 ± 0.129] (0.5878–1.0000)	0
	2-3+4-5	21	---	---	5 [0.612 ± 0.214] (0.4755–0.9796)	***16*** [0.890 ± 0.122] (0.6670–0.9998)	0
All major element-based diagrams	**{Σn} {Σprob} [%prob]**	**{105}**	**{3} {1.8531} [---]**	**{7} {5.1345} [6.4%]**	**{25} {18.5987} [23.1%]**	**{69} {60.5147} [69.9%]**	**{1} {0.5083} [0.6%]**

Table S18. (continued).

Western Tasmania, Australia (Brown & Jenner, 1989); Cambrian; major elements	1+2-3+4-5	39	***33*** [0.9811 ± 0.0319] (0.8849–1.0000)	---	---	0	6 [0.871 ± 0.148] (0.6857–0.9994)
	1-2-3+4	39	---	***33*** [0.903 ± 0.146] (0.5562–1.0000)	6 [0.758 ± 0.201] (0.5344–0.9948)	0	---
	1-2-5	39	---	***35*** [0.889 ± 0.145] (0.5197–1.0000)	3 [0.840 ± 0.235] (0.5685–0.9762)	---	1 [---] (0.5234)
	1-3+4-5	39	---	***38*** [0.9805 ± 0.0254] (0.8657–1.0000)	---	0	1 [---] (0.9038)
	2-3+4-5 *	39	---	---	28 [0.931 ± 0.129] (0.5537–1.0000)	0	11 [0.844 ± 0.160] (0.5664–0.9981)
All major element-based diagrams	**{Σn} {Σprob} [%prob]**	**{195}**	**{33} {32.3754} [---]**	**{106} {98.5682} [68.5%]**	**{36} {32.5718} [22.6%]**	**{0} {0} [0%]**	**{19} {15.9407} [8.9%]**
Alps, France-Italy-Switzerland (Debon & Lemmet, 1999); Late Carboniferous, 295 Ma; major elements	1+2-3+4-5	6	0	---	---	0	***6*** [0.981 ± 0.034] (0.9116–0.9995)
	1-2-3+4 *	6	---	0	0	***6*** [0.796 ± 0.264] (0.3700–0.9969)	---
	1-2-5	6	---	0	0	---	***6*** [0.977 ± 0.051] (0.8728–1.0000)
	1-3+4-5	6	---	0	---	0	***6*** [0.983 ± 0.028] (0.9256–0.9993)
	2-3+4-5	6	---	---	0	0	***6*** [0.973 ± 0.042] (0.8903–0.9991)
All major element-based diagrams	**{Σn} {Σprob} [%prob]**	**{30}**	**{0} {0} [0%]**	**{0} {0} [0%]**	**{0} {0} [0%]**	**{6} {4.7760} [16.9%]**	**{24} {23.4834} [83.1%]**
Alps, France-Italy-Switzerland (Debon & Lemmet, 1999); Late Carboniferous, 295 Ma; major and trace elements	1+2-3+4-5	5	0	---	---	0	***5*** [0.925 ± 0.083] (0.7936–0.9859)
	1-2-3+4	5	---	1 [---] (0.5085)	2 [0.979 ± 0.008] (0.9736–0.9850)	2 [0.8100 ± 0.053] (0.7723–0.8476)	---
	1-2-5	5	---	0	0	---	***5*** [0.846 ± 0.163] (0.6011–0.9959)
	1-3+4-5	5	---	0	---	0	***5*** [0.913 ± 0.111] (0.7312–0.9924)
	2-3+4-5	5	---	---	0	0	***5*** [0.927 ± 0.077] (0.8299–0.9943)
All major and trace element-based diagrams	**{Σn} {Σprob} [%prob]**	**{25}**	**{0} {0} [0%]**	**{1} {0.5857} [2.6%]**	**{2} {1.9586} [8.8%]**	**{2} {1.6200} [7.3%]**	**{20} {23.4834} [83.3%]**
Alps, France-Italy-Switzerland (Debon & Lemmet, 1999); Late Carboniferous, 295 Ma; trace elements	1+2-3+4-5	6	0	---	---	0	***6*** [0.957 ± 0.102] (0.7485–0.9993)
	1-2-3+4	6	---	0	1 [---] (0.5602)	5 [0.970 ± 0.045] (0.8940–1.0000)	---
	1-2-5	6	---	0	0	---	***6*** [0.953 ± 0.113] (0.7228–1.0000)
	1-3+4-5	6	---	0	---	0	***6*** [0.95613 ± 0.099] (0.7549–0.9983)
	2-3+4-5	6	---	---	0	0	***6*** [0.950 ± 0.114] (0.7184–0.9988)
All trace element-based diagrams	**{Σn} {Σprob} [%prob]**	**{30}**	**{0} {0} [0%]**	**{0} {0} [0%]**	**{1} {0.5602} [2.0%]**	**{5} {4.8494} [17.1%]**	**{24} {22.9374} [80.9%]**

Table S18. (continued).

Chichijima Island, Bonin Islands, Japan (Taylor *et al.*, 1994); Eocene, 48–40 Ma; major elements	1+2-3+4-5	35	***35*** [0.989 ± 0.040] (0.7583–0.9993)	---	---	0	0
	1-2-3+4	35	---	***35*** [0.944 ± 0.081] (0.6617–0.9994)	0	0	---
	1-2-5	35	---	***35*** [0.941 ± 0.087] (0.6453–0.9995)	0	---	0
	1-3+4-5	35	---	***35*** [0.988 ± 0.058] (0.6535–0.9998)	---	0	0
	2-3+4-5	35	---	---	33 [0.873 ± 0.123] (0.5252–0.9810)	0	2 [0.525 ± 0.019] (0.5156–0.5389)
All major element-based diagrams	**{Σn} {Σprob} [%prob]**	**{175}**	**{35} {34.6104} [---]**	**{105} {100.5573} [77.3%]**	**{33} {28.7943} [22.1%]**	**{0} {0} [0%]**	**{2} {1.0504} [0.6%]**

For more explanation, see footnote of Table S12.

Table S19. Evaluation of the first new major element-based multidimensional diagram for changes related to analytical errors, mobility, or alteration.

Element [+gain%, –loss%]	Probability change of the centroid [p_{gain}, p_{loss}] caused by element concentration changes Θ						
	IA+CA		Arc		Within-plate (CR+OI)		Collision Col
	IA	CA	IA	CA	CR	OI	
No change (1+2-3+4-5)	**0.92046**	**0.88378**	---	---	**0.92458**	**0.98888**	**0.94785**
SiO_2 [+10%, –10%]	[0.8898, 0.9363]	[0.8402, 0.9075]	---	---	[0.8624, 0.9599]	[0.9803, 0.9936]	[0.9710, 0.9005]
TiO_2 [+20%, –20%]	[0.8515, 0.9562]	[0.7928, 0.9341]	---	---	[0.9720, 0.7679]	[0.9963, 0.9568]	[0.9348, 0.9400]
Al_2O_3 [+20%, –20%]	[0.9420, 0.8818]	[0.9140, 0.8314]	---	---	[0.8914, 0.9515]	[0.9827, 0.9934]	[0.9415, 0.9505]
Fe_2O_3 [+20%, –20%]	[0.9343, 0.9460]	[0.9046, 0.9213]	---	---	[0.9333, 0.9454]	[0.9904, 0.9917]	[0.9644, 0.9534]
FeO [+20%, –20%]	[0.9124, 0.9562]	[0.7612, 0.9364]	---	---	[0.9162, 0.9541]	[0.9885, 0.9925]	[0.9748, 0.9401]
MnO [+40%, –40%]	[0.9466, 0.7373]	[0.9229, 0.6445]	---	---	[0.9706, 0.6257]	[0.9949, 0.9389]	[0.8366, 0.9915]
MgO [+20%, –20%]	[0.9128, 0.9288]	[0.8729, 0.8957]	---	---	[0.9192, 0.9304]	[0.9883, 0.9895]	[0.9538, 0.9395
CaO [+20%, –20%]	[0.9301, 0.8942]	[0.8966, 0.8494]	---	---	[0.8570, 0.9671]	[0.9776, 0.9953]	[0.9561, 0.9264]
Na_2O [+40%, –40%]	[0.9444, 0.7324]	[0.9199, 0.6386]	---	---	[0.9729, 0.5918]	[0.9953, 0.9334]	[0.8295, 0.9919]
K_2O [+40%, –40%]	[0.8559, 0.9663]	[0.7949, 0.9502]	---	---	[0.9000, 0.9374]	[0.9868, 0.9888]	[0.9733, 0.8599]
P_2O_5 [+20%, –20%]	[0.9144, 0.9268]	[0.8751, 0.8930]	---	---	[0.9159, 0.9338]	[0.9878, 0.9901]	[0.9540, 0.9392]
No change (1-2-3+4)	---	---	**0.61392**	**0.59320**	**0.95535**	**0.98472**	---
SiO_2 [+10%, –10%]	---	---	[0.6580, 0.5626]	[0.5513, 0.6365]	[0.9409, 0.9671]	[0.9798, 0.9887]	---
TiO_2 [+20%, –20%]	---	---	[0.6261, 0.5745]	[0.5312, 0.6466]	[0.9875, 0.8115]	[0.9958, 0.9275]	---
Al_2O_3 [+20%, –20%]	---	---	[*0.4618*, 0.7668]	[0.7344, *0.3998*]	[0.9329, 0.9695]	[0.9756, 0.9902]	---
Fe_2O_3 [+20%, –20%]	---	---	[0.5831, 0.5533]	[0.6391, 0.6664]	[0.9854, 0.9851]	[0.9930, 0.9927]	---
FeO [+20%, –20%]	---	---	[0.6207, 0.5157]	[*0.4423*, 0.6957]	[0.9858, 0.9847]	[0.9932, 0.9924]	---
MnO [+40%, –40%]	---	---	[0.8294, *0.2098*]	[*0.3053*, 0.9001]	[0.9689, 0.8657]	[0.9902, 0.9459]	---
MgO [+20%, –20%]	---	---	[0.5962, 0.6352]	[0.6095, 0.5728]	[0.9585, 0.9511]	[0.9858, 0.9833]	---
CaO [+20%, –20%]	---	---	[0.7110, *0.4800*]	[*0.4942*, 0.6953]	[0.9158, 0.9788]	[0.9712, 0.9926]	---
Na_2O [+40%, –40%]	---	---	[*0.3659*, 0.8747]	[0.8027, *0.2344*]	[0.9343, 0.9614]	[0.9756, 0.9880]	---
K_2O [+40%, –40%]	---	---	[0.6699, 0.5209]	[0.5275, 0.6860]	[0.9646, 0.9350]	[0.9882, 0.9768]	---
P_2O_5 [+20%, –20%]	---	---	[0.5665, 0.6689]	[0.6395, 0.5342]	[0.9553, 0.9548]	[0.9845, 0.9848]	---
No change (1-2-5)	---	---	**0.59424**	**0.59364**	---	---	**0.95095**
SiO_2 [+10%, –10%]	---	---	[0.6574, 0.5167]	[0.5130, 0.6763]	---	---	[0.9666, 0.9240]
TiO_2 [+20%, –20%]	---	---	[0.6426, 0.5252]	[0.5206, 0.6738]	---	---	[0.9712, 0.9061]
Al_2O_3 [+20%, –20%]	---	---	[*0.3942*, 0.7970]	[0.7586, *0.3571*]	---	---	[0.9458, 0.9474]
Fe_2O_3 [+20%, –20%]	---	---	[0.5870, 0.5549]	[0.6139, 0.6532]	---	---	[0.9819, 0.9702]
FeO [+20%, –20%]	---	---	[0.6226, 0.5127]	[0.4204, 0.6929]	---	---	[0.9901, 0.9527]
MnO [+40%, –40%]	---	---	[0.8355, *0.1693*]	[*0.3209*, 0.7570]	---	---	[0.8268, 0.9895]
MgO [+20%, –20%]	---	---	[0.5705, 0.6224]	[0.6105, 0.5715]	---	---	[0.9571, 0.9421]
CaO [+20%, –20%]	---	---	[0.6638, 0.4966]	[0.5000, 0.6971]	---	---	[0.9704, 0.9079]
Na_2O [+40%, –40%]	---	---	[*0.4067*, 0.7213]	[0.7771, *0.2366*]	---	---	[0.7803, 0.9949]
K_2O [+40%, –40%]	---	---	[0.6145, 0.5455]	[0.5327, 0.6640]	---	---	[0.9776, 0.8484]
P_2O_5 [+20%, –20%]	---	---	[0.5281, 0.6705]	[0.6501, 0.5191]	---	---	[0.9547, 0.9448]
No change (1-3+4-5)	---	---	**0.92792**	---	**0.93414**	**0.98914**	**0.95117**
SiO_2 [+10%, –10%]	---	---	[0.8947, 0.9450]	---	[0.8745, 0.9662]	[0.9798, 0.9940]	[0.9751, 0.8985]
TiO_2 [+20%, –20%]	---	---	[0.8580, 0.9628]	---	[0.9751, 0.7970]	[0.9963, 0.9590]	[0.9299, 0.9486]
Al_2O_3 [+20%, –20%]	---	---	[0.9567, 0.8655]	---	[0.8973, 0.9605]	[0.9812, 0.9941]	[0.9419, 0.9522]

Table S19. (continued).

Fe_2O_3 [+20%, –20%]	---	---	[0.9361, 0.9433]	---	[0.9387, 0.9505]	[0.9897, 0.9915]	[0.9598, 0.9501]
FeO [+20%, –20%]	---	---	[0.9232, 0.9492]	---	[0.9221, 0.9593]	[0.9873, 0.9928]	[0.9700, 0.9390]
MnO [+40%, –40%]	---	---	[0.9725, 0.5531]	---	[0.9665, 0.6457]	[0.9930, 0.9354]	[0.7864, 0.9958]
MgO [+20%, –20%]	---	---	[0.9224, 0.9340]	---	[0.9297, 0.9390]	[0.9885, 0.9898]	[0.9558, 0.9449]
CaO [+20%, –20%]	---	---	[0.9419, 0.8972]	---	[0.8824, 0.9686]	[0.9794, 0.9951]	[0.9580, 0.9319]
Na_2O [+40%, –40%]	---	---	[0.9153, 0.8890]	---	[0.9812, 0.6406]	[0.9968, 0.9269]	[0.8731, 0.9845]
K_2O [+40%, –40%]	---	---	[0.8669, 0.9712]	---	[0.9164, 0.9425]	[0.9874, 0.9886]	[0.9730, 0.8782]
P_2O_5 [+20%, –20%]	---	---	[0.9254, 0.9304]	---	[0.9251, 0.9437]	[0.9877, 0.9907]	[0.9562, 0.9441]
No change (2-3+4-5)	---	---	---	**0.84611**	**0.86404**	**0.96601**	**0.91793**
SiO_2 [+10%, –10%]	---	---	---	[0.7704, 0.8992]	[0.8144, 0.8975]	[0.9543, 0.9729]	[0.9523, 0.8544]
TiO_2 [+20%, –20%]	---	---	---	[0.7647, 0.8938]	[0.9424, 0.6647]	[0.9868, 0.8964]	[0.8912, 0.9223]
Al_2O_3 [+20%, –20%]	---	---	---	[0.9443, 0.5761]	[0.7633, 0.9161]	[0.9266, 0.9820]	[0.8356, 0.9468]
Fe_2O_3 [+20%, –20%]	---	---	---	[0.8347, 0.8660]	[0.8687, 0.8822]	[0.9668, 0.9695]	[0.9283, 0.9071]
FeO [+20%, –20%]	---	---	---	[0.7641, 0.8942]	[0.8499, 0.8919]	[0.9630, 0.9708]	[0.9496, 0.8821]
MnO [+40%, –40%]	---	---	---	[0.8292, 0.8141]	[0.9443, 0.5795]	[0.9865, 0.8665]	[0.8553, 0.9593]
MgO [+20%, –20%]	---	---	---	[0.8423, 0.8477]	[0.8311, 0.8966]	[0.9570, 0.9745]	[0.9291, 0.9012]
CaO [+20%, –20%]	---	---	---	[0.8385, 0.8451]	[0.7975, 0.9187]	[0.9473, 0.9801]	[0.9369, 0.8843]
Na_2O [+40%, –40%]	---	---	---	[0.8736, 0.7187]	[0.9367, 0.5981]	[0.9838, 0.8798]	[0.8297, 0.9737]
K_2O [+40%, –40%]	---	---	---	[0.7119, 0.9396]	[0.7991, 0.9005]	[0.9511, 0.9713]	[0.9630, 0.7492]
P_2O_5 [+20%, –20%]	---	---	---	[0.8410, 0.8520]	[0.8581, 0.8709]	[0.9646, 0.9677]	[0.9223, 0.9122]

Θ p_{gain} and p_{loss} here refer to the probability of the modified concentrations from the gain or loss of an element; the probability values in *italics* underlined are for the centroids that are misdiscriminated in a given diagram, generally as the other arc setting (i.e. IA was misdiscriminated as CA and vice versa).

Table S20. Evaluation of the second set of major and trace element-based multidimensional diagrams for compositional changes related to analytical errors, mobility, or alteration.

Element [+gain%, –loss%]	Probability change of the centroid [p_{gain}, p_{loss}] caused by element concentration changes						
	IA+CA		Arc		Within-plate (CR+OI)		Collision Col
	IA	CA	IA	CA	CR	OI	
No change (1+2-3+4-5)	**0.86377**	**0.84043**	---	---	**0.92193**	**0.99002**	**0.96549**
TiO_2 [+20%, –20%]	[0.9031, 0.7965]	[0.8867, 0.7623]	---	---	[0.8970, 0.9431]	[0.9862, 0.9930]	[0.9577, 0.9702]
MgO [+20%, –20%]	[0.8419, 0.8361]	[0.7720, 0.8148]	---	---	[0.9934, *0.3425*]	[0.9992, 0.8156]	[0.8453, 0.9813]
P_2O_5 [+20%, –20%]	[0.8732, 0.8505]	[0.8526, 0.8224]	---	---	[0.8894, 0.9497]	[0.9854, 0.9937]	[0.9674, 0.9609]
Nb [+20%, –20%]	[0.8075, 0.9131]	[0.7763, 0.8976]	---	---	[0.9304, 0.9093]	[0.9912, 0.9883]	[0.9718, 0.9525]
Ni [+20%, –20%]	[0.8414, 0.8874]	[0.8148, 0.8678]	---	---	[0.9264, 0.9160]	[0.9906, 0.9892]	[0.9685, 0.9609]
V [+20%, –20%]	[0.8739, 0.8395]	[0.8554, 0.7970]	---	---	[0.7843, 0.9804]	[0.9683, 0.9976]	[0.9717, 0.9330]
Y [+20%, –20%]	[0.8870, 0.8300]	[0.8672, 0.8020]	---	---	[0.9189, 0.9253]	[0.9896, 0.9905]	[0.9606, 0.9702]
Zr [+20%, –20%]	[0.8154, 0.9029]	[0.7899, 0.8771]	---	---	[0.8140, 0.9753]	[0.9735, 0.9970]	[0.9798, 0.9268]
No change (1-2-3+4)	---	---	**0.58700**	**0.64616**	**0.98474**	**0.99858**	---
TiO_2 [+20%, –20%]	---	---	[0.5623, 0.6167]	[0.6728, 0.6078]	[0.9698, 0.9933]	[0.9969, 0.9993]	---
MgO [+20%, –20%]	---	---	[0.5509, 0.6096]	[0.6106, 0.6320]	[0.9985, 0.7923]	[0.9998, 0.9749]	---
P_2O_5 [+20%, –20%]	---	---	[*0.4775*, 0.7082]	[0.7413, 0.5122]	[0.9729, 0.9921]	[0.9973, 0.9992]	---
Nb [+20%, –20%]	---	---	[0.5794, 0.5958]	[0.6492, 0.6410]	[0.9898, 0.9752]	[0.9990, 0.9975]	---
Ni [+20%, –20%]	---	---	[0.5839, 0.5906]	[0.6470, 0.6447]	[0.9878, 0.9800]	[0.9988, 0.9980]	---
V [+20%, –20%]	---	---	[0.6200, 0.5413]	[0.6197, 0.6640]	[0.9554, 0.9960]	[0.9954, 0.9996]	---
Y [+20%, –20%]	---	---	[0.6848, *0.4581*]	[0.5475, 0.7492]	[0.9805, 0.9883]	[0.9980, 0.9988]	---
Zr [+20%, –20%]	---	---	[0.6220, 0.5425]	[0.6153, 0.6800]	[0.9768, 0.9908]	[0.9977, 0.9991]	---
No change (1-2-5)	---	---	**0.54861**	**0.59639**	---	---	**0.94769**
TiO_2 [+20%, –20%]	---	---	[0.5292, 0.5626]	[0.6412, 0.5318]	---	---	[0.9214, 0.9687]
MgO [+20%, –20%]	---	---	[0.5291, 0.5705]	[0.6266, 0.5576]	---	---	[0.9378, 0.9577]
P_2O_5 [+20%, –20%]	---	---	[*0.4576*, 0.6516]	[0.6848, 0.4790]	---	---	[0.9370, 0.9566]
Nb [+20%, –20%]	---	---	[0.5190, 0.5785]	[0.5873, 0.5990]	---	---	[0.9638, 0.9187]
Ni [+20%, –20%]	---	---	[0.5422, 0.5555]	[0.5902, 0.6029]	---	---	[0.9545, 0.9381]
V [+20%, –20%]	---	---	[0.5946, 0.4912]	[0.5584, 0.6396]	---	---	[0.9446, 0.9508]
Y [+20%, –20%]	---	---	[0.6373, *0.4363*]	[0.5173, 0.6815]	---	---	[0.9432, 0.9509]
Zr [+20%, –20%]	---	---	[0.5714, 0.5098]	[0.5352, 0.6630]	---	---	[0.9656, 0.9129]
No change (1-3+4-5)	---	---	**0.83946**	---	**0.91525**	**0.98628**	**0.96261**
TiO_2 [+20%, –20%]	---	---	[0.8795, 0.7753]	---	[0.8919, 0.9358]	[0.9817, 0.9900]	[0.9572, 0.9655]
MgO [+20%, –20%]	---	---	[0.8094, 0.8161]	---	[0.9914, *0.3714*]	[0.9987, 0.7981]	[0.8351, 0.9806]
P_2O_5 [+20%, –20%]	---	---	[0.8347, 0.8444]	---	[0.8896, 0.9391]	[0.9817, 0.9903]	[0.9673, 0.9552]
Nb [+20%, –20%]	---	---	[0.7806, 0.8933]	---	[0.9237, 0.9031]	[0.9877, 0.9842]	[0.9680, 0.9516]
Ni [+20%, –20%]	---	---	[0.8158, 0.8650]	---	[0.9198, 0.9093]	[0.9871, 0.9852]	[0.9651, 0.9588]
V [+20%, –20%]	---	---	[0.8481, 0.8155]	---	[0.7788, 0.9770]	[0.9591, 0.9965]	[0.9716, 0.9230]
Y [+20%, –20%]	---	---	[0.8840, 0.7673]	---	[0.9114, 0.9192]	[0.9856, 0.9869]	[0.9533, 0.9701]
Zr [+20%, –20%]	---	---	[0.7929, 0.8775]	---	[0.8024, 0.9726]	[0.9643, 0.9958]	[0.9782, 0.9195]
No change (2-3+4-5)	---	---	---	**0.94673**	**0.89487**	**0.97756**	**0.97595**

Table S20. (continued).

TiO_2 [+20%, –20%]	---	---	---	[0.9653, 0.9084]	[0.8506, 0.9314]	[0.9661, 0.9861]	[0.9771, 0.9703]
MgO [+20%, –20%]	---	---	---	[0.9293, 0.9098]	[0.9891, *0.3172*]	[0.9978, 0.7060]	[0.8353, 0.9952]
P_2O_5 [+20%, –20%]	---	---	---	[0.9645, 0.9125]	[0.8653, 0.9227]	[0.9705, 0.9839]	[0.9762, 0.9726]
Nb [+20%, –20%]	---	---	---	[0.8856, 0.9800]	[0.8916, 0.8970]	[0.9768, 0.9781]	[0.9809, 0.9618]
Ni [+20%, –20%]	---	---	---	[0.9311, 0.9613]	[0.8996, 0.8886]	[0.9787, 0.9761]	[0.9769, 0.9740]
V [+20%, –20%]	---	---	---	[0.9546, 0.9223]	[0.7475, 0.9688]	[0.9381, 0.9937]	[0.9859, 0.9362]
Y [+20%, –20%]	---	---	---	[0.9403, 0.9537]	[0.9044, 0.8820]	[0.9798, 0.9745]	[0.9750, 0.9768]
Zr [+20%, –20%]	---	---	---	[0.9338, 0.9532]	[0.7751, 0.9625]	[0.9463, 0.9924]	[0.9877, 0.9410]

For more explanation, see Table S19.

Table S21. Evaluation of the third set of major and trace element-based multidimensional diagrams for compositional changes related to analytical errors, mobility, or alteration.

Element [+gain%, –loss%]	Probability change of the centroid [p_{gain}, p_{loss}] caused by element concentration changes						
	IA+CA		Arc		Within-plate (CR+OI)		Collision Col
	IA	CA	IA	CA	CR	OI	
No change (1+2-3+4-5)	**0.96541**	**0.91223**	---	---	**0.97804**	**0.99661**	**0.98297**
Yb [+20%, –20%]	[0.9951, 0.7020]	[0.9868, 0.4732]	---	---	[0.9636, 0.9729]	[0.9962, 0.9953]	[0.9484, 0.9911]
La [+20%, –20%]	[0.9693, 0.9599]	[0.9213, 0.8997]	---	---	[0.9792, 0.9765]	[0.9968, 0.9963]	[0.9812, 0.9849]
Ce [+20%, –20%]	[0.9681, 0.9485]	[0.9226, 0.8636]	---	---	[0.9433, 0.9933]	[0.9908, 0.9990]	[0.9917, 0.9523]
Sm [+20%, –20%]	[0.9343, 0.9845]	[0.8413, 0.9595]	---	---	[0.9798, 0.9733]	[0.9967, 0.9963]	[0.9851, 0.9775]
Nb [+20%, –20%]	[0.9494, 0.9738]	[0.8688, 0.9359]	---	---	[0.9902, 0.9421]	[0.9985, 0.9908]	[0.9675, 0.9908]
Th [+20%, –20%]	[0.9521, 0.9757]	[0.8835, 0.9355]	---	---	[0.9697, 0.9846]	[0.9951, 0.9978]	[0.9887, 0.9720]
Y [+20%, –20%]	[0.9088, 0.9899]	[0.7884, 0.9733]	---	---	[0.9793, 0.9703]	[0.9966, 0.9963]	[0.9865, 0.9710]
Zr [+20%, –20%]	[0.9659, 0.9641]	[0.9122, 0.9105]	---	---	[0.9826, 0.9708]	[0.9974, 0.9954]	[0.9788, 0.9869]
No change (1-2-3+4)	---	---	**0.71546**	**0.64256**	**0.98757**	**0.99908**	---
Yb [+20%, –20%]	---	---	[0.7870, 0.5795]	[0.5673, 0.6142]	[0.9233, 0.9987]	[0.9941, 0.9999]	---
La [+20%, –20%]	---	---	[0.6275, 0.8036]	[0.7289, 0.5233]	[0.9835, 0.9909]	[0.9987, 0.9994]	---
Ce [+20%, –20%]	---	---	[0.6716, 0.7590]	[0.6974, 0.5597]	[0.9697, 0.9958]	[0.9977, 0.9997]	---
Sm [+20%, –20%]	---	---	[0.6413, 0.7899]	[0.6900, 0.5595]	[0.9944, 0.9668]	[0.9996, 0.9976]	---
Nb [+20%, –20%]	---	---	[0.7135, 0.7144]	[0.6238, 0.6548]	[0.9944, 0.9677]	[0.9996, 0.9976]	---
Th [+20%, –20%]	---	---	[0.7600, 0.6545]	[0.5870, 0.7055]	[0.9896, 0.9844]	[0.9992, 0.9988]	---
Y [+20%, –20%]	---	---	[0.7366, 0.6816]	[0.5890, 0.6903]	[0.9956, 0.9569]	[0.9997, 0.9967]	---
Zr [+20%, –20%]	---	---	[0.7500, 0.6692]	[0.5986, 0.6931]	[0.9901, 0.9835]	[0.9993, 0.9988]	---
No change (1-2-5)	---	---	**0.71670**	**0.63668**	---	---	**0.98681**
Yb [+20%, –20%]	---	---	[0.7825, 0.5642]	[0.5778, 0.5512]	---	---	[0.9154, 0.9987]
La [+20%, –20%]	---	---	[0.6392, 0.7955]	[0.7165, 0.5282]	---	---	[0.9821, 0.9908]
Ce [+20%, –20%]	---	---	[0.6866, 0.7502]	[0.6566, 0.6070]	---	---	[0.9905, 0.9804]
Sm [+20%, –20%]	---	---	[0.6322, 0.8023]	[0.7087, 0.5331]	---	---	[0.9890, 0.9832]
Nb [+20%, –20%]	---	---	[0.7097, 0.7251]	[0.6429, 0.6289]	---	---	[0.9874, 0.9861]
Th [+20%, –20%]	---	---	[0.7624, 0.6514]	[0.5691, 0.7112]	---	---	[0.9917, 0.9767]
Y [+20%, –20%]	---	---	[0.7503, 0.6575]	[0.5491, 0.7152]	---	---	[0.9957, 0.9485]
Zr [+20%, –20%]	---	---	[0.7326, 0.6965]	[0.6177, 0.6594]	---	---	[0.9876, 0.9958]
No change (1-3+4-5)	---	---	**0.96450**	---	**0.97209**	**0.99371**	**0.97546**
Yb [+20%, –20%]	---	---	[0.9946, 0.7164]	---	[0.9657, 0.9622]	[0.9944, 0.9908]	[0.9434, 0.9859]
La [+20%, –20%]	---	---	[0.9526, 0.9749]	---	[0.9778, 0.9630]	[0.9949, 0.9918]	[0.9714, 0.9789]
Ce [+20%, –20%]	---	---	[0.9685, 0.9418]	---	[0.9218, 0.9924]	[0.9815, 0.9983]	[0.9897, 0.9205]
Sm [+20%, –20%]	---	---	[0.9305, 0.9847]	---	[0.9759, 0.9646]	[0.9944, 0.9926]	[0.9753, 0.9729]
Nb [+20%, –20%]	---	---	[0.9498, 0.9725]	---	[0.9869, 0.9315]	[0.9971, 0.9841]	[0.9527, 0.9879]
Th [+20%, –20%]	---	---	[0.9593, 0.9689]	---	[0.9621, 0.9807]	[0.9912, 0.9958]	[0.9822, 0.9637]
Y [+20%, –20%]	---	---	[0.9170, 0.9879]	---	[0.9708, 0.9701]	[0.9931, 0.9941]	[0.9800, 0.9645]
Zr [+20%, –20%]	---	---	[0.9693, 0.9574]	---	[0.9751, 0.9677]	[0.9945, 0.9926]	[0.9715, 0.9795]
No change (2-3+4-5)	---	---	---	**0.94219**	**0.97245**	**0.99233**	**0.97787**

Table S21. (continued).

Yb [+20%, –20%]	---	---	---	[0.9878, 0.6863]	[0.9637, 0.9635]	[0.9917, 0.9890]	[0.9428, 0.9890]
La [+20%, –20%]	---	---	---	[0.9604, 0.9082]	[0.9648, 0.9792]	[0.9904, 0.9941]	[0.9786, 0.9755]
Ce [+20%, –20%]	---	---	---	[0.9533, 0.9091]	[0.9414, 0.9893]	[0.9832, 0.9971]	[0.9874, 0.9509]
Sm [+20%, –20%]	---	---	---	[0.8980, 0.9717]	[0.9782, 0.9613]	[0.9938, 0.9897]	[0.9774, 0.9756]
Nb [+20%, –20%]	---	---	---	[0.8958, 0.9663]	[0.9879, 0.9265]	[0.9966, 0.9791]	[0.9589, 0.9870]
Th [+20%, –20%]	---	---	---	[0.9105, 0.9654]	[0.9649, 0.9778]	[0.9898, 0.9943]	[0.9852, 0.9632]
Y [+20%, –20%]	---	---	---	[0.8688, 0.9799]	[0.9725, 0.9665]	[0.9920, 0.9917]	[0.9832, 0.9630]
Zr [+20%, –20%]	---	---	---	[0.9522, 0.9270]	[0.9736, 0.9705]	[0.9928, 0.9916]	[0.9746, 0.9812]

For more explanation, see Table S19.

Table S22. Evaluation of the 3 sets of multidimensional diagrams for bulk assimilation of upper continental crust (UCC).

Diagram type [Assimilation %, %]	Probability change of the centroid [p_{gain}, p_{loss}] caused by element concentration changes Θ						
	IA+CA		Arc		Within-plate (CR+OI)		Collision Col
	IA	CA	IA	CA	CR	OI	
Major element-based diagrams							
(1+2-3+4-5) **UCC**							**0.98306**
(1+2-3+4-5) **No change**	**0.92046**	**0.88378**	---	---	**0.92458**	**0.98888**	**0.94785**
(1+2-3+4-5) [10%, 20%]	[0.8618, 0.7701]	[0.8084, 0.6991]	---	---	[0.8681, 0.7698]	[0.9778, 0.9531]	[0.9546, 0.9604]
(1-2-3+4) **UCC**					**0.74767**		
(1-2-3+4) **No change**	---	---	**0.61392**	**0.59320**	**0.95535**	**0.98472**	---
(1-2-3+4) [10%, 20%]	---	---	[0.6044, 0.5867]	[0.5861, 0.5859]	[0.9336, 0.8995]	[0.9752, 0.9587]	---
(1-2-5) **UCC**							**0.91900**
(1-2-5) **No change**	---	---	**0.59424**	**0.59364**	---	---	**0.95095**
(1-2-5) [10%, 20%]	---	---	[0.5700, 0.5320]	[0.5699, 0.5398]	---	---	[0.9503, 0.9495]
(1-3+4-5) **UCC**							**0.99496**
(1-3+4-5) **No change**	---	---	**0.92792**	---	**0.93414**	**0.98914**	**0.95117**
(1-3+4-5) [10%, 20%]	---	---	[0.8596, 0.7436]	---	[0.8825, 0.7892]	[0.9782, 0.9531]	[0.9610, 0.9689]
(2-3+4-5) **UCC**							**0.97334**
(2-3+4-5) **No change**	---	---	---	**0.84611**	**0.86404**	**0.96601**	**0.91793**
(2-3+4-5) [10%, 20%]	---	---	---	[0.7492, 0.6220]	[0.7936, 0.6900]	[0.9415, 0.8958]	[0.9278, 0.9365]
Major and trace elements-based diagrams							
(1+2-3+4-5) **UCC**							**0.98581**
(1+2-3+4-5) **No change**	**0.86377**	**0.84043**	---	---	**0.92193**	**0.99002**	**0.96549**
(1+2-3+4-5) [10%, 20%]	[0.6037, *0.4021*]	[0.5970, *0.3562*]	---	---	[0.8937, 0.8520]	[0.9854, 0.9776]	[0.9697, 0.9731]
(1-2-3+4) **UCC**					**0.47778**		
(1-2-3+4) **No change**	---	---	**0.58701**	**0.64616**	**0.98474**	**0.99848**	---
(1-2-3+4) [10%, 20%]	---	---	[0.5944, 0.6032]	[0.6089, 0.5675]	[0.9827, 0.9798]	[0.9981, 0.9976]	---
(1-2-5) **UCC**							**0.99520**
(1-2-5) **No change**	---	---	**0.54861**	**0.59639**	---	---	**0.94769**
(1-2-5) [10%, 20%]	---	---	[0.4666, *0.3467*]	[0.4828, *0.3289*]	---	---	[0.9581, 0.9665]
(1-3+4-5) **UCC**							**0.98058**
(1-3+4-5) **No change**	---	---	**0.83946**	---	**0.91525**	**0.98628**	**0.96261**
(1-3+4-5) [10%, 20%]	---	---	[0.6287, *0.4129*]	---	[0.8854, 0.8421]	[0.9802, 0.9701]	[0.9657, 0.9684]
(2-3+4-5) **UCC**							**0.99072**
(2-3+4-5) **No change**	---	---	---	**0.94673**	**0.89487**	**0.99756**	**0.97595**
(2-3+4-5) [10%, 20%]	---	---	---	[0.6347, *0.2257*]	[0.8579, 0.8047]	[0.9680, 0.9526]	[0.9798, 0.9826]
Trace element-based diagrams							
(1+2-3+4-5) **UCC**					**0.57012**		
(1+2-3+4-5) **No change**	**0.96541**	**0.91223**	---	---	**0.97804**	**0.99661**	**0.98297**
(1+2-3+4-5) [10%, 20%]	[0.8800, 0.7376]	[0.7379, 0.5410]	---	---	[0.9733, 0.9669]	[0.9958, 0.9947]	[0.9739, 0.9601]
(1-2-3+4) **UCC**					**0.79084**		
(1-2-3+4) **No change**	---	---	**0.71546**	**0.64256**	**0.98757**	**0.99908**	---

Table S22. (continued).

(1-2-3+4) [10%, 20%]	---	---	[0.6666, 0.5930]	[0.5585, 0.4788]	[0.9858, 0.9834]	[0.9989, 0.9986]	---
(1-2-5) **UCC**							**0.82762**
(1-2-5) **No change**	---	---	**0.71670**	**0.63668**	---	---	**0.98681**
(1-2-5) [10%, 20%]	---	---	[0.6646, 0.5970]	[0.5619, 0.4943]	---	---	[0.9835, 0.9791]
(1-3+4-5) **UCC**					**0.54487**		
(1-3+4-5) **No change**	---	---	**0.96450**	---	**0.97209**	**0.99371**	**0.97546**
(1-3+4-5) [10%, 20%]	---	---	[0.8882, 0.7628]	---	[0.9663, 0.9588]	[0.9925, 0.9907]	[0.9635, 0.9461]
(2-3+4-5) **UCC**					**0.61370**		
(2-3+4-5) **No change**	---	---	---	**0.94219**	**0.97245**	**0.99233**	**0.97787**
(2-3+4-5) [10%, 20%]	---	---	---	[0.7382, 0.4818]	[0.9675, 0.9611]	[0.9910, 0.9892]	[0.9671, 0.9511]

For more explanation, see Table S19.

Table S23. Evaluation of the third trace element-based multidimensional diagrams for petrogenetic process of fractional crystallization applied to basic magmas.

Diagram type [petrogenetic process of fractional crystallization]	Probability change of the centroid [p_{gain}, p_{loss}] caused by fractional crystallization applied to basic magmas *					
	Arc			CR	OI	Collision Col
	IA+CA	IA	CA	Within-plate (CR+OI)		
(1+2-3+4-5) **Centroid of basic magmas**	**0.86271**	---	---	**0.98273 (CR)**	**0.98691 (OI)**	No data
[FC of olivine: F = 0.50]	[0.8240]	---	---	[0.9827]	[0.9869]	
[FC of cpx: F = 0.50]	[0.5298]	---	---	[0.9795]	[0.9845]	
[FC of opx: F = 0.50]	[0.9484]	---	---	[0.9803]	[0.9850]	
[FC of plg: F = 0.50]	[0.8598]	---	---	[0.9847]	[0.9884]	
(1-2-3+4) **Centroid of basic magmas**	---	***0.42952*– 0.55888**		**0.99620**	**0.99730**	---
[FC of olivine: F = 0.50]	---	[*0.4290*]	[0.5585]	[0.9966]	[0.9976]	---
[FC of cpx: F = 0.50]	---	[*0.3384*]	[0.6214]	[0.9988]	[0.9992]	---
[FC of opx: F = 0.50]	---	[*0.3612*]	[0.6356]	[0.9853]	[0.9895]	---
[FC of plg: F = 0.50]	---	[*0.4785*]	[0.5107]	[0.9964]	[0.9974]	---
(1-2-5) **Centroid of basic magmas**	---	***0.46586*–0.48481**		---	---	No data
[FC of olivine: F = 0.50]	---	[0.4686]	[*0.4653*]	---	---	
[FC of cpx: F = 0.50]	---	[*0.3045*]	[0.4228]	---	---	
[FC of opx: F = 0.50]	---	[*0.3826*]	[0.6001]	---	---	
[FC of plg: F = 0.50]	---	[0.5185]	[*0.4318*]	---	---	
(1-3+4-5) **Centroid of basic magmas**	---	**0.80111**	---	**0.97864**	**0.98237**	No data
[FC of olivine: F = 0.50]	---	[0.7545]	---	[0.9785]	[0.9822]	
[FC of cpx: F = 0.50]	---	[*0.4338*]	---	[0.9730]	[0.9776]	
[FC of opx: F = 0.50]	---	[0.9093]	---	[0.9794]	[0.9831]	
[FC of plg: F = 0.50]	---	[0.8137]	---	[0.9808]	[0.9842]	
(2-3+4-5) **Centroid of basic magmas**	---	---	**0.88619**	**0.98231**	**0.98649**	No data
[FC of olivine: F = 0.50]	---	---	[0.8500]	[0.9823]	[0.9865]	
[FC of cpx: F = 0.50]	---	---	[0.5926]	[0.9747]	[0.9818]	
[FC of opx: F = 0.50]	---	---	[0.9517]	[0.9800]	[0.9827]	
[FC of plg: F = 0.50]	---	---	[0.8696]	[0.9849]	[0.9884]	

Table S24. Evaluation of the third trace element-based multidimensional diagrams for petrogenetic process of assimilation and fractional crystallization (AFC) applied to basic magmas.

Diagram type mineral [petrogenetic process of AFC; r–F_{remain}]	Probability change of the centroid [p_{gain}, p_{loss}] caused by AFC applied to basic magmas*					
	Arc			CR	OI	Collision Col
	IA+CA	IA	CA	Within-plate (CR+OI)		
(1+2-3+4-5) **Centroid of basic magmas**	**0.86271**	---	---	**0.98273 (CR)**	**0.98691 (OI)**	No data
olivine [0.2–0.7, 0.4–0.5]	[0.7007, *0.3509*]	---	---	[0.9774, 0.9567]	[0.9814, 0.9589]	
cpx [0.2–0.7, 0.4–0.5]	[0.4986, *0.0773*]	---	---	[0.9752, 0.9455]	[0.9795, 0.9472]	
opx [0.2–0.7, 0.4–0.5]	[0.8450, 0.7934]	---	---	[0.9760, 0.9437]	[0.9803, 0.9492]	
plg [0.2–0.7, 0.4–0.5]	[0.7315, 0.4229]	---	---	[0.9791, 0.9633]	[0.9828, 0.9654]	
(1-2-3+4) **Centroid of basic magmas**	---	**0.42952–0.55888**		**0.99620**	**0.99730**	---
olivine [0.2–0.7, 0.4–0.5]	---	[*0.4273, 0.3047*]	[0.5218, 0.3975]	[0.9958, 0.9934]	[0.9971, 0.9959]	---
cpx [0.2–0.7, 0.4–0.5]	---	[*0.3568, 0.1002*]	[0.5428, *0.2208*]	[0.9978, 0.9984]	[0. 9985, 0.9990]	---
opx [0.2–0.7, 0.4–0.5]	---	[*0.3955, 0.3133*]	[0.5819, 0.6311]	[0.9894, 0.9438]	[0.9928, 0.9627]	---
plg [0.2–0.7, 0.4–0.5]	---	[*0.4574*, 0.3725]	[0.4957, *0.3719*]	[0.9956, 0.9925]	[0.9970, 0.9954]	---
(1-2-5) **Centroid of basic magmas**	---	**0.46586–0.48481**		---	---	No data
olivine [0.2–0.7, 0.4–0.5]	---	[*0.4382, 0.2952*]	[0.4399, 0.3487]	---	---	
cpx [0.2–0.7, 0.4–0.5]	---	[*0.3205, 0.0513*]	[0.3995, *0.1019*]	---	---	
opx [0.2–0.7, 0.4–0.5]	---	[*0.4049, 0.2841*]	[0.5395, 0.6494]	---	---	
plg [0.2–0.7, 0.4–0.5]	---	[0.4708, 0.3787]	[*0.4254, 0.3532*]	---	---	
(1-3+4-5) **Centroid of basic magmas**	---	**0.80111**	---	**0.97864**	**0.98237**	No data
olivine [0.2–0.7, 0.4–0.5]	---	[0.6347, *0.3267*]	---	[0.9725, 0.9492]	[0.9757, 0.9497]	
cpx [0.2–0.7, 0.4–0.5]	---	[*0.4304, 0.0731*]	---	[0.9685, 0.9315]	[0.9720, 0.9310]	
opx [0.2–0.7, 0.4–0.5]	---	[0.7818, 0.7169]	---	[0.9733, 0.9496]	[0.9765, 0.9516]	
plg [0.2–0.7, 0.4–0.5]	---	[0.6798, 0.4250]	---	[0.9743, 0.9561]	[0.9773, 0.9567]	
(2-3+4-5) **Centroid of basic magmas**	---	---	**0.88619**	**0.98231**	**0.98649**	No data
olivine [0.2–0.7, 0.4–0.5]	---	---	[0.6675, *0.2492*]	[0.9775, 0.9588]	[0.9821, 0.9636]	
cpx [0.2–0.7, 0.4–0.5]	---	---	[0.4794, *0.0609*]	[0.9721, 0.9301]	[0.9783, 0.9375]	
opx [0.2–0.7, 0.4–0.5]	---	---	[0.8113, 0.6542]	[0.9765, 0.9512]	[0.9804, 0.9548]	
plg [0.2–0.7, 0.4–0.5]	---	---	[0.6843, *0.2727*]	[0.9797, 0.9575]	[0.9837, 0.9712]	